

THESIS ON NATURAL AND EXACT SCIENCES B209

**Applications of Marine Scatterometer Winds and
Quality Aspects of their Assimilation into
Numerical Weather Prediction Model HIRLAM**

JEKATERINA SLUŽENIKINA

TALLINN UNIVERSITY OF TECHNOLOGY

Marine Systems Institute

Dissertation was accepted for the defence of the degree of Doctor of Philosophy in Earth Sciences on April 6, 2016

Supervisors: Prof. Sirje Keevallik, Marine Systems Institute at Tallinn University of Technology, Estonia
Dr. Aarne Männik, Institute of Environmental Physics at University of Tartu, Estonia.

Opponents: Dr. Ad Stoffelen, Group Leader Active Satellite Sensing, Royal Netherlands Meteorological Institute, Netherlands
Prof. Tiit Nilson, Senior Research Fellow, Tartu Observatory

Defence of the thesis: May 26, 2016 at the Marine Systems Institute at Tallinn University of Technology, Akadeemia tee 15a, Tallinn, Estonia

Declaration:

Hereby I declare that this thesis, submitted for the doctoral degree at Tallinn University of Technology, is my original investigation and achievement and has not been submitted for any other academic degree.

/Jekaterina Služenikina/

Copyright: Jekaterina Služenikina, 2016

ISSN 1406-4723

ISBN 978-9949-23-940-5 (publication)

ISBN 978-9949-23-941-2 (PDF)

LOODUS- JA TÄPPISTEADUSED B209

Skatteromeetri meretuulte rakendused ja kvaliteedihinnang nende assimileerimisele numbrilise prognoosi mudelisse HIRLAM

JEKATERINA SLUŽENIKINA

CONTENTS

1. INTRODUCTION.....	9
1.1 Background	9
1.2 Scatterometers and their evolution	10
1.3 SeaWinds scatterometer on QuikSCAT	11
1.3.1 Overview and measurement technique.....	11
1.3.2 Data processing	12
1.3.3 Rain contamination.....	13
1.3.4 Data quality	14
1.4 ASCAT scatterometer on MetOp	15
1.4.1 Overview and measurement technique.....	15
1.4.2 Data processing	16
1.4.3 High resolution winds	17
1.4.5 Data Quality	18
1.5 Motivation and objectives	18
ABBREVIATIONS.....	21
2. DATA AND METHODS.....	23
2.1 QuikSCAT data	23
2.2 ASCAT data	25
2.3 Severe storms cases	27
2.4 Surface-based measurements.....	27
2.5 HIRLAM and data assimilation.....	29
2.5.1 ASCAT data assimilation into the HIRLAM	31
2.6 HIRLAM winds.....	32
3. MARINE WINDS IN THE GULF OF RIGA FROM QUIKSCAT AND GROUND BASED MEASUREMENTS	34
3.1 SeaWinds – analysis with strict criteria	34
3.2 SeaWinds – analysis with more lenient criteria	36
3.3 Wind measurements on the islands and correlation with satellite data	36

4. MARINE WINDS IN THE BALTIC SEA REGION FROM THE ASCAT AND HIRLAM FORECASTS	40
4.1 Statistical comparison of the HIRLAM and ASCAT	40
4.2 A case with phase error in cyclonic activity	41
4.3 Discussion	43
5. IMPACT OF THE ASCAT WINDS ON THE HIRLAM ANALYSIS QUALITY IN CASE OF SEVERE STORMS.....	45
5.1 Storm Christian (St Jude, Allan) 28.10.2013	45
5.2 Stormy winds in the Baltic Sea 01.12.2013	49
5.3 Storm Xaver 05.12.2013	51
5.4 Discussion	55
CONCLUSIONS	57
Acknowledgements	60
ABSTRACT	61
RESÜMEE	63
REFERENCES.....	65
ELULOOKIRJELDUS.....	71
CURRICULUM VITAE	73
APPENDIX A: PAPERS.....	75

List of original publications

This thesis is based on the following papers, which will be referred to in the text by their Roman numerals.

- I. Služenikina, J., Keevallik, S. 2013. Winds in the Gulf of Riga from QuikSCAT and ground-based measurements. *International Journal of Remote Sensing*, 34 (16), 5731–5747.
- II. Služenikina, J., Männik, A. 2011. A comparison of ASCAT wind measurements and the HIRLAM model over the Baltic Sea. *Oceanologia*, 53 (1, SI), 229–244.
- III. Služenikina, J., Männik, A. [accepted for publication]. Impact of the ASCAT scatterometer winds on the HIRLAM analysis quality in case of severe storms. *Proceedings of the Estonian Academy of Sciences*, 2016, 65, 3, 177–194.

In Appendix A, copies of the papers are included.

Author's contribution

- I. The author was responsible for data analysis and writing of the manuscript.
- II. The author was responsible for data analysis and writing of the manuscript. The author presented the results at international conferences.
- III. The author was responsible for data analysis and writing of the manuscript. The author presented the results at the EUMETSAT international training course.

Approbations of the results

The results have been presented in the following international conferences:

1. The 6th Study Conference on BALTEX “Changing Water, Energy and Biogeochemical Cycles in the Baltic Sea Basin, Międzyzdroje, Poland, 14-18 June 2010: poster – A study of ASCAT wind measurements near coastal region of Estonia (in cooperation with A. Männik).
2. The 8th Baltic Sea Science Congress, St. Petersburg, Russia, 22-26 August 2011: poster – A comparison of ASCAT wind measurements and the HIRLAM model over the Baltic Sea (in cooperation with A. Männik).
3. EUMETSAT Baltic+ Training Course 2015, Tallinn, Estonia, 17-19 March 2015: oral presentation – Impact of the ASCAT data assimilation into the HIRLAM model in case of severe storms.

1. INTRODUCTION

1.1 Background

Enormous progress has been done in the weather forecasting during the second half of the 20th century due to the advent of powerful computers and launching meteorological satellites. Before the 1940s, the meteorologists forecasted weather with the aid of typical weather patterns, assuming that the forecast could be given on the basis of the formerly observed evolution of similar patterns over time. Meteorological data used for initiation of the forecast were sparse and situation in the upper layers of the atmosphere could be estimated only by means of radiosoundings and balloons. Although it was already clear that the weather forecast can be regarded as a physical problem, the calculation power was too weak to solve the complicated system of equations.

Unprecedented development of computer technology contributed to development of numerical weather prediction (NWP) models and introducing them into operational weather forecasting, offering a tool for giving the weather forecasts for several days ahead and even longer. Nowadays, the usage of different types of NWPs such as global models or limited area models and even ensemble of NWP models speeds up everyday work of operational forecaster and give an excellent opportunity to make more accurate forecast of atmospheric flow.

One of the important aspects playing vital role in NWP accuracy is the quality and accessibility of observational data. Regular surface-based observations, radiosonde data and the data from ships, buoys and lightships are the basic *in situ* observations used as the input of NWP models. In addition to surface-based measurements, global observations from satellites started in the 1960s. It is widely known that satellite measurements offer the best spatial coverage to describe properties of the underlying surface and atmosphere. This is especially important in marine areas where *in situ* measurements are rather sparse.

This work is focused on wind scatterometers – the instruments on polar-orbiting satellites that are used to infer data on wind speed and wind direction from the radar measurements of the sea surface. They rely for their operation on the fact that winds blowing over the sea influence the radar backscattering properties of the surface in a manner that is related to wind speed and wind direction (Stoffelen, 1998; Portabella, 2002). Wind stress over the ocean generates ripples and small waves, which roughen the sea surface, therefore modify the radar cross section (σ^0) of the ocean surface and hence the magnitude of backscattered power (Lungu and Callahan, 2006).

1.2 Scatterometers and their evolution

The first scatterometer launched into space was the National Aeronautics and Space Administration (NASA) SeaSat-A Scatterometer System, SASS that flew in 1978 for three months. SASS had four antennas, two on both sides of the satellite. Each set of two antennas covered a swath; one to the right of the sub-satellite (ground) track and one to the left. In the horizontal plane, the fore and aft beams were pointing at respectively 45° and 135° with respect to the ground track (Stoffelen, 1998). In spite of its short period of the measurements, the preliminary assessment of the SASS data assimilation into the global NWP forecast experiments studied by Yu and McPherson (1984) showed that the influence of scatterometer winds was beneficial, especially in the Southern Hemisphere, where the number of marine observations is limited.

The next scatterometer launched in 1996 was the NASA Scatterometer (NSCAT) on Japanese Advanced Earth Observation Satellite (ADEOS) and the basic difference from SASS was that this time a beam was added in between the fore and aft beams to both sides of the swath. The two additional measurements helped to resolve a unique wind vector solution (Stoffelen, 1998). Somewhat later, after the loss of NSCAT scatterometer, in 1999 a new scatterometer SeaWinds on Quick Scatterometer (QuikSCAT) satellite was launched. SeaWinds scatterometer measured globally marine winds for nearly ten years, it was the first satellite that operated for such a long time and for a wide swath (about 1800 km) giving a good opportunity to make climatological overview of marine winds. The main difference of SeaWinds from previous instruments lays on the technique of measurement. SeaWinds was the first pencil-beam scanning scatterometer making circular measurements near the ocean surface and therefore making the measurements on a wider swath.

The next AMI (Advanced Microwave Instrument) scatterometer was a fan-beam instrument operated at C-band (5.6 GHz) on ERS-1 (European Remote-Sensing Satellite) and ERS-2, launched in 1991 and 1995 respectively by ESA (European Space Agency). AMI used a similar principle of work as NSCAT, however, with antennas on either sides of the nadir track. In continuation of AMI measurements, the ASCAT (Advanced Scatterometer) was successfully launched by ESA and European Organization for the Exploitation of Meteorological Satellites (EUMETSAT) in 2006 and 2012 on board of (Meteorological Operational) MetOp-A and MetOp-B satellites and presently work operationally.

In 2009 the Indian Space Research Organization (ISRO) launched a Ku-band OSCAT scatterometer on Oceansat-2 which was aimed to enlarge data coverage of the ASCAT satellite swaths. Unfortunately, the OSCAT finished its work in February 2014 due to irrecoverable instrument failure. Today the newest scatterometer RapidScat with a similar measurement technique as OSCAT started its operational dissemination in May 2015. The RapidScat instrument is a conically scanning pencil-beam scatterometer that operates at Ku-band (13.5 GHz). The RapidScat is a speedy and cost-effective replacement for the NASA

SeaWinds instrument, which provided a decade-long ocean wind vector observations. The RapidScat observation swath of approximately 1100 kilometres covers the majority of the oceans between 56° north and south latitude in 48 hours (Verhoef and Stoffelen, 2015).

1.3 SeaWinds scatterometer on QuikSCAT

1.3.1 Overview and measurement technique

The SeaWinds scatterometer was an active microwave instrument launched 19 June 1999 on board of polar-orbiting QuikSCAT satellite, operated by Jet Propulsion Laboratory (JPL) and managed by NASA. Throughout its long operational lifetime (19 June 1999 - 23 November 2009) the SeaWinds measurements have helped in the estimation of the intensity of tropical storms, in determining the radial extent of winds of tropical storm force in tropical storms and hurricanes, and in locating circulation centres for tropical depressions and tropical storms (National Research Council, 2007). The QuikSCAT data were not only used for tropical storms detection, but globally in everyday operational marine forecasting and warning systems, NWP models and in detection of low-pressure systems at high-latitudes.

The SeaWinds instrument was a conical-scanning pencil-beam scatterometer that used a rotating 1-meter dish antenna with two spot beams, a horizontally-polarized (H-pol) beam and a vertically-polarized (V-pol) beam at incidence angles of 46° and 54° respectively, that swept in a circular pattern (Fig. 1.1). The antenna radiated microwave pulses at a frequency of 13.4 GHz (Ku-Band) across a 1800-km-wide swath centred on the spacecraft's nadir sub-track, making approximately 1.1 million 25-km ocean surface wind vector measurements and covering 90% of the Earth's surface every day (Portabella and Stoffelen, 2002).

The backscatter (σ^0) signals measured by SeaWinds were collected over special equidistant wind vector cells (WVCs) with grid resolution of 25 x 25 km and 12.5 x 12.5 km. In the standard QuikSCAT data product, slices from overlapping current and previous across-track sweeps of the radar beam were then combined and averaged to provide 25 km by 25 km WVC. The output was not used if any part of the field of view was contaminated by land, so the QuikSCAT wind data were masked within 30 km of the coast (Pickett *et al.*, 2003). The high-resolution 12.5-km Level 2B winds were produced from the "slices" of the ellipsoidal instantaneous antenna footprint with a simplified backscatter averaging scheme and different land contamination criteria that was particularly useful to resolve the coastal winds (Tang *et al.*, 2004).

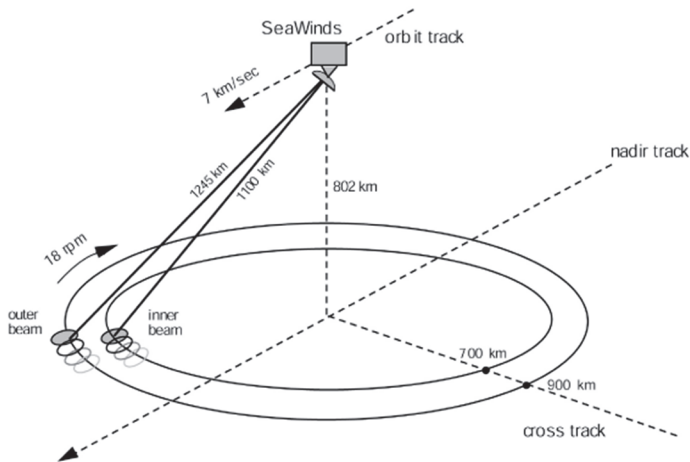


Figure 1.1. SeaWinds viewing geometry (Spencer *et al.*, 2000).

1.3.2 Data processing

In order to extract wind velocity from the backscatter (σ^0) signal, one must know the relationship between σ^0 and near-surface winds – this relationship is known as the geophysical model function (GMF) (Lungu and Callahan, 2006). The GMF was used to transform SeaWinds backscattered signals from the sea surface into wind speed and wind direction at each WVC. Multiple measurements at different azimuth angles were performed in order to remove the ambiguities appeared after the measurements. The wind retrieval algorithm computed a set of wind vectors together with their relative likelihoods for each WVC. According to the Bayes' theorem, the Maximum Likelihood Estimation (MLE) value represented the probability of a trial wind vector (solution) being the “true” wind, the SeaWinds optimization technique consisted of looking for the minima, which represented the local solutions with maximum probability (Portabella and Stoffelen, 2004). The MLE incorporated the NWP, by the National Centers of Environmental Prediction (NCEP), output as the initial field, or “first guess”, to choose the best solution (nudging technique). The NWP wind field was spatially interpolated: 2.5° resolution 1000 mb (≈ 100 m) global data analysis model outputs closest in time to the QuikSCAT pass (Sharma and D'Sa, 2008). It should be noted that NWP winds, used in ambiguity removal algorithm are about 100 m above the sea level while the QuikSCAT winds are 10 m neutral winds, such difference in reference heights may bring along some uncertainty. The QuikSCAT neutral winds were defined as the equivalent winds obtained with the stress and roughness length consistent with the atmospheric stratification when the stability adjustment was set to zero (Nghiem *et al.*, 2004).

In addition to general ambiguity removal, some special techniques were applied for the wind direction retrieval due to ambiguities appeared at different viewing angles. The specification of pencil-beam measurements is that the azimuth angle “mix” of the σ^0 measurements going into the wind retrieval is not constant, but varies from nadir out to the edge of the swath. Near nadir the forward and aft measurements are approximately 180 degrees apart, while at the extreme edge of the swath the azimuth angle between the measurements approaches 0 degrees. Thus, the wind retrieval performance of SeaWinds varied as a function of the distance from the nadir track, in general being optimum when the azimuth differences of the measurements are near 90 degrees (Tsai *et al.*, 2000). As a result, near nadir, due to non-optimal measurement geometry, there was a marked decrease in directional accuracy even when ambiguity removal worked correctly. Two algorithms were developed in order to improve the wind directional accuracy: direction interval retrieval (DIR) to address the nadir performance issue, and threshold nudging (TN) to improve ambiguity removal at far swath (Stiles, 1999). Both algorithms worked independently and were used together to obtain the (DIRTH) solutions in the Level 2B product (Lungu and Callahan, 2006). More information about the DIRTH algorithm can be found in the manuscript of Stiles (1999).

1.3.3 Rain contamination

Rain is known to both attenuate and backscatter the microwave signal, affecting the quality of wind measurements. Raindrops are small compared to radar wavelengths and cause Rayleigh scattering (inversely proportional to the fourth power of the wavelength) (Portabella and Stoffelen, 2002). In presence of large raindrops the impact is higher and the „splashing“ effect occurs. The roughness of the sea surface is increased because of splashing due to raindrops. This increases the radar backscatter (σ^0) signal, which in turn will affect the quality of wind speed (positive bias due to σ^0 increase) and direction (loss of anisotropy in the backscatter signal) retrievals (Portabella and Stoffelen, 2002). In addition, as the rain rate increases, the space-borne instrument sees less and less of the radiation emitted by the surface, and increasingly sees the radiation emitted by the rainy layer that becomes optically thick due to volumetric Rayleigh scattering (Portabella and Stoffelen, 2002).

Several algorithms were developed to detect rain-contaminated data for rain-flagging: Normalized Object Function (NOF) Rain Flag (Mears *et al.*, 2000) and Multidimensional Histogram (MUDH) Rain Flag (Huddleston and Stiles, 2000). Both techniques are included to detect rain contamination in the QuikSCAT Level 2B data, however, the impact-based MUDH (IMUDH) algorithm is used in processing of Level 2B JPL data, NOF is incorporated as additional parameter

into wind dataset (Lungu and Callahan, 2006). The new IMUDH rain probability does not flag a specific rain rate, but shows the likelihood that the wind speed is perturbed by more than 2 m s^{-1} or in the wind direction by more than 15 degrees. The previous MUDH showed the probability of encountering a columnar rain rate that is greater than $2 \text{ km}^3 \text{ mm h}^{-1}$ (Lungu and Callahan, 2006). The primary improvement of IMUDH over MUDH is in the reduction of the overflagging of strong wind speeds and the removal of swath artefacts including overflagging in the outer swath (Lungu and Callahan 2006). Instead of flagging for rain IMUDH algorithm flag detects rain contamination of wind data and as a result flags fewer high winds and fewer overall (Stiles *et al.*, 2006). In addition, the NOF rain flag validation by (Mears *et al.*, 2000) showed that NOF rain flag removes erroneous wind vectors almost as effectively as SSM/I (Special Sensor Microwave Imager for rain rate measurements) collocated rain measurements, but does not require the SSM/I collocated measurements.

In general, rain contamination of QuikSCAT data causes two main effects, 1) higher derived wind speeds in low wind fields and 2) the presence of wind vectors turned perpendicular to the satellite track in high wind and rain locations (referred to as cross-track winds) (Smith *et al.*, 2002). These two indicators of wrong wind speed and wind direction are used in operational forecasting when the rain-flagging technique is turned off to get more wind observations inside tropical or extra-tropical cyclones.

1.3.4 Data quality

The QuikSCAT wind data are in general of high quality, however, the accuracy of scatterometer winds can be affected by different factors, such as land, ice and rain contamination, very strong or very weak winds. The accuracy of QuikSCAT 25-km product is required to have a root mean square error (RMSE) less than 2 m s^{-1} in wind speed interval $3\text{--}30 \text{ m s}^{-1}$ or 10% in the interval $20\text{--}30 \text{ m s}^{-1}$, the wind direction RMSE (root mean square error) is required to be less than 20 degrees ($3\text{--}30 \text{ m s}^{-1}$) (Lungu and Callahan, 2006). The buoy comparison with 25-km QuikSCAT winds by Stoffelen *et al.* (2010) show similar results. The QuikSCAT winds weaker than 3 m s^{-1} or stronger than 30 m s^{-1} are generally flagged as “low” or “high” wind speed. At light winds for example, the uncertainties of wind retrievals are higher as the smoother sea surface appears more as a reflector than a scatterer. Direction errors decrease with increasing wind speed (Hoffman and Leidner, 2005), therefore, it is not recommended to analyse winds weaker than 1 m s^{-1} .

1.4 ASCAT scatterometer on MetOp

1.4.1 Overview and measurement technique

The ASCAT is the real aperture radar on MetOp-A (launched on 19 October 2006) and MetOp-B (launched on 17 September 2012) satellites that successfully measure global marine winds near the sea surface. The main application foreseen is the assimilation of those winds into NWP models. Furthermore, its dense coverage makes the winds useful for direct use by operational weather forecasters when performing the necessary real-time interpretation of NWP model results to elaborate a forecast (Figa-Saldaña *et al.*, 2002). In addition to marine wind measurements, the ASCAT measures the soil moisture on the land surface, and indirectly such land surface variables as snow cover fraction, frozen land surface fraction, vegetation can be estimated (Bartalis *et al.*, 2008).

As the SeaWinds instrument, the ASCAT gives information about the wind speed and wind direction at 10 m height. Calculations of the wind parameters at the height of 10 m are chosen for better validation with *in situ* wind measurement and the wind retrieval from NWP models. In contrast to the SeaWinds instrument, the ASCAT operates at the frequency of 5.255 GHz (C-band) which makes it rather insensitive to rain (OSI-SAF Project Team, 2013). The data are also organized into WVCs with the same grid spacing of 12.5 km (spatial resolution of 25 km) and with a grid spacing of 25 km (spatial resolution of 50 km) across and along two 550-km wide swaths on both sides of the nadir track. Unlike the SeaWinds instrument, the ASCAT fan-beam measurements are provided in three azimuth directions – fore, mid and aft respectively (Fig. 1.2) pointing 45°, 90° and 135° away from the satellite propagation vector, to resolve the wind direction and speed (OSI-SAF Project Team, 2013).

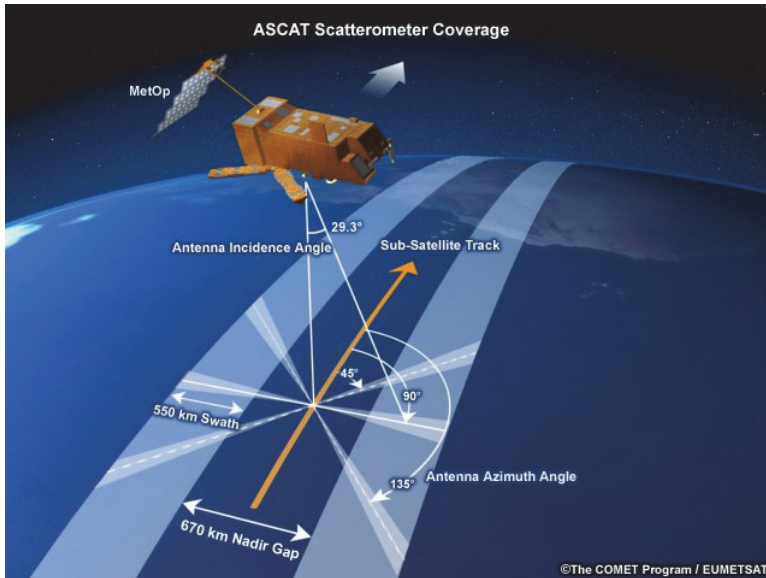


Figure 1.2. The ASCAT Scatterometer Coverage.

Source: COMET® <http://www.moisturemap.monash.edu.au/aaces/aaces-1/ascat.php>; accessed 28 April 2010

1.4.2 Data processing

Processing of the ASCAT measurements leads to the generation of two main products: (1) ASCAT Level 1b data that consist of rows of nodes along-track, containing σ^0 estimates (three values, one from each beam within a swath), with a fixed node grid across the swath; and (2) ASCAT Level 2 data that contain values of wind speed and direction retrieved on a node by node basis from the σ^0 triplets (Figa-Saldaña *et al.*, 2002). The Level 1b data processing lies in the spatial averaging of all available σ^0 measurements into WVCs performed by EUMETSAT ground segment. The ASCAT Level 2 data are processed and distributed in near real-time jointly by the EUMETSAT Ocean and Sea Ice Satellite Application Facility (OSI SAF) and Advanced Retransmission Service (EARS) ground system, both implemented at the Royal Netherlands Meteorological Institute (KNMI). The quality control (QC) of the ASCAT data is carried out during the wind retrieval process by KNMI.

In the wind retrieval the CMOD5.n GMF for calculating equivalent neutral winds is used (Verhoef and Stoffelen, 2014). For each scatterometer measurement it shows the wind speed solution as a function of all possible wind directions. Given the basic harmonic wind direction dependency of the backscatter signal, four solutions exist in this general case (Stoffelen, 1998). Each wind ambiguity is

characterized by a solution probability that is determined on the basis of the distance-to-cone residual in the inversion. The wind ambiguities, solution probabilities, and prior information from the ECMWF model 10-m background winds are used in a 2D variational ambiguity removal procedure to produce an analysed surface wind field. This wind field is then used to select the wind vector ambiguity in each WVC that is closest to the analysis, based on vector difference, as the solution for the observed surface wind (De Haan *et al.*, 2013). Finally, the backscatter measurements, wind ambiguities, scanning geometry, and wind vector solution flag, among others, are made available in the ASCAT Wind Product. The observations flagged as rain or land contaminated, or sea-ice contaminated are eliminated from observations (OSI-SAF Project Team, 2013).

1.4.3 High resolution winds

The high resolution ASCAT 12.5-km Wind Product is very important for detecting the mesoscale processes over the marine areas, however more random wind noise is expected. Noise reduction is beneficial and further progress is being made by implementing the so-called Multiple Solution Scheme (MSS) (Portabella and Stoffelen, 2004). It was noted by the authors that the improved verification of MSS is mainly due to the reduction of occasional erratic noise; coherent mesoscale structures remain present and become more visible due to the noise reduction.

Another development of 12.5-km ASCAT Wind Product is the Coastal Wind Product that was aimed to make the wind measurements closer to the coastal area and the narrow marine areas. The main difference in processing of the Coastal ASCAT 12.5-km Wind Product lies in the backscatter averaging procedure. The full resolution backscatter data are averaged using a spatial box filter rather than the Hamming filter that is used in the spatial averaging of the σ^0 s of the nominal Level 1 products, in more detail described by Verhoef and Stoffelen (2011). During the averaging only those full resolution σ^0 s are used that are placed entirely over sea (OSI-SAF Project Team, 2013). As a result, the box-averaging technique makes it possible to retrieve marine winds about 15 km off the coast, while the former product gave information only 35 km off the coast.

The ASCAT Coastal Wind Products operated in testing mode on MetOp-A since 2011. Validation with buoy data and with triple collocated data showed that the error characteristics of the coastal product are very similar to those of the operational 12.5-km product (Verhoef and Stoffelen, 2011). As a result, since the end of April 2015 the global MetOp-A Hamming window based 12.5-km Wind Product discontinued its measurements and was totally replaced by the ASCAT Coastal 12.5-km Wind Product. For Metop-B the ASCAT Coastal 12.5-km Wind Product is produced from the beginning of operation.

1.4.5 Data Quality

The accuracy of the ASCAT winds is validated against *in situ* wind measurements from buoys, platforms or ships, and against NWP data. The performance of the products issued by the OSI SAF and the EARS is characterized by a wind component RMS (Root Mean Square) error smaller than 2 m s^{-1} and a bias of less than 0.5 m s^{-1} in wind speed (OSI-SAF Project Team, 2013). According to Gelsthorpe *et al.* (2000), determination of speeds in the range $4\text{--}24 \text{ m s}^{-1}$ with an accuracy of 2 m s^{-1} (or 10%) and directions with an accuracy of ± 20 degrees is required. As reported by OSI SAF (2013), both MetOp-A and MetOp-B ASCAT winds have expected the following accuracy (compared with buoy data): the wind speed bias of -0.02 m s^{-1} for MetOp-A and 0.05 m s^{-1} for MetOp-B, the standard deviation is 1.78 m s^{-1} for MetOp-A and 1.80 m s^{-1} for MetOp-B, respectively. Buoy collocations and a triple collocation study made by Verspeek *et al.* (2013) show also that there are no significant differences in wind quality between the ASCAT-A and ASCAT-B wind products and therefore both data sets can be successfully used in operational work or in the data assimilation procedure.

1.5 Motivation and objectives

The primary mission of scatterometers is to provide operationally the users with the sea-surface wind measurements in marine areas over the globe. The main applications of scatterometer data are operational nowcasting and assimilation of marine winds into NWP models (Figa-Saldaña *et al.*, 2002; Stoffelen *et al.*, 2013). The use of scatterometer observations in data assimilation systems can extend their usefulness substantially and lead to improved sea level pressure analyses, improved upper air analyses of both wind and geopotential, and improved short and extended-range numerical weather forecasts (Atlas *et al.*, 2001).

Most prominent weather centres such as ECMWF (European Centre for Medium-Range Weather Forecasting), Met Office (UK's national weather service), Japan Meteorological Agency and Environment Canada already use the ASCAT data in the data assimilation process. The ECMWF was the first centre that assimilated the ASCAT winds into the global NWP model in 2007 and showed positive effect on forecast skills, especially over the Southern Hemisphere where the number of marine observations is limited. In addition, for ocean waves significant positive impact was observed in the tropics (Hersbach and Janssen, 2007).

The impact of the ASCAT data assimilation into numerical models is mainly analysed for global models and in general, the impact is neutral to positive (Takashi, 2010; Bi *et al.*, 2010; Payan, 2010; Hesbach and Janssen, 2007). More recent studies of scatterometer data assimilation into the ECMWF model by De Chiara *et al.* (2014) also show positive effect after the ASCAT data assimilation

from both MetOp satellites together with OSCAT winds. In addition, Cotton (2013) evaluated the impact of the ASCAT data measured from both satellites into the global model in Met Office. To better exploit data from parallel ASCAT measurements, a new thinning scheme is proposed.

For limited area models several studies by Ollinaho (2010), De Valk (2013) and De Haan *et al.* (2013) showed positive to neutral impact on the forecasts of the HIRLAM (High Resolution Limited Area Model), which serves as the main NWP platform for short-range (up to three days) operational weather forecasting and NWP applications in many European countries. Valkonen and Schyberg (2015) assessed the impact of the ASCAT assimilation into the HARMONIE (Hirlam Aladin Regional/Mesoscale Operational NWP In Europe) model in case of severe storms and showed slight improvement of the forecasts in comparison with observations over land.

Because of the scarcity of marine wind observations in the Baltic Sea region, Estonian Weather Service is interested, first of all, in the quality of scatterometer winds as a complementary data source for weather and climate analyses over the sea. In addition, operational ASCAT measurements can be used as a possible solution for the operational monitoring of marine winds. This is of vital importance for the storms warnings, as the network of coastal weather stations is insufficient for assessing weather conditions over the sea. The potential of ASCAT wind measurements is also foreseen in improving the HIRLAM forecasts by assimilation scatterometer winds.

The main objectives of this thesis are:

- To verify the quality of scatterometer data in a relatively closed Baltic Sea region by comparing scatterometer winds with surface-based measurements on the islands and to study wind climatology in the Gulf of Riga, where combination of high sea level and strong wind may cause destructive floods (Suursaar *et al.*, 2006). In addition, this study is supported by the GORWIND (The Gulf of Riga as a Resource for Wind Energy) Project to study the wind energy resources in the gulf.
- To verify the quality of the ASCAT winds in the Baltic Sea region by comparing instantaneous ASCAT measurements with the HIRLAM wind forecasts. The comparison also aims to assess the quality and uncertainty range of both the HIRLAM NWP model predictions and the ASCAT measurements. The quality of the HIRLAM wind forecasts in marine areas are of special interest, as its output is often used for driving marine models in operational forecasting and hindcasting regimes.
- To perform the ASCAT data assimilation into operational HIRLAM (in Estonian Weather Service) and to compare the model behaviour with and without data assimilation.
- To assess the impact of the ASCAT data assimilation into the HIRLAM in some cases of severe storms as the impact in such cases is expected to

be more evident. Accurate calculations of the HIRLAM with the ASCAT data assimilation may improve the quality of severe weather forecasts, which is of great importance for the society.

ABBREVIATIONS

2D	Two-dimensional
ADEOS	ADvanced Earth Observation Satellite
3DVAR	Three-Dimensional Variational data assimilation
AIREP	AIRcraft REPorts
AMI	Advanced Microwave Instrument
AMO	Assimilated Marine Observations
ASCEXP	Experiments with ASCAT data assimilation
ASCII	American Standard Code for Information Interchange
ATS-1	Applications Technology Satellite
BSH	Federal Maritime and Hydrographic Agency of Germany
C-band	4.0–8.0 GHz electromagnetic spectrum frequency range
DIR	Direction interval retrieval
DIRTH	Direction interval retrieval threshold nudging
DRIBU	Drifting Buoys
EARS	EUMETSAT Advanced Retransmission Service
ECMWF	European Centre for Medium-Range Weather Forecasts
ERS	European Remote-Sensing Satellite
ESA	European Space Agency
EUMETCast	EUMETSAT's Digital Video Broadcast Data Distribution System
EUMETSAT	European Organisation for the Exploitation of Meteorological Satellites
FGAT	First Guess at Appropriate Time
GMF	Geophysical Model Function
GORWIND	Gulf of Riga as a Resource for Wind Energy project
HDF	Hierarchical Data Format
HIRLAM	HIgh Resolution Limited Area Model
H-pol	Horizontally polarized beam
IMO	Independent Marine Observation
IMUDH	Impact-based MUDH algorithm
ISRO	Indian Space Research Organization
JPL	Jet Propulsion Laboratory
KNMI	Royal Netherlands Meteorological Institute
Ku-band	12.0–18.0 GHz electromagnetic spectrum frequency
MARNET	MARine Environmental Monitoring NETwork in the North Sea and the Baltic Sea
MetOp	Meteorological Operational satellite
MLE	Maximum Likelihood Estimator
MSLP	Mean Sea Level Pressure
MSS	Multiple Solution Scheme

MUDH	Multidimensional Histogram
NASA	National Aeronautics and Space Administration
NCEP	National Centres of Environmental Prediction
NOF	Normalized Object Function
NSCAT	NASA Scatterometer
NWP	Numerical Weather Prediction
O–A	<i>In situ</i> Observation minus HIRLAM Analysis
O–B	ASCAT Observation minus HIRLAM Background
OSCAT	Oceansat-2 scatterometer
OSE	Observing System Experiments
OSI SAF	Ocean and Sea Ice Satellite Application Facility
PILOT	Pilot-balloon stations
PO.DAAC	Physical Oceanography Distributed Active Archive Centre
QC	Quality Control
QuikSCAT	Quick Scatterometer
REFEXP	Experiments without ASCAT data assimilation
RMS	Root Mean Square
RMSD	Root Mean Square Deviation
RMSE	Root Mean Square Error
SASS	SeaSat-A Scatterometer System
SHIP	Synoptic observations from ships
SMHI	Swedish Meteorological and Hydrological Institute
SSM/I	Special Sensor Microwave Imager
STDEV	Standard deviation
SYNOP	Surface synoptic stations
TEMP	Upper air soundings
TIROS-1	Television and Infrared Observational Satellite
TN	Threshold Nudging
UK	United Kingdom
UTC	Coordinated Universal Time
V-pol	Vertically polarized beam
WVC	Wind Vector Cell

2. DATA AND METHODS

2.1 QuikSCAT data

For the study of marine wind climatology in the relatively small basin as the Gulf of Riga, it was necessary to use the high-resolution winds with the longest period of measurements. For this purpose 12.5-km gridded ocean wind vectors were obtained from the Physical Oceanography Distributed Active Archive Centre (PO.DAAC) (<http://podaac-ftp.jpl.nasa.gov/OceanWinds/quikscat/L2B12>). Before the analysis, it was necessary to convert data from Hierarchical Data Format (HDF) to ASCII (by Fortran program provided with PO.DAAC dataset). Changes in the wind direction were also necessary due to non-conventional wind direction detection of the QuikSCAT winds. For example, in the QuikSCAT data the wind direction of 0° means the northward wind instead of meteorological northerly direction.

At the first step of the wind data analysis, the wind vectors were selected geographically (57°N – 58.5°N , 22.5°E – 24.5°E). The period of acquired data is 1999–2009, however, the year 2003 was eliminated due to the large amount of missing values. In addition, the year 1999 started on the 1st of August and the year 2009 lasted till the end of October. The measurements in the Gulf of Riga were from two time intervals: 02–04 UTC and 16–18 UTC. Then, scatterometer data were filtered out by quality flags at each WVC.

The winds used for this study are with a good σ^0 values for wind retrieval (Lungu and Callahan, 2006), without presence of ice, but in some cases with the land contamination. Although the Coastal Flag presence means that some portion of the WVC is over the land and it may indicate noisy wind measurements, elimination of this data significantly reduces the number of data points in the small area near the coastline. The difference when using high-resolution (12.5 km) data is that the slice data may not fall on land while another fraction or part of the cell data may fall on land. Thus, the high-resolution data have a lesser impact due to land effects and can be used to obtain winds closer to land (Nghiem *et al.*, 2004).

Next, the data with Low Wind Speed Flag (less than 3 m s^{-1}) and High Wind Speed Flag (greater than 30 m s^{-1}) were eliminated due to some factors influencing the quality of data mentioned before. As to the rain contamination, two methods were used: 1) conservative elimination of all rain-contaminated data detected by IMUDH algorithm and 2) more lenient filtering of rain-contaminated data. For filtering the wind data by the strict criteria, the IMUDH algorithm was used that can provide a reasonably accurate estimate of the probability of the rain and the rain probability is detected. For more lenient rain filtering special thresholds were used: MUDH less than 0.2 and NOF index less than 50 as done by Kleiss *et al.* (2010). A more lenient method was used to increase the number of data points, especially for the northern part in the Gulf of Riga. The coverage of QuikSCAT measurements for all period with strict criteria are shown in Figure 2.1(a) and with

more lenient criteria in Figure 2.1(b). The total number of data points in the Gulf of Riga with more lenient criteria is shown in Paper I, Table 1.

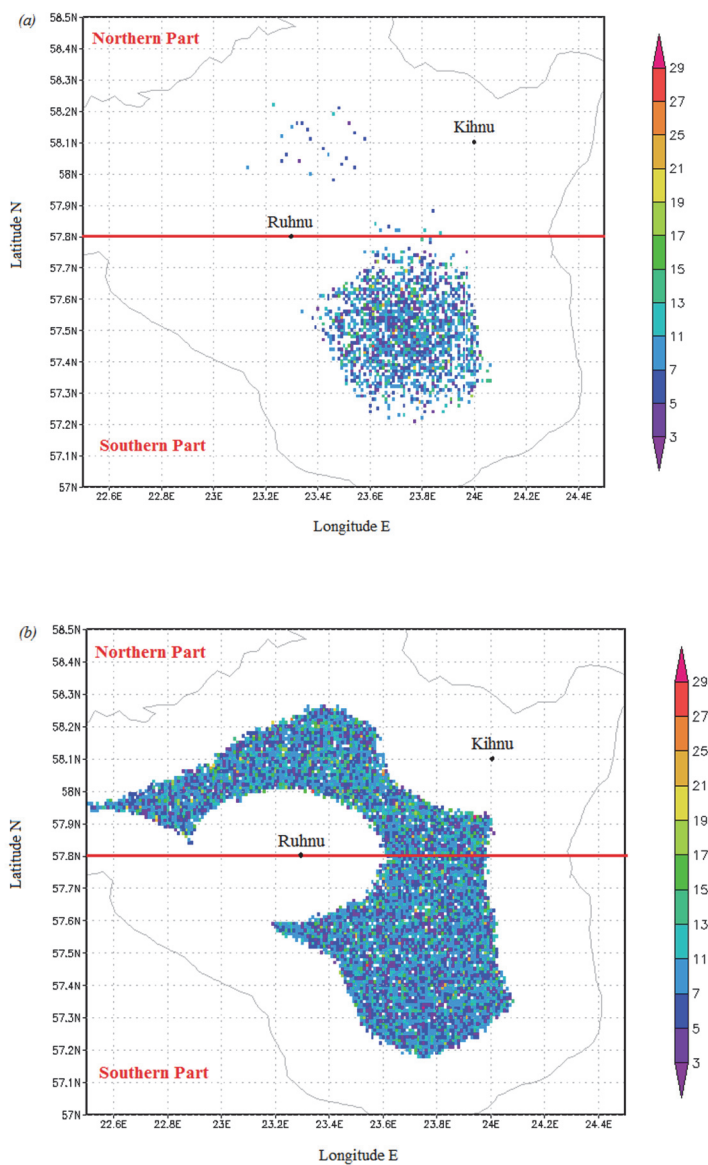


Figure 2.1. The coverage of QuikSCAT measurements for January 1999–2009 with strict criteria (a) and more lenient criteria (b).

2.2 ASCAT data

In the first study, which is focused on the comparison of the ASCAT measurements with the HIRLAM forecasts, the EARS ASCAT 12.5-km gridded wind speed and wind direction from MetOp-A were obtained during the two-month period of 01.10 – 03.12.2009. The ASCAT measurements were collected from the Baltic Sea region ($55^{\circ}\text{N} - 62.3^{\circ}\text{N}$, $14.5^{\circ}\text{E} - 27.8^{\circ}\text{E}$). The measurements in this area were made only 1–3 times per day and in the time interval about 17–20 UTC. For the comparison of the ASCAT and HIRLAM winds, the time of the ASCAT data measurements had to be collocated with time of the HIRLAM wind forecasts. If the ASCAT measurements, performed in the selected area were available more than once per day, the ASCAT data were chosen with the minimal time difference between NWP model and the ASCAT winds (less than one hour). The ASCAT Level 2 data were received via the EUMETCast service in BUFR format, decoded and then converted into the ASCII format by the software developed at KNMI.

In the second study, which is aimed to assess the impact of the ASCAT data assimilation into the HIRLAM, the ASCAT measurements in cases of severe storms of 2013 were chosen. Unlike the first study, here both the ASCAT-A and ASCAT-B 25-km gridded Level 2 data were used for assimilation into the HIRLAM. As the coverage of the EARS ASCAT data in the HIRLAM assimilation window is not uniform during the day, it was decided to study the HIRLAM analyses at 12 UTC and 18 UTC. In selected analyses the HIRLAM domain is more densely filled with the ASCAT data (Fig. 2.2). In recalculations of the HIRLAM analyses, the ASCAT measurements from previous day before each case of severe storm were used to avoid the “cold start” in the analysis.

The ASCAT Level 2 data, used in both studies, include the information on the backscatter measurements, selected wind solution from calculated ambiguous (up to four) wind solutions, scanning geometry, and the WVC quality flag in case of poor data quality (too large inversion residual, or too high noise value in the input product such as sea-ice or land contamination) among others. The procedure and improvements of the QC performed at KNMI are described in more detail by Portabella *et al.* (2012).

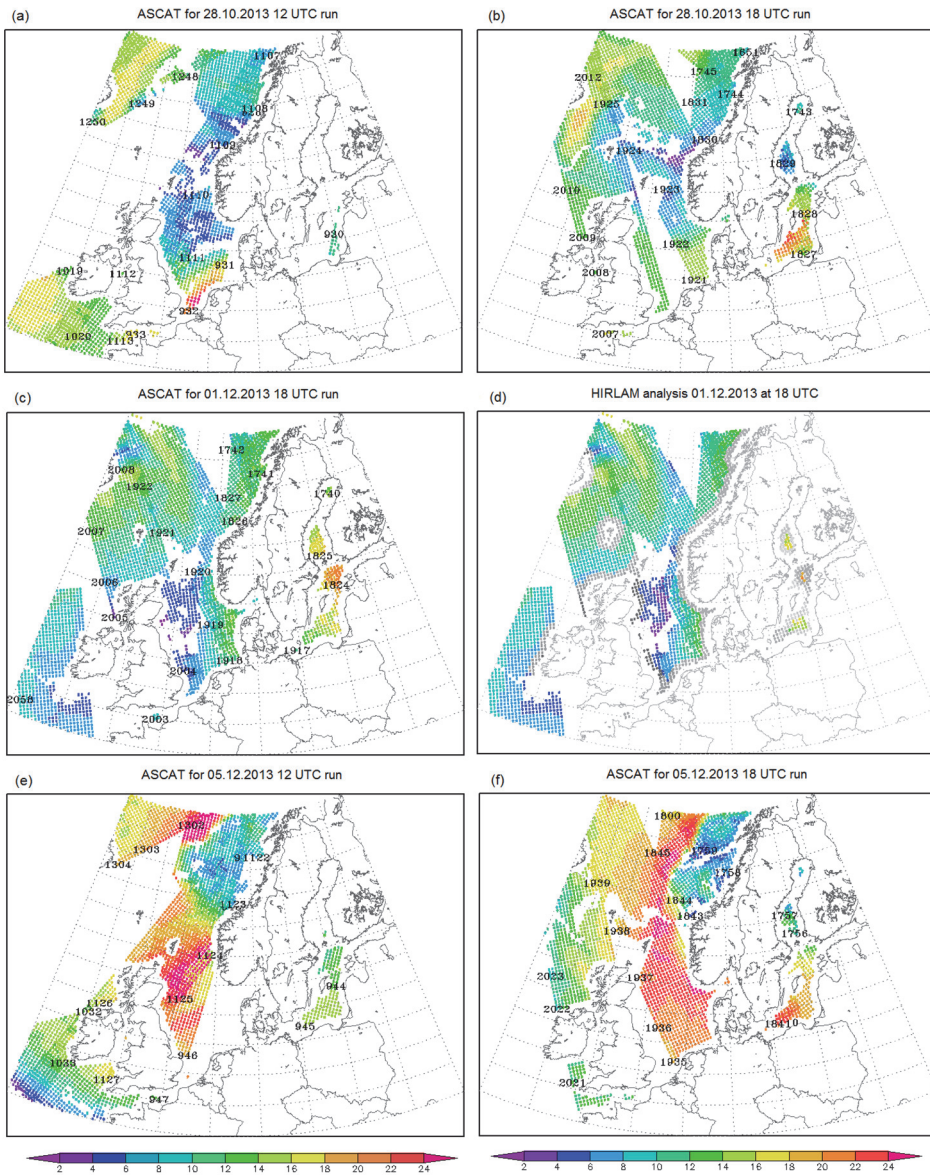


Figure 2.2. Coverage of the EARS ASCAT overpasses in HIRLAM assimilation windows at 12 UTC and 18 UTC 28.10.2013 (a,b), 01.12.2013 (c,d), 05.12.2013 (e,f). The ASCAT winds in the HIRLAM analysis (after data assimilation) 01.12.2013 at 18 UTC (d): grey dots represent the ASCAT measurements rejected after quality control, probably due to proximity to the land. Three and/or four digit numbers show the ASCAT overpass time in UTC.

2.3 Severe storms cases

Three different cases of severe storms in 2013 are selected to study the impact of the ASCAT measurements on the HIRLAM analysis output with the emphasis of the impact on the storm initialization accuracy. The storm cases are chosen to contain the highest possible density of the ASCAT stormy wind measurements (over 15 m s^{-1}) in the marine areas of the HIRLAM modelling domain (Fig. 2.2), where the impact of the ASCAT data is expected to be visible.

The first study case is the strong storm on October 28, 2013 named in Germany “Christian”, in Denmark “Allan”, and in UK “St Jude” that moved across northern Europe and caused massive damages and interruptions. The impact of the storm was considerable. At least 15 people perished, a large number of trees were blown down, power supply broke down, train connections were interrupted, streets were impassable, and the Øresund Bridge between Denmark and Sweden had to be closed (Storch *et al.*, 2014). In Germany, peak wind speeds ranking 11 ($28.5\text{--}32.6 \text{ m s}^{-1}$) and 12 ($\geq 32.7 \text{ m s}^{-1}$) on the Beaufort scale (Bft) were observed at many stations along the coasts of the North and the Baltic Sea as well as further inland, with a maximum of 47.7 m s^{-1} at St Peter Ording, a location facing the North Sea (Storch *et al.*, 2014).

The second stormy wind situation on December 1, 2013 observed in the current study was not as dramatic as the event in October, but the storm took place in the Baltic Sea region and it was possible to analyse the impact of the ASCAT winds for the closed marine area near the Baltic countries.

The third interesting case is the severe storm Xaver on December 5, 2013, where the ASCAT measured widely the winds over 20 m s^{-1} indicating high power of the storm. The storm moved across northern Europe and caused severe winds with gusts of hurricane force across northern Germany and at higher sites. Shipping and rail traffic was shut down in several places and flights were cancelled. In addition, dangerous street conditions and road accidents affected by the storm Xaver were reported in other European countries. More than 10 people died Europe-wide due to the storm (Deutschländer *et al.*, 2013).

2.4 Surface-based measurements

For the comparison of the SeaWinds scatterometer winds with surface-based measurements two wind observational stations located in marine area of the Gulf of Riga were used during the same period as the QuikSCAT measurements. Observational stations are located on the islands Kihnu ($58^{\circ} 06' \text{ N}$, $23^{\circ} 58' \text{ E}$) and Ruhnu ($57^{\circ} 47' \text{ N}$, $23^{\circ} 15' \text{ E}$) as it is shown in Figure 2.1. The winds are reported every 3 hours at 00, 03, 06, 09, 12, 15, 18 and 21 UTC. The wind speed is 10-minute average value before the observation time and the wind direction is a 2-

minute average accordingly. Data were drawn from the archives of Estonian Weather Service.

In the impact study of the ASCAT data assimilation into the HIRLAM analyses, the availability of the surface-based measurements was very important. As the most significant impact of scatterometer observations on NWP forecasts is expected over sea and near coastal regions, close to where the observations are made (De Valk, 2013), two types of surface-based measurements located in the HIRLAM domain were used. Independent Marine Observation (denoted here as IMO) from moored buoys, lighthouses, lightships, oil platforms and from some marine stations, which are not used in data assimilation cycle, and Assimilated Marine Observations (denoted here as AMO), which belong also to conventional data located mainly on islands or near the shoreline. The historical IMO data from UK Met Office buoys, lightships and Private Industry Oil Platforms were obtained manually from webpage <http://www.wunderground.com/MAR/ukm.html>. The measurements from Väderöarna buoy were provided by Swedish Meteorological and Hydrological Institute (SMHI), wind data from the island Vaindloo from Estonian Weather Service, marine data from some German buoys, lighthouses and lightships were obtained via Marine Environmental Monitoring Network in the North Sea and the Baltic Sea (MARNET) (http://www.bsh.de/en/Marine_data/Observations/MARNET_monitoring_network/index.jsp) and received from Federal Maritime and Hydrographic Agency of Germany (BSH). In addition, it was a good opportunity to use free access climate database <http://eklima.met.no/> for marine data from Norwegian Meteorological Institute. All surface-based measurements used in the analysis were carried out mainly at 12:00 UTC and 18:00 UTC, except measurements on the Kiel lighthouse with 09-minute delay (at 12:09 UTC, 18:09 UTC). The overview of IMO data can be seen in Paper III, Table 1.

As reported by Ingleby (2009) all selected here Private Industry Oil Platforms report the wind measurements adjusted to 10-meter height. In addition, marine winds measured in the Norwegian Sea were also adjusted to 10 meters. Marine winds measured from other heights were recalculated to 10 meters using the method described by Hsu *et al.* (1994), the formula is given in Paper III.

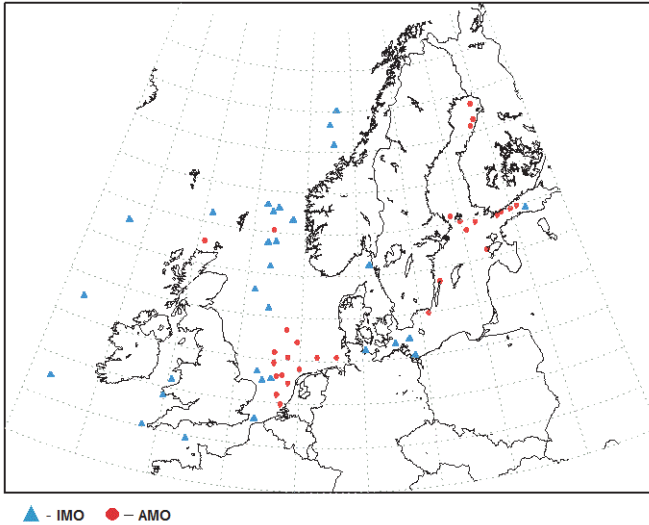


Figure 2.3. Geographical location of the marine wind observations in the HIRLAM domain. The IMO data points are marked by blue colour, AMO data points are red.

The geographical location of IMO and AMO observations is shown in Figure 2.3. The AMO measurements were carried out mainly on islands and chosen manually depending on the location from the shoreline or in case it is checked that the measurements can represent marine winds. However, the effects of slowing down the wind speed and wind turning caused by land friction should be taken into account.

2.5 HIRLAM and data assimilation

The HIRLAM is a hydrostatic grid-point model which dynamics is based on a semi-implicit semi-Lagrangian discretization using hybrid vertical coordinates. The model equations and their numerical aspects are described in more detail by Undén *et al.* (2002). HIRLAM gained operational status in Estonian Weather Service in 2007. At present, the Estonian Weather Service uses the HIRLAM 7.4 version. The HIRLAM model in Estonia has two domains: operational ETA with the horizontal resolution of 11.1 km and the experimental ETB with the grid of 3.3 km. Figure 2.4 illustrates the Estonian HIRLAM modelling areas and their geographical location.

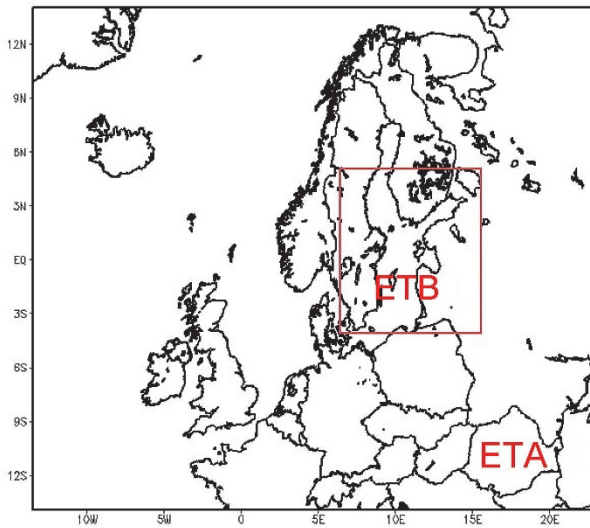


Figure 2.4. HIRLAM ETA and ETB modelling areas. The geographical coordinates are the latitudes and longitudes in the Earth's system with rotated poles as defined in HIRLAM.

The boundary fields for the HIRLAM operational model are provided by ECMWF model. The 54-hour forecasts of the HIRLAM are calculated four times a day with forecast starting-points at 00, 06, 12 and 18 UTC. For the ETB domain the 36-hour forecasts are calculated twice a day with starting-points at 00 and 12 UTC. To maintain the analysis cycle, 6-hour forecasts at 06 and 18 UTC are calculated for ETB as well. Besides its usual application as the weather prediction model, HIRLAM acts as the driving model for the local HIROMB (High Resolution Operational Model for the Baltic) marine modelling system, which is currently used for storm surge warnings (Služenikina and Männik, 2011).

The current data assimilation system in the HIRLAM is 3DVAR (three-dimensional variational data assimilation), the assimilation window is 06 hours, -03 hours from the analysis time and +03 hours ahead. There are some conventional observations generally assimilated into the local HIRLAM. The surface observations include the observations from synoptic stations (SYNOP), ships (SHIP) and from drifting buoys (DRIBU). The upper air observations include the measurements from radiosoundings (TEMP), aircraft reports (AIREP) and from pilot-balloon stations (PILOT). The overview of meteorological parameters assimilated into the HIRLAM can be seen from Table 2.1.

Table 2.1. Conventional observations assimilated into the HIRLAM 3DVAR system, where z is geopotential height, u is zonal wind component, v is meridional wind component, T is temperature and q is specific humidity.

	Observation type	Parameters assimilated
Surface	SYNOP	z
	SHIP	z
	DRIBU	z
Upper air	TEMP	u, v, T, q
	AIREP	u, v, T
	PILOT	u, v

The First Guess at Appropriate Time (FGAT) is applied for both conventional and the ASCAT data assimilation in operational HIRLAM. Traditionally, 3DVAR uses only a short-range forecast valid at the analysis time to compute the innovations (observations minus background), however, in the FGAT option all short-range forecasts are taken into account in the assimilation time window, and for each observation the closest forecast is selected (Huang *et al.*, 2002). This option helps to approximate the model analysis time with observational data sampled at asynoptic time and improve the accuracy of initial conditions in the model. However, in the HIRLAM 3DVAR such scheme is not used for *in situ* observation such as SYNOP, TEMP and PILOT data to avoid data redundancy associated with assumption about static observation increment (HIRLAM System Documentation www.hirlam.org).

2.5.1 ASCAT data assimilation into the HIRLAM

The algorithm of the ASCAT data assimilation is written by De Valk (2013) and De Vries and is optional for calculations in HIRLAM version 7.4. The principle of SeaWinds data assimilation is applied for the ASCAT. As the ASCAT and SeaWinds have different data structures, the reading routines had to be adapted. Once the WVC information is ingested, the consecutive steps for ASCAT and SeaWinds data assimilation are similar (De Valk, 2013). More detailed description of the SeaWinds 3DVAR assimilation algorithm is given by Tveter (2006).

The coverage of the EARS ASCAT Level 2 data used in the HIRLAM assimilation window is not uniform during the day. The overpasses are quite sparse for HIRLAM 00 UTC and 06 UTC analysis while for HIRLAM analysis at

12 UTC and 18 UTC the ASCAT measurements are more densely filled with the ASCAT data.

The spatial and temporal screening procedure of the ASCAT observations is performed before admission of the ASCAT data into the HIRLAM analysis: location of each WVC is compared with the HIRLAM domain and the ASCAT observational time should fit into the time window of a given assimilation cycle. Then, the WVC quality flag from the ASCAT wind product is used to ensure the high quality of the backscatter measurements and successful inversion. The ASCAT data that are flagged as land or sea ice contaminated, as well as the data with the wind speeds exceeding 30 m s^{-1} are rejected during the quality control. In addition, the HIRLAM checks the number of ambiguities calculated for each WVC and takes the wind solutions only from the WVCs where up to two ambiguities exist. As the ASCAT wind information consists of wind ambiguities, no first-guess check is carried out and, in the analysis, variational quality control is not active for ASCAT (De Valk, 2013). The wind vector ambiguous solutions at each WVC is compared with the HIRLAM background winds, and the closest solution is finally selected, other wind solutions are rejected in HIRLAM analysis.

2.6 HIRLAM winds

In the first study the ASCAT measurements were compared with the respective numerical predictions of the operational HIRLAM during the stormy season in 2009. Two different resolutions of the NWP model were compared to see whether the resolution increase can play a significant role in forecasting over the enclosed Baltic Sea. The forecasts of the HIRLAM version 7.1.2 were obtained from the archive of operational runs at Estonian Weather Service for the same time period. In this study 06-hour, 18-hour and 30-hour forecasts of both ETA and ETB domain (Fig. 2.4) for geographical area ($55^{\circ}\text{N} - 62.3^{\circ}\text{N}$, $14.5^{\circ}\text{E} - 27.8^{\circ}\text{E}$) were used. HIRLAM wind components at 10-m height were interpolated into the ASCAT points of measurements using the bilinear interpolation method. The bias, RMS deviation and correlation coefficient were calculated between the ASCAT and HIRLAM models for two wind speed intervals $0-22 \text{ m s}^{-1}$ and $4-22 \text{ m s}^{-1}$. For wind verification, a speed of over 4 m s^{-1} is often used to estimate quality characteristics (Gelsthorpe *et al.*, 2000, Verspeek *et al.*, 2007, Verhoef and Stoffelen, 2009); this approach was followed here also. The upper limit of the wind speed is the maximum wind speed during the observed period. Comparison of the wind data was performed through the wind speed and direction, and the wind velocity components, where u is the zonal and v is the meridional wind component. All statistical characteristics were computed on homogenized dataset.

In the impact study of the ASCAT data assimilation into the HIRLAM analyses two different observing system experiments (OSE) were carried out: with

ASCAT data assimilated into HIRLAM (named “ASCEXP”) and without ASCAT data assimilation (named “REFEXP”). The OSEs were performed in selected HIRLAM analyses where the HIRLAM domain was more densely covered by the ASCAT measurements:

- 28.10.2013 at 12 UTC, 18 UTC
- 01.12.2013 at 18 UTC
- 05.12.2013 at 12 UTC, 18 UTC

The experiments were recalculated for chosen cases in the past using the backgrounds from operational HIRLAM archive. For each case the calculations were started with the backgrounds one day before the cases at 06 UTC to avoid “cold start” of the model. In the current study surface-based measurements in marine areas were compared with OSEs analyses results (O–A) to investigate, first of all, the impact of the ASCAT wind data assimilation into the model in case of stormy wind situation. The bias, root mean square error (RMSE) and correlation coefficients were calculated for wind data and mean sea level pressure (MSLP). In addition, the differences between the ASCAT winds as observation and HIRLAM background winds (O–B) were calculated for each case, which helped to detect the areas with the highest deviations before data assimilation.

3. MARINE WINDS IN THE GULF OF RIGA FROM QUIKSCAT AND GROUND BASED MEASUREMENTS

3.1 SeaWinds – analysis with strict criteria

The analysis of the wind field is focused on seasonal histograms of wind speed and direction for the two time intervals 02–04 UTC and 16–18 UTC. While interpreting the data, one must keep in mind that wind speeds $<3 \text{ m s}^{-1}$ are not considered. The results show that the wind is the strongest in winter and autumn, when prevailing wind speed V is $6 < V \leq 9 \text{ m s}^{-1}$ (Fig. 3.1(a), 3.1(b)). In spring and summer the most frequent wind speed is $3 \leq V \leq 6 \text{ m s}^{-1}$, more than 50% of cases, while in the evening the frequency of those winds is somewhat higher.

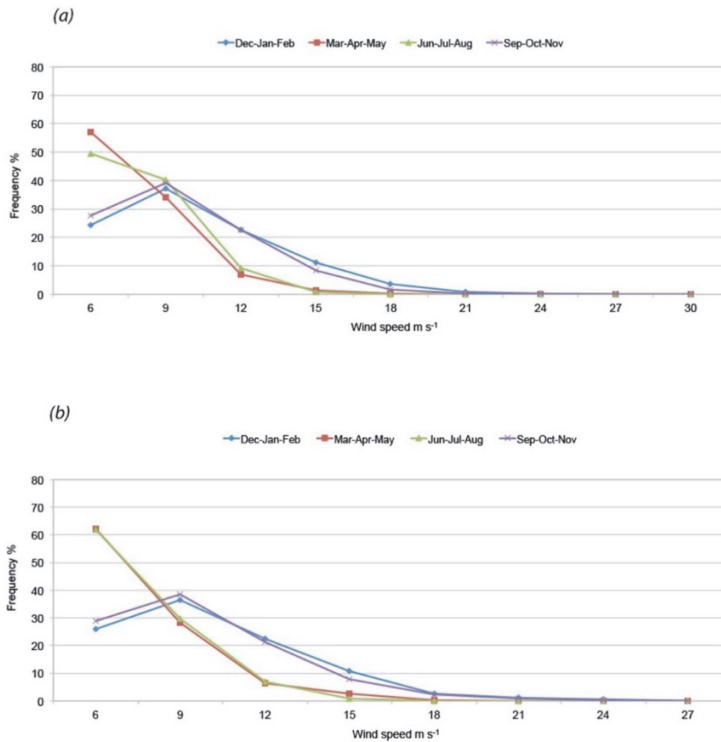


Figure 3.1. SeaWinds wind speed seasonal histogram at 02–04 UTC (a) and 16–18 UTC (b).

Some differences were observed in comparing the wind direction for different seasons at different measurement time (Fig. 3.2(a) and Fig. 3.2(b)). In winter and autumn the most frequent wind direction is S or SW with minor differences between morning and evening recordings: At 02–04 UTC SW winds prevail and at 16–18 UTC – S winds dominate. In spring the prevalence of SW and W winds is only weakly expressed in the morning wind rose, but the evening wind rose is highly anisotropic showing 27% of NW winds and 17% of N winds while S winds are very seldom. The same feature can be noticed in summer with the exception that morning wind rose shows sharp maximum (25%) in the frequency of SW winds.

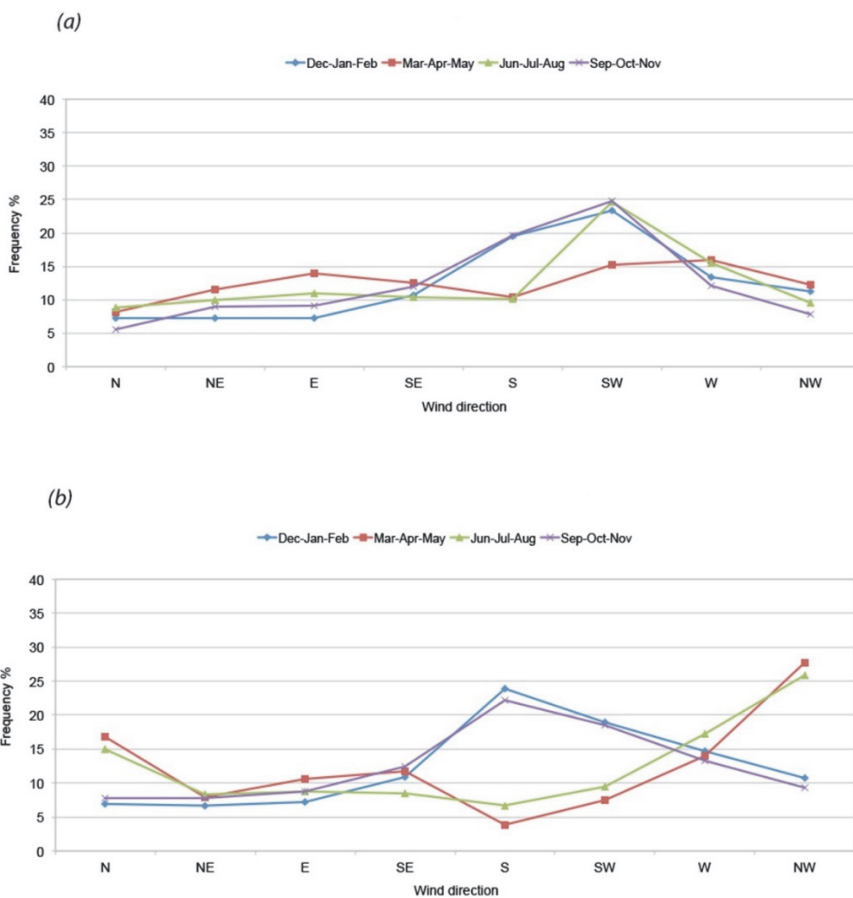


Figure 3.2. SeaWinds wind direction seasonal histogram (wind rose) at 02–04 UTC (a) and 16–18 UTC (b).

3.2 SeaWinds – analysis with more lenient criteria

For a more detailed analysis of the wind speed distribution and the wind direction differences in the Gulf of Riga, the area of interest was divided into northern part (57.8° N–58.5° N) and southern part (57° N–57.8° N) as it is shown in Figure 2.1. Comparing the wind speed distribution in these areas with the wind speed chosen on the basis of strict criteria, no significant difference was found. The average wind for both areas is somewhat stronger than without presence of rain (Paper I, Tables 2–3), however, the maximum difference between the values is not more than 0.9 m s⁻¹. This difference may be attributed to more lenient filtering of rain-contaminated data. The winds in the northern part are slightly stronger than in the southern part.

The wind direction frequency distributions in the southern part of the gulf got by means of the lenient criteria (Paper I, Fig. 5(b)) are similar to those for the whole gulf got by means of the strict criteria (Fig. 3.2). This is understandable as the data for the analysis with strict criteria come mostly from the southern part (Fig. 2.1(a)). The same can be said for the northern part in early morning, but the evening frequency distributions are somewhat different: in winter and autumn the differences are not noticeable, but in spring and summer the most frequent winds are in the northern part W and in the southern part NW (Paper I, Fig. 5(a) and Fig. 5(b) and Fig. 3.2(b)).

3.3 Wind measurements on the islands and correlation with satellite data

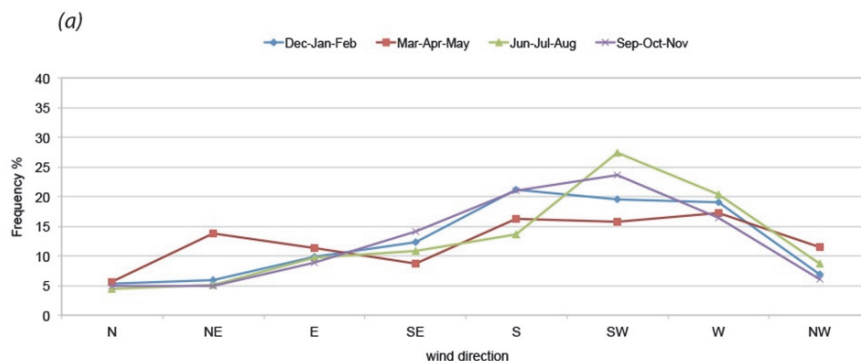
As presented in the paper by Keevallik *et al.* (2009), Kihnu observational station is sheltered from the north and northeast directions and only partly open from the east, southeast and northwest directions, on Ruhnu the winds are totally sheltered from the north and northwest and partly from the northeast and west direction. As a result, the average wind speed is reduced (Table 3.1).

Table 3.1. Average seasonal wind speed (winds <3 m s⁻¹ are not considered) and the wind speed standard deviation (STDEV) estimated from the satellite data (with strict criteria) and measured at the meteorological stations.

Season		Kihnu 03 UTC	Satellite 02–04 UTC	Kihnu 18 UTC	Ruhnu 18 UTC	Satellite 16–18 UTC
Winter	MEAN	7.6	8.6	7.6	7.0	8.5
	STDEV	3.1	3.4	3.2	2.9	3.5
Spring	MEAN	5.5	6.0	5.4	5.0	5.8
	STDEV	2.2	2.2	2.4	1.9	2.3
Summer	MEAN	6.0	6.3	5.8	5.3	5.8
	STDEV	2.4	2.1	2.5	2.0	2.1
Autumn	MEAN	7.3	8.1	7.5	6.8	8.1
	STDEV	2.9	3.1	3.1	2.6	3.2

The difference between satellite winds and winds at the stations is the largest during the period of the strongest winds, winter and autumn. Domination of weaker winds is more evident in the wind speed histograms (Paper I, Fig. 6(a) and Fig. 6(b)), where almost in all seasons prevailing winds are between 3–6 m s⁻¹. At the same time satellite measured 30–40% of all winds between 6.1–9 m s⁻¹ practically in all seasons with the maximum in winter and autumn (Fig. 3.1(a) and Fig. 3.1(b)). In addition, the standard deviation of wind speed (Table 3.1) shows that the higher wind speed variation appears in winter and autumn both measured at ground-based stations and satellite. The wind speed variation is about 2–3 m s⁻¹.

Comparing the results with the wind direction on Kihnu and Ruhnu, it was noticed that in the evening Kihnu and Ruhnu wind directional histograms are very similar, only some slight quantitative differences can be seen in the N and NE directions, therefore the histogram of Ruhnu is not shown in analysis. In addition, Ruhnu observations at 03 UTC were not available. The Kihnu station is situated in the northern part of the gulf, therefore the comparison with satellite is done with the same area.



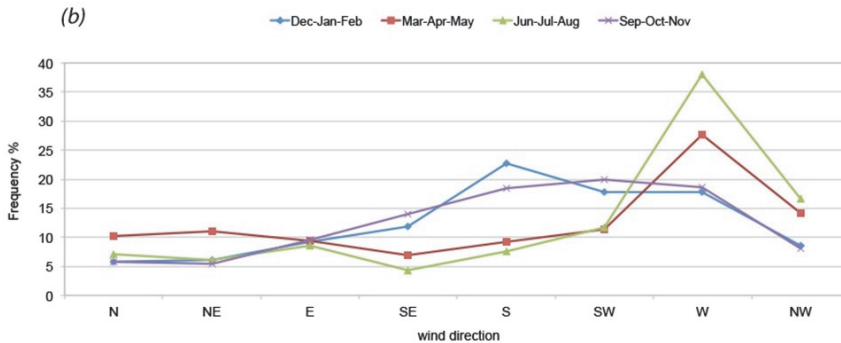


Figure 3.3. Wind direction seasonal histogram (wind rose) of Kihnu at 03 UTC (a) and 18 UTC (b).

The results show that in the morning measurements in winter at Kihnu more frequent winds are S, whereas the frequency of SW and W winds is slightly less (Fig. 3.3(a)). The QuikSCAT measured more than 20% of SW winds (Fig. 3.2(a)). In spring the morning measurements at Kihnu show equal frequency of SW, S and W winds (about 15% of each), satellite measured also SW and W winds with the same value of frequency, but S winds were less frequent. Attention should be drawn to the secondary maximum in spring that is typical to the wind roses of the Baltic Sea area. Ground measurements show this for NE winds (Fig. 3.3(a)), satellite measurements for E winds (Fig. 3.2(a)). In the evening recordings at Kihnu in summer the frequency of W wind is more than 35% (Fig. 3.3(b)), whereas satellite measures the frequency less than 30% (Fig. 3.2(b)).

To find out the correlation between ground-based and satellite measurements, the closest QuikSCAT recordings to Kihnu station were chosen. For the cases (winter and summer at 02– 04 UTC) shown in Paper I, Figure 8 and Figure 9, the correlation coefficient for wind direction was 0.94 in summer and 0.95 in winter. At the calculation of the correlation coefficients it was kept in mind that the difference between the measurements did not exceed 180°. The correlation coefficient for wind speed was somewhat less – around 0.6.

Table 3.2. The bias and the root mean square deviation (RMSD) between the satellite and ground-based measurements.

SEASON		Satellite 02–04 UTC, Kihnu 03 UTC		Satellite 16–18 UTC, Kihnu 18 UTC	
		SPEED, m s ⁻¹	DIR, degrees	SPEED, m s ⁻¹	DIR, degrees
Winter	BIAS	1.6	3.5	1.6	2.9
	RMSD	3.2	25.0	3.1	25.9
Summer	BIAS	0.9	-2.3	0.4	8.5
	RMSD	2.1	29.2	2.6	36.7

As can be seen in Table 3.2, the bias of the wind speed (average satellite record minus ground-based record) is positive, larger in winter and smaller in summer. A positive bias in wind speed can be explained by the reported site obstructions that clearly affect the ground-based measurements but not the satellite measurements. The bias of the wind direction is negligible, but the RMSD estimates exceed the root mean square error foreseen by the scatterometer design. It must be taken into account that the coordinates of the measurement sites are not exactly the same and it cannot be expected that the measurements are carried out at the same moment.

4. MARINE WINDS IN THE BALTIC SEA REGION FROM THE ASCAT AND HIRLAM FORECASTS

4.1 Statistical comparison of the HIRLAM and ASCAT

Over the evaluation period the ASCAT winds in general showed remarkably good coincidence with those predicted by the HIRLAM. Some quality characteristics are computed for all forecast periods for both the ETA and the ETB models and are summarized in Table 4.1 and Table 4.2. Statistical output shows that the quality characteristics are worse when all wind speeds are taken into account (compared to the range 4–22 m s⁻¹), which can be explained by the fact that, according to Stoffelen (1998), in the presence of weak winds, wind speed error distributions are skewed at low winds with slightly increased variance differences. The differences are related mostly to effects of atmospheric wind variability and differences in spatial representation, which are well expressed as constant errors in the wind components. As far as the wind speed is concerned, the bias (HIRLAM forecasts minus ASCAT measurements) of both the ETA and ETB models in the 4–22 m s⁻¹ range is almost non-existent, whereas a weak, negative bias growth may be noted with increasing forecast length. In the case of wind direction, the bias is appreciable, and a weak anticlockwise turning with growing forecast length may be observed.

The RMS difference of the wind speed was mostly less than 2 m s⁻¹ in all forecasts and wind speed intervals. The results in Table 4.2 show that the bias of the wind component is quite small and in some cases even decreases to 0 m s⁻¹. However, the RMS difference gradually increases with the forecasting length.

Table 4.1. ASCAT and HIRLAM models: statistical characteristics (bias, RMS difference, correlation coefficient) of wind speed and direction.

HIRLAM ETA		06-hour forecast			18-hour forecast			30-hour forecast		
		Bias	RMS	Corr	Bias	RMS	Corr	Bias	RMS	Corr
0-22 m/s	Wind speed	0.12	1.30	0.94	0.14	1.46	0.92	-0.10	2.05	0.85
	Wind direction	5.34	24.89	0.75	4.53	27.13	0.76	2.14	33.23	0.72
4-22 m/s	Wind speed	0.03	1.28	0.93	0.01	1.39	0.91	-0.31	1.97	0.84
	Wind direction	3.46	16.19	0.82	2.45	18.60	0.82	1.40	27.52	0.75
HIRLAM ETB		06-hour forecast			18-hour forecast			30-hour forecast		
		Bias	RMS	Corr	Bias	RMS	Corr	Bias	RMS	Corr
0-22 m/s	Wind speed	0.12	1.38	0.94	0.12	1.51	0.92	-0.07	2.08	0.85
	Wind direction	5.13	25.36	0.73	4.90	28.43	0.72	2.80	32.76	0.71
4-22 m/s	Wind speed	0.03	1.35	0.93	-0.01	1.46	0.91	-0.28	2.03	0.83
	Wind direction	3.26	16.31	0.80	3.10	19.72	0.78	1.79	26.68	0.75

Table 4.2. ASCAT and HIRLAM models: statistical characteristics (bias, RMS difference, correlation coefficient) of wind components.

HIRLAM ETA		06-hour forecast			18-hour forecast			30-hour forecast		
		Bias	RMS	Corr	Bias	RMS	Corr	Bias	RMS	Corr
0-22 m/s	<i>u</i>	0.16	1.61	0.96	0.04	1.80	0.94	-0.01	2.22	0.92
	<i>v</i>	0.34	1.58	0.98	0.15	1.77	0.97	-0.09	2.72	0.92
4-22 m/s	<i>u</i>	0.17	1.59	0.96	0.00	1.77	0.95	0.01	2.16	0.93
	<i>v</i>	0.29	1.52	0.98	0.13	1.72	0.97	-0.15	2.78	0.93
HIRLAM ETB		06-hour forecast			18-hour forecast			30-hour forecast		
		Bias	RMS	Corr	Bias	RMS	Corr	Bias	RMS	Corr
0-22 m/s	<i>u</i>	0.20	1.69	0.95	0.03	1.89	0.94	-0.01	2.24	0.92
	<i>v</i>	0.28	1.66	0.97	0.15	1.84	0.96	-0.08	2.77	0.92
4-22 m/s	<i>u</i>	0.20	1.68	0.96	0.00	1.90	0.94	-0.01	2.20	0.93
	<i>v</i>	0.23	1.61	0.98	0.12	1.82	0.97	-0.12	2.84	0.93

Comparison of the results in Tables 4.1 and 4.2 shows high correlation between the ASCAT and HIRLAM wind components (> 0.90 for all the forecasts), whereas the correlation coefficients of the wind speed and wind direction are much lower. According to Stoffelen (1998), the wind component errors are better described than those of wind speed or wind direction. The wind component errors have the symmetrical distribution for the scatterometer and model forecast, and as mentioned before, the random errors of wind direction clearly depend on wind speed.

If we compare the models, ETA seems to perform slightly better than the high-resolution ETB model, whereas the expectation was that the high-resolution model would perform better. An explanation of that fact could be that more small scales are represented in ETB than in ETA, these scales do not appear to tally with the scatterometer winds. The reason for this might be that the forcing of these scales in the HIRLAM model is weak and the phases of these small-scales are not well determined. In such a case, the added small-scale variance will not reduce the variance of the differences, but will tend to cause the difference variances to increase. To determine small scales, they need to be either observed or generated by downscale cascading and parameterizations. Other possible explanations may be that the HIRLAM parameterization schemes are fine-tuned to 15 km resolution and therefore do not work so well at high resolution, or that the proximity of the boundary conditions introduces distortions in small domains.

4.2 A case with phase error in cyclonic activity

Another application of the ASCAT measurements is the correction of the NWP model output in operational weather forecasting.

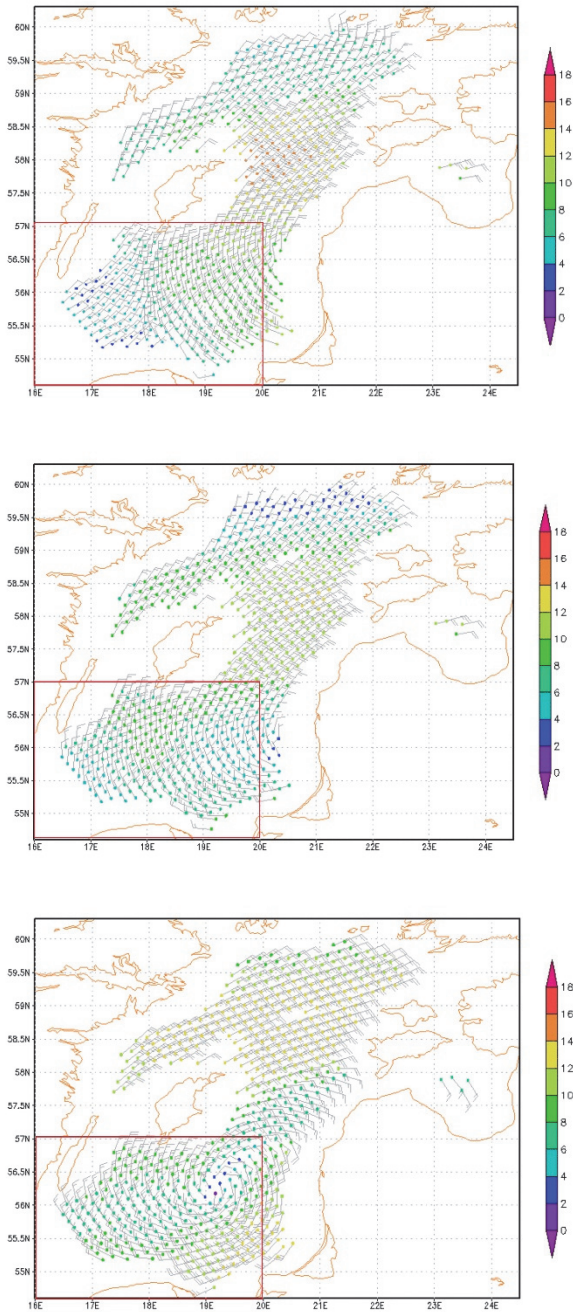


Figure 4.1. The winds of the ASCAT – 02.12.2009 at 18:09 UTC (a), HIRLAM ETA model – 02.12.2009 at 12 UTC 06-hour forecast (b), HIRLAM ETA model – 01.12.2009 at 12 UTC 30-hour forecast (c).

The difference between the ASCAT and HIRLAM 06-hour forecast is not significant: only a few differences in the wind direction can be noticed in the southern Baltic Sea at 18°E (Fig. 4.1). However, the comparison with the HIRLAM ETA 30-hour forecast shows that there is a significant difference in the wind directions. On the southern part of the region, the HIRLAM ETA generates cyclonic winds, which do not fit with the ASCAT winds. The results of the same forecasts from ETB model data show practically the same difference. This is a clear signal that HIRLAM predicted a cyclonic development with a phase shift in the forecast with start time 12 UTC 01.12.2009 and corrected it later. The situation can be used to study the reasons for such phase shifts over the open sea and find the solutions to correct them.

4.3 Discussion

The uncertainty ranges in both HIRLAM domain forecasts fit well with the expected quality characteristics of the ASCAT 25-km product in the wind speed range 4–24 m s⁻¹ defined by Gelsthorpe *et al.* (2000). These criteria are met in both domains up to the 18-hour forecast lengths. In the case of the 30-hour forecasts the uncertainty ranges are slightly exceeded, more noticeably in wind direction.

According to Figa-Saldaña *et al.* (2002), the accuracy target for ASCAT winds generated by the OSI SAF is 2 m s⁻¹ RMSD for wind component and 0.5 m s⁻¹ bias for all speeds below 25 m s⁻¹. The wind components of the HIRLAM and ASCAT presented in Table 4.2 show that the wind component statistics fit the required accuracy thresholds well. The RMSD of wind components higher than 2 m s⁻¹ is present only in the 30-hour forecasts. The bias of the components is lower than that required in all HIRLAM forecasts.

The comparison of the ASCAT 25-km winds and ECMWF analysis in northern oceanic areas (30°N–60°N) by Bentamy *et al.* (2008) determined the bias of -0.03 m s⁻¹ and the standard deviation of 1.77 m s⁻¹ for wind speed, and the bias of 2 degrees and the standard deviation of 20 degrees for wind direction. The validation of the global ASCAT 25-km winds with the ECMWF background winds by Verspeek *et al.* (2007) reported the standard deviation for wind speed 1.26 m s⁻¹ and for wind direction about 15 degrees. The *u* wind component standard deviation of the ASCAT-ECMWF winds is 1.45 m s⁻¹; the corresponding *v* component is 1.63 m s⁻¹. In line with these results, Hersbach and Janssen (2010) reported the ASCAT vector RMS difference with the ECMWF winds about 2.2 m s⁻¹ in the Baltic. Concerning these reports, the HIRLAM forecasts show similar or slightly over these ranges.

Slightly worse results may indicate that the HIRLAM model may contain smaller scales than ECMWF that are not well resolved by the physical parameterizations and the observing systems. Generally, 100-km scales evolve fast and need to be sampled densely in both time and space. To reduce the uncertainty in HIRLAM wind predictions, more observations over the Baltic may be necessary.

The results of the higher resolution ETB model tend to be slightly worse than those of the operational suite; we may speculate that they are the result of the poor determination of 50-km scales over the Baltic, due to the relatively weak forcing and the lack of observations, or perhaps they are due to the proximity of the boundary zone, which introduces dynamic distortions in too small domain, or it may be the effect of physical parameterizations not being tuned to such a high resolution.

Nevertheless, the results from comparison of ASCAT and HIRLAM winds are generally in line with results from other similar studies, which confirms that the ASCAT 10-m winds are reliable data source over the Baltic Sea, which is of great importance for marine and NWP communities operating in the region. Unfortunately, sea buoy or ship measurements in the Baltic Sea region were not available for the study.

5. IMPACT OF THE ASCAT WINDS ON THE HIRLAM ANALYSIS QUALITY IN CASE OF SEVERE STORMS

5.1 Storm Christian (St Jude, Allan) 28.10.2013

The case of storm Christian is evaluated for two assimilation cycles at 12 and 18 UTC. It is notable from Figure 2.2(a) and 2.2(b) that the highest wind speeds measured by ASCAT for 12 UTC assimilation window are across the coast of Belgium, the Netherlands and Germany (max 25.8 m s^{-1}) and for 18 UTC assimilation window in the southern part of the Baltic Sea (max 23.9 m s^{-1}).

The fields of the wind speed and the MSLP analysis at 12 UTC mainly differ in the centre of the storm Christian, as it is shown in Figures 5.1 and 5.2. The REFEXP calculated stormy winds in the larger marine area, while in the ASCEXP stormy winds are pressed together and shifted more to the east. The area with the strongest winds near the coastline of the Netherlands is more accurate in the ASCEXP (area in blue circle), however, the area of weak winds has already developed in the tail of rapidly moving storm. Verification with surface-based observations (O–A) detects wind speed underestimation in the tail of the storm (area in the red box), in some points even up to 7 m s^{-1} and 8 m s^{-1} . In Figure 5.1 it is shown that the ASCAT measurements were significantly lower than the HIRLAM background winds before assimilation and after data assimilation HIRLAM winds decreased.

What could be the reason that the ASCAT winds were lower than actual winds? Haeseler and Lefebvre (2013) analysed the storm Christian in more detail and report that with the forward speed of 1200 km in 12 hours, Christian was a rapid moving low. On 28 October at 07 UTC the centre of the storm with a pressure of 977 hPa was located over the East Midlands, UK. Inspection of the ASCAT overpasses in the same area reveals that the ASCAT measurements were made at 09:31–09:32 UTC. This fact confirms that the centre of the low has moved slightly in two hours and the ASCAT still gave accurate measurements. The problem lies in the fact that the ASCAT measured weaker winds in the tail of the moving storm in this time moment and the analysis at 12 UTC follows the ASCAT measurements made about two hours before the analysis time moment.

28.10.2013 at 12 UTC wind speed analysis

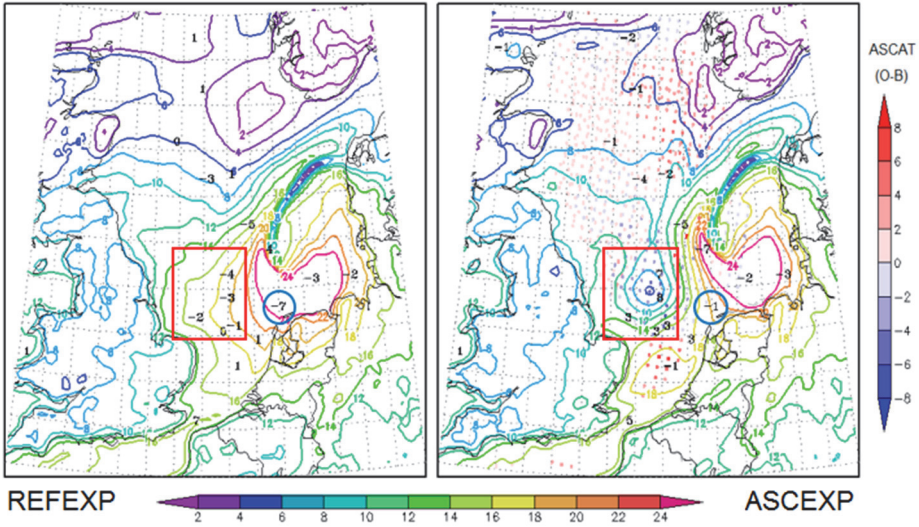


Figure 5.1. The HIRLAM 10-m wind speed analyses 28.10.2013 at 12 UTC: REFEXP (left), ASCEXP (right). The number values: surface-based observation minus analysis (O–A); colour dots: ASCAT observation minus HIRLAM background (O–B) before assimilation.

28.10.2013 at 12 UTC MSLP analysis

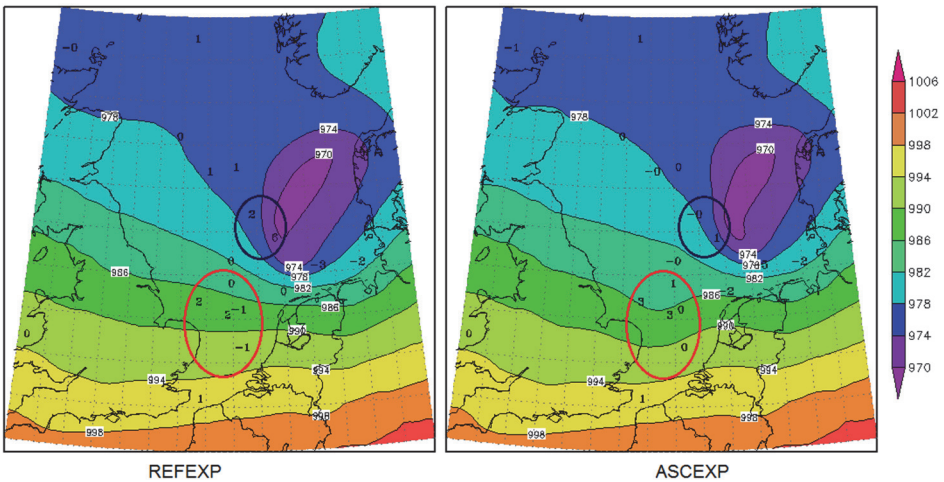
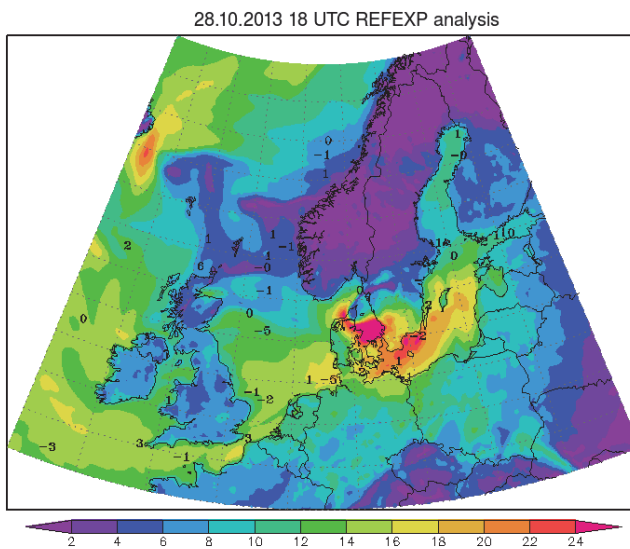


Figure 5.2. The HIRLAM MSLP analyses 28.10.2013 at 12 UTC: REFEXP (left), ASCEXP (right). The number values: surface-based observation minus analysis (O–A).

The most notable in the MSLP analysis is that the isobars between the UK and the Netherlands (Fig. 5.2) are slightly shifted to the south in the ASCEXP (area in red circle). Deepening of the low in this region probably is related to the strong winds registered by the ASCAT in this area. In spite of that fact, the field of the lowest pressure is more accurate in ASCEXP (area in blue circle), which is moved more to the east unlike the REFEXP.

The visual comparison of OSEs analyses 28.10.2013 at 18 UTC (Fig. 5.3) does not show significant differences. In the ASCEXP the area of stronger winds is extended more to the southern part of the Baltic Sea and the winds are stronger in the northern part of the Norwegian Sea. In this case we have two ASCAT overpasses across the Baltic Sea region – starting at 17:43 UTC and 18:27 UTC, both showing strong winds in the Baltic Sea region. Unfortunately, the southern part of the Baltic Sea is not covered enough with observational data and we cannot check model accuracy sufficiently.



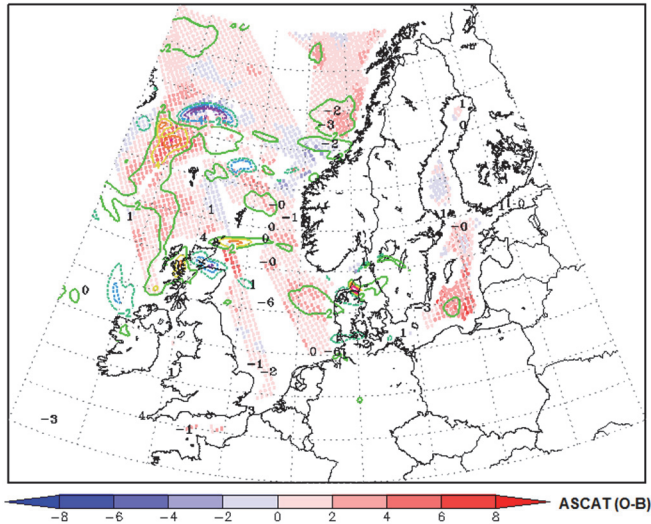


Figure 5.3. The HIRLAM 10-m wind speed analyses 28.10.2013 at 18 UTC: REFEXP (top), ASCEXP-REFEXP (bottom). The number values: surface-based observation minus analysis (O-A); colour dots: ASCAT observation minus HIRLAM background (O-B) before assimilation; colour contours (2 m s⁻¹ step) wind speed analyses difference (ASCEXP-REFEXP).

The statistics for 28.10.2013 at 12 UTC for wind speed and MSLP (Table 5.1) shows that the results of OSEs are either more or less accurate depending on the area of inspection. Statistical parameters in the wind speed analysis at 18 UTC are worse in the ASCEXP compared to IMO data. The differences with IMO data points are clearly observed near the coast of the Norwegian Sea, where the ASCEXP follows the ASCAT wind speed values registered in this assimilation window. Unfortunately, the comparison with IMO data points detects overestimation. This overestimation stems from the stronger ASCAT wind measurements in comparison with IMO (Fig. 2.2(b) and Fig. 5.3(bottom)). The model assimilates ASCAT winds and becomes “incorrect” in respect to IMO. It is difficult to assess to which observations should be given priority here.

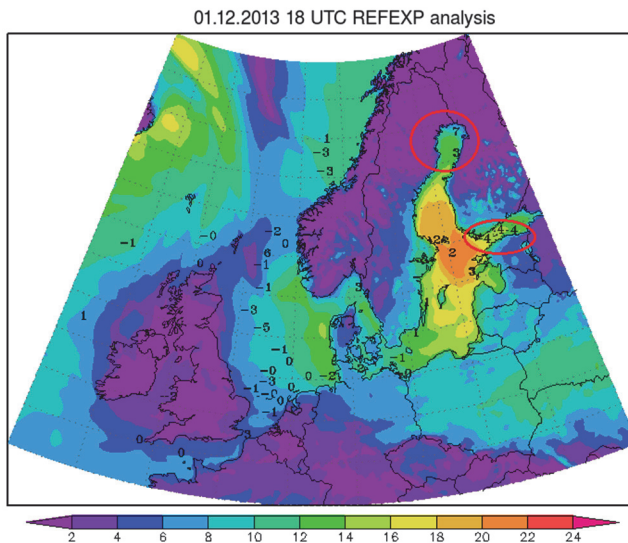
The MSLP statistics is more accurate in AMO data points in the ASCEXP analysis when all marine MSLP observations are taken into account. The visual comparison of the MSLP 28.10.2013 at 18 UTC can be seen in Paper III, Figure 6. The output in the MSLP for both OSEs is very similar, only some differences are detected in the areas, where the accuracy cannot be checked by surface-based observations.

Table 5.1. The HIRLAM REFEXP and ASCEXP bias, RMSE and correlation with observed values of the 10-m wind speed and MSLP 28.10.2013 at 12 UTC (left) and 18 UTC (right).

10-m wind speed					10-m wind speed				
20131028 12 UTC		BIAS	RMSE	CORREL	20131028 18 UTC		BIAS	RMSE	CORREL
ASCEXP	IMO	0.00	2.17	0.95	ASCEXP	IMO	-0.63	2.11	0.91
REFEXP		0.45	2.25	0.94	REFEXP		-0.08	1.68	0.94
ASCEXP	AMO	0.56	3.24	0.81	ASCEXP	AMO	0.37	2.13	0.89
REFEXP		-0.36	3.11	0.87	REFEXP		0.53	2.12	0.89
ASCEXP	ALL	0.29	2.77	0.88	ASCEXP	ALL	-0.23	2.11	0.88
REFEXP		0.03	2.73	0.90	REFEXP		0.16	1.87	0.92
MSLP					MSLP				
ASCEXP	IMO	-0.08	2.07	0.98	ASCEXP	IMO	-0.20	0.98	1.00
REFEXP		-0.28	1.57	0.99	REFEXP		-0.15	0.98	1.00
ASCEXP	AMO	-0.50	1.26	0.98	ASCEXP	AMO	-0.71	0.77	1.00
REFEXP		-0.02	1.49	0.97	REFEXP		-0.78	0.83	1.00
ASCEXP	ALL	-0.31	1.67	0.98	ASCEXP	ALL	-0.41	0.90	1.00
REFEXP		-0.13	1.52	0.98	REFEXP		-0.41	0.92	1.00

5.2 Stormy winds in the Baltic Sea 01.12.2013

In this case we omit the OSE for 01.12.2013 at 12 UTC because of relatively sparse coverage of the ASCAT data in the HIRLAM domain, with missing measurements in the Baltic Sea. Fortunately, for the 18 UTC run the ASCAT overpasses in the Baltic Sea region started at 17:40 UTC and 18:24 UTC providing a good coverage with ASCAT measurements (Fig. 2.2(c)).



01.12.2013 18 UTC analysis ASCEXP-REFEXP

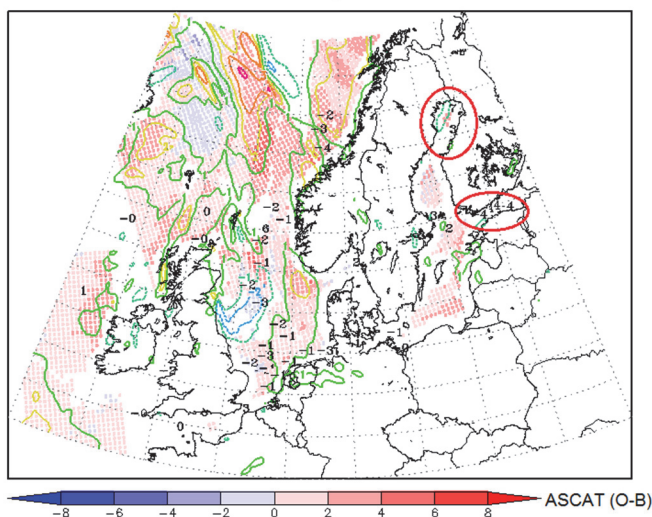


Figure 5.4. The HIRLAM 10-m wind speed analyses 01.12.2013 at 18 UTC: REFEXP (top), ASCEXP–REFEXP analysis difference (bottom). The number values: surface-based observation minus analysis (O–A); colour dots: ASCAT observation minus HIRLAM background (O–B) before assimilation; colour contours (1 m s⁻¹ step) wind speed analysis difference (ASCEXP–REFEXP).

In Figure 5.4 two HIRLAM wind speed analyses of 01.12.2013 at 18 UTC are shown. The basic OSEs differences appear in the Baltic Sea, in the North Sea and in the northwestern part of the HIRLAM domain, in all mentioned areas the ASCEXP calculate stronger winds. Unfortunately, the most distinctive analysis difference features appear in places, which are not verifiable with independent data.

In both OSEs strong underestimation of the wind is detected in the Gulf of Bothnia (7 m s⁻¹) and widely in the Gulf of Finland (4 m s⁻¹), areas in red circles. It is well known that the ASCAT wind product with the grid spacing of 25 km measures the winds about 70 km away from the coastline, the WVCs closer than ~70 km from the coast are flagged because of land contamination (Verhoef *et al.*, 2012). The ASCAT winds in these areas are not admitted, most likely due to proximity to the land (Fig. 2.2(d)), though it was full of ASCAT measurements. Unfortunately, the ASCAT measurements could not improve the analysis of the storm over the Baltic Sea as it was expected.

The results of statistical comparison with surface-based observations are presented in Table 5.2. The RMSEs in the ASCEXP are slightly lower in both the wind speed and the MSLP in comparison with the IMO data, however, the RMSEs of AMO data in both parameters are higher than in the REFEXP. Overestimation of the wind speed analysis is detected (Fig. 5.4, bottom) in the ASCEXP, which

shows larger differences with AMO data points in the North Sea. The ASCAT overpasses after 19 UTC in the North Sea and in the northwestern part of the HIRLAM domain may cause the wind speed overestimations in these regions. The cause of wind speed overestimations in the Norwegian Sea is unknown, the ASCAT measurements are quite close to assimilation moment.

Table 5.2. The HIRLAM REFEXP and ASCEXP bias, RMSE and correlation coefficients of 10-m wind speed and MSLP 01.12.2013 at 18 UTC.

10-m wind speed					MSLP				
20131201 18 UTC		BIAS	RMSE	CORREL	20131201 18 UTC		BIAS	RMSE	CORREL
ASCEXP	IMO	-1.10	2.13	0.79	ASCEXP	IMO	-0.27	0.84	0.99
REFEXP		-0.96	2.18	0.75	REFEXP		-0.16	0.89	0.99
ASCEXP	AMO	0.48	2.82	0.86	ASCEXP	AMO	-0.65	0.85	1.00
REFEXP		0.87	2.72	0.88	REFEXP		-0.45	0.75	1.00
ASCEXP	ALL	-0.34	2.49	0.88	ASCEXP	ALL	-0.47	0.85	1.00
REFEXP		-0.08	2.46	0.88	REFEXP		-0.31	0.82	1.00

Visual comparison of the MSLP shows similar results except the difference in the Norwegian Sea; the isobars of the ASCEXP are more extended to the north and shifted slightly to the east (Paper III, Fig. 8).

5.3 Storm Xaver 05.12.2013

The storm Xaver brought very strong wind speeds over large marine area of Europe, The ASCAT registered the maximum of 28.6 m s^{-1} for the 12 UTC HIRLAM run and 25.5 m s^{-1} for the 18 UTC run. Here two HIRLAM runs are evaluated: at 12 UTC and 18 UTC. The results of the two experiments at 12 UTC (Figure 5.5) differ considerably in the Norwegian Sea, showing only small differences in other marine areas. The statistical output in this case (Table 5.3) shows more accurate wind speed analysis in the REFEXP compared with IMO data. Here very strong wind speed overestimation is detected in the North Sea (-11 m s^{-1} , area in red circle), such overestimation is caused again by differences in the measurement time: the ASCAT measurements in this area are carried out at 09:45 UTC. However, in the Norwegian Sea the ASCEXP analysis is very accurate and fits with IMO data points (area in blue circle) because of more appropriate time of measurement (11:23 UTC).

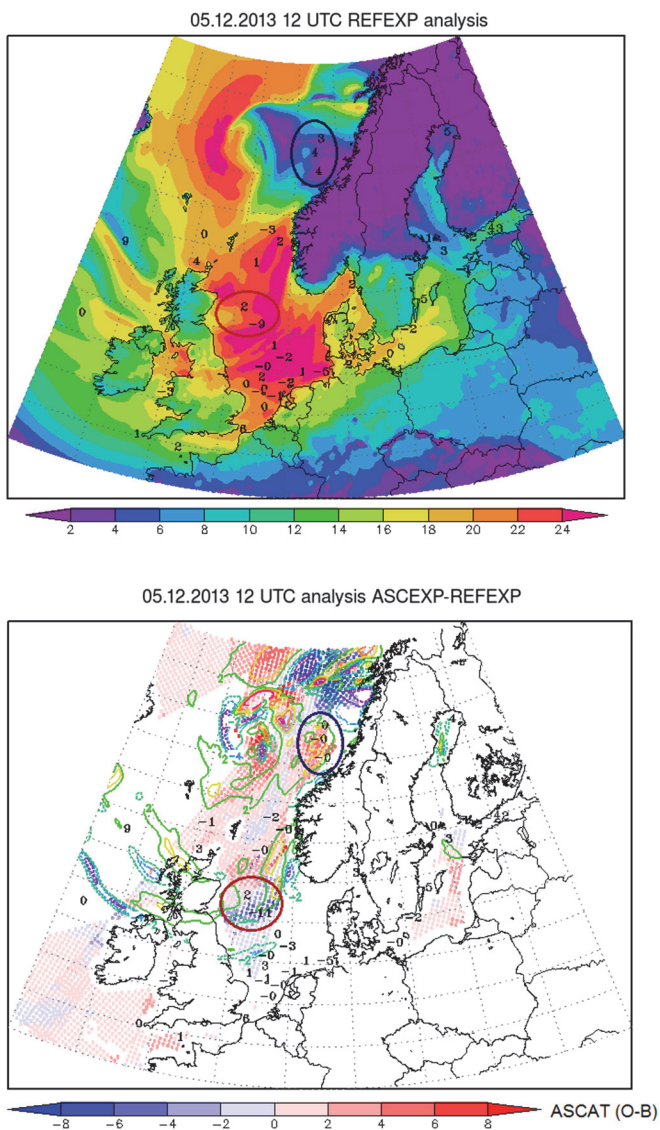
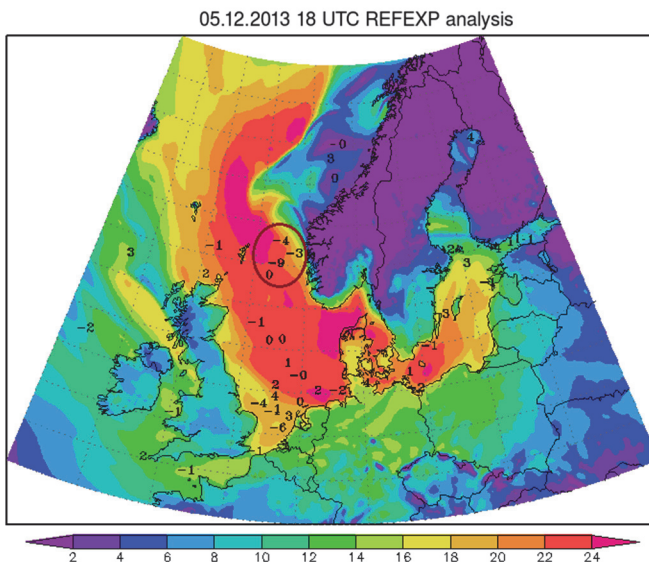


Figure 5.5. The HIRLAM 10-m wind speed analyses 05.12.2013 at 12 UTC: REFEXP (top), ASCEXP–REFEXP analysis difference (bottom). The number values: surface-based observation minus analysis (O–A); colour dots: ASCAT observation minus HIRLAM background (O–B) before assimilation; colour contours (2 m s⁻¹ step) wind speed analysis difference (ASCEXP–REFEXP).

The important fact in this case is that about 2.0 percent of all ASCAT measurements used in the current assimilation window are the winds over 25 m s⁻¹. The ASCAT Wind Product User Manual (OSI-SAF Project Team, 2013) shows the data range of the ASCAT winds 0–50 m s⁻¹, however, the wind speeds over 25

m s^{-1} are generally known to be less reliable. At strong winds wave breaking will further intensify, causing air bubbles, foam and spray at the ocean surface, and a more and more complicated ocean topography (Verhoef and Stoffelen, 2014). The buoy measurements in high wind/wave conditions may also show underestimated wind due to the flow disturbance extending beyond the anemometer height (Ingleby, 2009). It is also known that the model calculations may not be perfectly fitted for severe weather conditions. All these facts may lead to larger variations between observed and analysed wind speed differences, even in closely located observational data points.

The storm Xaver 05.12.2013 at 18 UTC intensified and winds are very strong already in the southern part of the Baltic Sea (Fig. 5.6). The ASCEXP calculate stronger winds across the Norwegian coast and in the southern part of the Norwegian Sea, and the differences with marine observations may reach -12 m s^{-1} (area in red circle). Here, again the strong variation of the wind speed measurements is observed in closely located data points inside the storm. At 18 UTC the wind speed statistics is more accurate in the REFEXP for all marine observations (Table 5.3), this is most likely caused by wind speed overestimations in the ASCEXP analysis. The wind speed analyses in the Baltic Sea region are very similar in both OSEs.



05.12.2013 18 UTC analysis ASCEXP-REFEXP

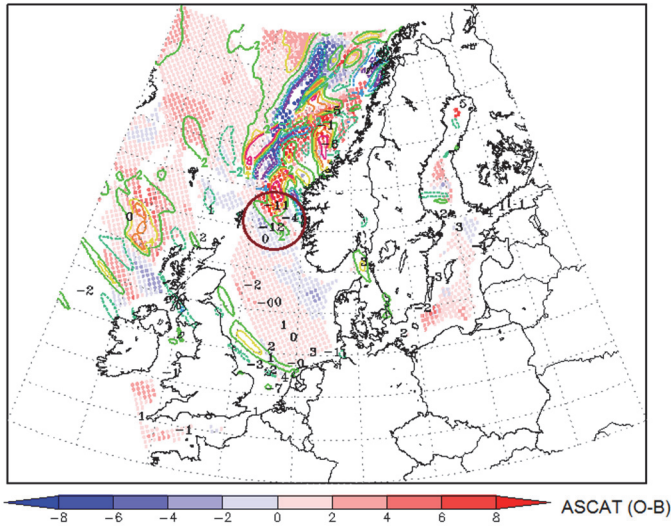


Figure 5.6. The HIRLAM 10-m wind speed analyses 05.12.2013 at 18 UTC: REFEXP (top), ASCEXP–REFEXP analyses difference (bottom). The number values: surface-based observation minus analysis (O–A); colour dots: ASCAT observation minus HIRLAM background (O–B) before assimilation; colour contours (2 m s⁻¹ step) wind speed analysis difference (ASCEXP–REFEXP).

The visual comparison of the MSLP in both analysis cycles shows significant differences in the Norwegian Sea (Paper III, Fig. 12). Most likely, the strong ASCAT winds and their assimilation in this area (Fig. 2.2(f)) deepen the low-pressure system in comparison with the REFEXP. Unfortunately, the accuracy of OSEs output cannot be checked with observational data in these areas due to missing MSLP measurements.

Statistics of the MSLP 05.12.2013 at 12 UTC (Table 5.3) give smaller errors in the ASCEXP for all types of marine observations and, in general, show better fit with observed MSLP. The MSLP statistics at 18 UTC is also rather similar for both experiments.

Table 5.3. The HIRLAM REFEXP and ASCEXP bias, RMSE and correlation with observed values of 10-m wind speed and MSLP 05.12.2013 at 12 UTC (left) and 18 UTC (right).

10-m wind speed					10-m wind speed				
20131205 12 UTC		BIAS	RMSE	CORREL	20131205 18 UTC		BIAS	RMSE	CORREL
ASCEXP	IMO	0.20	3.35	0.82	ASCEXP	IMO	-1.77	4.12	0.81
REFEXP		0.90	3.27	0.86	REFEXP		-0.73	3.46	0.86
ASCEXP	AMO	-0.45	4.06	0.84	ASCEXP	AMO	0.42	3.41	0.80
REFEXP		-0.33	4.10	0.84	REFEXP		0.55	2.89	0.85
ASCEXP	ALL	-0.12	3.71	0.83	ASCEXP	ALL	-0.67	3.78	0.79
REFEXP		0.30	3.70	0.85	REFEXP		-0.09	3.19	0.85
MSLP					MSLP				
ASCEXP	IMO	-0.45	1.53	1.00	ASCEXP	IMO	-0.03	1.42	1.00
REFEXP		-0.45	1.54	1.00	REFEXP		0.10	1.35	1.00
ASCEXP	AMO	-0.91	1.16	1.00	ASCEXP	AMO	-0.61	0.86	1.00
REFEXP		-0.99	1.29	1.00	REFEXP		-0.72	0.99	1.00
ASCEXP	ALL	-0.69	1.35	1.00	ASCEXP	ALL	-0.34	1.16	1.00
REFEXP		-0.73	1.42	1.00	REFEXP		-0.34	1.17	1.00

5.4 Discussion

The results from verification with surface-based measurements show that sometimes the ASCAT data assimilation improves the analysis, but in some cases the REFEXP shows more accurate analysis. It is clear that case studies provide fewer statistics for the overall quality assessment of the ASCAT data assimilation in comparison with statistics collected over longer period. On the other hand, the case studies may give more information about model behaviour in specific synoptic situations. Valkonen and Schyberg (2015) also demonstrated strong day-to-day variations in the standard deviations of the ASCAT data compared to the model background (O–B) and the analysis (O–A). Such variations show how the model fits with instantaneous ASCAT measurements performed in assimilation time window.

Verification of the OSEs in this study was performed separately for each case. The smallest RMSE of the wind speed appeared in the storm Christian 2.11 m s^{-1} and the highest in the storm Xaver 3.78 m s^{-1} . Formerly, De Valk (2013) has analysed the impact of the ASCAT 25-km wind data assimilation on the HIRLAM during one-week experiments in winter time and showed similar results, the mean standard deviation of the model initial state (00 length forecast) from marine observations was about 3.5 m s^{-1} . Statistical calculations of the MSLP showed also that the ASCAT data assimilation impacts on the changes in the MSLP and in locations of the low-pressure systems.

Assimilation of extremely strong ASCAT winds is also highlighted in this study. In the storm Xaver HIRLAM assimilated the ASCAT winds over 25 m s^{-1} .

The analysis winds mainly followed HIRLAM background winds, which are weaker than the ASCAT measurements (Paper III, Fig. 10). This result is contrary to the study by Valkonen and Schyberg (2015) which showed that in case of the strong ASCAT winds (over 23 m s^{-1}) HARMONIE background winds were always higher than ASCAT. This may be attributed to the different tunings or systematic differences of HIRLAM and HARMONIE background forecast models.

No adjustments in the system as data thinning or observation error setting done in the study, similar to the studies by De Valk (2013) and De Haan *et al.* (2013) gave more weight to the ASCAT measurements. Some negative results detected in the study raise question of the optimal use of the ASCAT data. Probably, the ASCAT observations should be thinned to get better results, especially in the areas where the measurements are performed simultaneously from both satellites. Such technique is applied by Valkonen and Schyberg (2015), De Chiara *et al.* (2014) and Ollinaho (2010) and shows positive to neutral results. Another aspect which could improve the quality of the HIRLAM analyses is to shorten time interval between the analyses. In our studies the FGAT is applied, but it still seems to be insufficient to avoid large differences in observations and background in the assimilation cycle. Further research is necessary to improve the data assimilation methods for ASCAT winds to avoid such negative impact as improving the quality of severe storm forecasting is very important for the society.

CONCLUSIONS

The quality of scatterometer winds are usually validated against *in situ* wind measurements, but complimentary numerical weather prediction (NWP) data can be used, especially in such marine areas where *in situ* measurements are missing. On the other hand, comparison of scatterometer data with ground-based or NWP winds permits one to estimate quality of both measurement systems and detect systematic errors that may affect the prediction of hazardous weather. Such comparisons are also a prerequisite to assimilation of scatterometer data into the NWP model.

The QuikSCAT 12.5-km measurements during the period 19 June 1999 – 23 November 2009 gave a possibility to study marine winds at the standard height of 10 m in the Gulf of Riga from climatological point of view and compare them with ground-based measurements on the islands of Kihnu and Ruhnu. As the QuikSCAT measurements are sensitive to the presence of rain, two methods were applied to filter the rain-contaminated data: by strict and more lenient criteria. It was shown that:

- More lenient criteria applied for rain-contaminated measurements enlarged significantly the number of data points, especially in the northern part of the gulf.
- Wind speed in the northern part of the gulf is slightly larger than that in the southern part. Strong winds prevail from September to February, most probably from SW or S.
- Wind speed measured at meteorological stations on the islands is weaker than that estimated from satellite even in the case when rain contamination is removed through the application of strict criteria. This can be explained by site obstructions – on both islands the northern directions are sheltered by forest.
- Correlation between satellite and island measurements is strong for wind direction (correlation coefficient over 0.9) and somewhat weaker for wind speed (correlation coefficient around 0.6).

Taking into account that the coordinates of the measurement sites are not exactly the same and the measurements may not be carried out simultaneously, it can be said that both measurement systems – ground based and QuikSCAT – describe the main features of the wind climate satisfactorily. On the other hand, in case wind speed is considered, satellite data should be preferred, as they are free of orographic disturbances.

Comparison of the ASCAT 12.5-km winds with the HIRLAM version 7.1.2 forecasts in the Baltic Sea region during October 1 – December 3, 2009 showed that:

- The HIRLAM 10-m wind speed forecasts show good correspondence (correlation coefficient over 0.9 up to 18-hour forecast) with the ASCAT measurements. The wind speed predictions practically lack systematic errors, although a very weak negative bias (HIRLAM minus ASCAT) in wind speed appears with growing forecast length. This shows that the friction parameterization over the sea is roughly correct in HIRLAM.
- The HIRLAM 10-m wind direction forecasts and ASCAT wind directions correlate better when the wind speed exceeds 4 m s^{-1} showing correlation coefficients from 0.82 for the 6-hour forecast and not less than 0.72 for the 30-hour forecast.
- The uncertainty ranges fit well with the expected ASCAT quality characteristics and meet the requirements up to the 18-hour forecast lengths. In the case of the 30-hour forecast these criteria are exceeded only slightly for both the wind speed and the wind direction.
- The ASCAT wind components – zonal and meridional – correlate better with those of the HIRLAM forecasts; they fit the required accuracy thresholds well. The RMS difference of wind components higher than 2 m s^{-1} is present only in the 30-hour forecasts. The bias of the components is smaller than that required in all HIRLAM forecasts.
- The results of the higher resolution ETB model tend to be slightly less consistent with scatterometer winds than the results of ETA model. The reason for this might be that the forcing of these scales in the HIRLAM model is weak and the phases of these small-scales are not well determined. Other possible explanations may be that the HIRLAM parameterization schemes are fine-tuned to 15 km resolution and therefore do not work so well at high resolution, or that the proximity of the boundary conditions introduces distortions in small domains.
- A case of phase error in the HIRLAM 30-hour predictions of cyclonic development over Baltic Sea was spotted on 2.12.2009. This situation needs further analysis to identify the causes of this discrepancy. Nevertheless, it illustrates the potential of ASCAT measurements to identify such phase shift errors over open sea areas and may contribute to the development of better deterministic models in the future.

As a result, ASCAT 10-m winds are a reliable data source over the Baltic Sea that is of great value for marine and NWP communities operating in the region.

In the newer HIRLAM version 7.4 the option of the ASCAT assimilation into the HIRLAM was made available by means of the algorithm written by John de Vries and Paul de Valk and enabled us to test it in Estonian Weather Service after the new cluster setup in 2013. The impact of the ASCAT 25-km data assimilation into the HIRLAM is assessed in cases of severe storms of 2013 and inspects the quality of HIRLAM analyses. The following can be concluded:

- Depending on the spatial and temporal availability of ASCAT data in the HIRLAM domain, the model may show more or less accurate wind and mean sea level pressure analysis.
- The errors in HIRLAM analysis occur mainly in the cases of considerable time difference between the ASCAT measurements and HIRLAM analysis.
- The areas of no impact after the ASCAT data assimilation are close to the shoreline where HIRLAM rejects most of the ASCAT observations after the procedure of quality control. As a result, in some cases the model wind speeds are significantly underestimated. It is of interest to investigate possibilities of application of the ASCAT Coastal Wind Product that may increase the impact of the ASCAT data assimilation in these areas.
- Assimilation of extremely strong ASCAT winds (over 25 m s^{-1}) is highlighted in the case of storm Xaver. The analysis winds mainly followed HIRLAM background winds, which are weaker than the winds from the ASCAT measurements.
- No adjustments in the system as data thinning or observation error setting done in the study gave more weight to the ASCAT measurements.

IMPLICATIONS FOR FURTHER RESEARCH

The following recommendations for further investigations could be given:

- Some negative results such as significant phase errors in case of relatively fast moving severe storms detected in the study raise question of the optimal use of the ASCAT data. Probably, the ASCAT observations should be thinned to get better results, especially in the areas where the measurements were performed simultaneously from both satellites.
- The quality of the HIRLAM analyses could be improved by shortening the time interval between the analyses. In our studies the FGAT is applied, but it still seems to be insufficient to avoid large differences in observations and background in the assimilation cycle.
- Further research is necessary to improve the data assimilation methods for ASCAT winds as the high quality of severe storm forecasting is very important for the society.

Acknowledgements

First, I would like to thank my supervisors Prof. Sirje Keevallik and Dr. Aarne Männik for guiding and giving me good advice during my study. Both of my supervisors were the co-authors of my papers as well and I would like to express the deepest gratitude for their contribution. I would like greatly to thank Prof. Sirje Keevallik for her inspiration and support, the review of my thesis and valuable comments related to it.

I would like to thank Kalle Eerola, Pirkka Ollinaho and Tuuli Perttula from Finnish Meteorological Institute for their advice and consultations in the ASCAT assimilation into NWP (numerical weather prediction) models. I am very thankful for cooperation and consultations to my colleague Vello Loorits, who provided me with the environment to make the HIRLAM experiments possible.

The ASCAT data used in these studies were processed and distributed jointly by the EUMETSAT Ocean and Sea Ice (OSI) Satellite Application Facility (SAF) project both implemented at the Royal Netherlands Meteorological Institute (KNMI).

The usage of the HIRLAM data was possible owing to the participation of Estonia in the HIRLAM project. The marine observational data used in the final study are provided by Federal Maritime and Hydrographic Agency of Germany (BSH), Estonian Weather Service and Swedish Meteorological Institute.

The QuikSCAT data used in the study were obtained from the freely available NASA Jet Propulsion Laboratory Physical Oceanography Distributed Active Archive Centre (PO.DAAC) and I would like to thank David Moroni for valuable consultations related to the QuikSCAT data quality flags.

This work was financially supported by the Estonian Science Foundation (grant no. 9140; SF0140017s08; SF0180038s08) and institutional research funding IUT20-11 of the Estonian Ministry of Education and Research; the European Social Fund's Doctoral Studies and Internationalisation Programme DoRa.

A special gratitude goes to my family for their greatest support. I would like to thank my husband Mihhail, who has been a great motivator for me, supporting emotionally to go through all the challenges met in this work. And finally, I would like to thank my son Yaroslav for his great love and cheerfulness.

ABSTRACT

Scatterometers are the radar instruments on board of polar-orbiting satellites that give an excellent opportunity to estimate the wind speed and wind direction at 10 m height in marine areas over the globe. These measurements help to get information about the wind conditions in the areas where *in situ* measurements are sparse or missing. The main aim of the thesis was to study the differences between satellite and ground-based wind measurements, to compare HIRLAM (High Resolution Limited Area Model) wind forecasts with corresponding scatterometer records and, finally, to test the quality of assimilation of satellite wind data to the NWP (Numerical Weather Prediction) model HIRLAM analyses in cases of severe storms.

The SeaWinds instrument on the QuikSCAT satellite was operational from 19 June 1999 to 23 November 2009. These data were used to describe marine winds in the Gulf of Riga where dangerous combinations of high sea level and wave height in stormy seasons may cause disasters. The quality of the data was carefully checked and necessary adjustment was applied to remove the contaminated recordings. It was shown that allowing lenient filtering of rain-contaminated data leads to larger wind speed estimates but increases considerably the quantity of data, allowing separate analysis of the northern and southern parts of the gulf. The wind speed and direction from the SeaWinds with the highest resolution of 25 km and grid spacing of 12.5 km were used in the study and compared with surface-based measurements on islands Kihnu and Ruhnu. It was found that the wind speed measured on the islands is weaker than that estimated from the satellite even in the case when rain contamination is removed through application of strict criteria, some differences in wind roses on islands are demonstrated as well. In spite of that fact, ground-based wind directions are well correlated with those measured by the satellite showing correlation coefficients of over 0.9. For wind speed, this quantity is somewhat lower, around 0.6.

The ASCAT (Advanced Scatterometer) on MetOp (Meteorological Operational) satellites is operational since 2006. The ASCAT data (25-km resolution winds with the grid spacing of 12.5 km) were compared in the Baltic Sea region during the stormy season in 2009 with HIRLAM forecasts. Two domains of HIRLAM with different resolutions were used in the comparison. Mutual quality and uncertainty characteristics of the measurements and predictions were determined during this study. The results showed that the ASCAT wind data are well correlated with the HIRLAM predicted winds, which raises the credibility of both data sources in operational and hindcasting applications over the Baltic Sea. A case of phase shift error in a HIRLAM forecast of cyclonic activity over the Baltic Sea is highlighted as well.

Further steps of improving the HIRLAM forecasts were performed by assimilation the ASCAT winds (50-km resolution data with grid spacing of 25 km) into model. The impact of the ASCAT data assimilation into HIRLAM is

assessed in case-studies of rapidly-developing severe storms of 2013. Mainly the impact on the model analysis output is evaluated. The HIRLAM quality is analysed for two experiments: with and without the ASCAT data assimilation. Marine observations of 10-m wind speed and mean sea level pressure are used as measures of quality. The results show that depending on ASCAT data coverage in the HIRLAM domain and temporal availability of the data in assimilation time moment, the analysis may be either more or less accurate. It is also detected that some narrow places of the Baltic Sea (Bothnia Bay, Gulf of Finland) are not affected by the ASCAT data assimilation. Due to the ASCAT Wind Product specification, the ASCAT measurements near the shoreline are usually flagged as land contaminated. The ASCAT winds in these areas are not admitted to the analysis after the procedure of the HIRLAM quality control, most likely due to the proximity to the land. The usage of the ASCAT Coastal Wind Product in the future may enlarge the ASCAT data coverage in these areas. In addition, some weaknesses of the ASCAT data assimilation were detected in the study and the question of the optimal ASCAT data usage was raised. Further attempts to improve the quality of the HIRLAM analyses are expected in the ASCAT data thinning before assimilation or reducing time differences between the HIRLAM analyses.

RESÜMEE

Skatteromeetrid on polaarorbiidil tiirlevatele satelliitidele paigutatud radarid, mis annavad suurepärase võimaluse hinnata tuule kiirust ja suunda 10 m kõrgusel merepinna kohal. Iseäranis kasulikud on need olukordades, kus *in situ* mõõtmisi on vähe või need puuduvad hoopis. Väitekirja eesmärk oli uurida erinevusi tuule satelliidilt hinnatud ja maapealsetes meteoroloogiajaamades mõõdetud parameetrite vahel, võrrelda HIRLAMi (High Resolution Limited Area Model) tuuleprognoose vastavate skatteromeetri mõõtmistega ja uurida satelliidiandmete assimileerimise mõju numbrilise ilmaprognoosimudeli HIRLAM kvaliteedile tugevate tormide korral.

Satelliidil QuikSCAT paiknenud SeaWinds instrument oli operatiivne 19. juunist 1999 kuni 23. novembrini 2009. Neid andmeid kasutati meretuule kirjeldamiseks Liivi lahe kohal, kus kõrge veetaseme ja lainetuse koosmõju tormide ajal võib kaasa tuua katastroofilisi üleujutusi. Andmed läbisid kvaliteedikontrolli ja võimalikud ebatäpsused eemaldati hoolikalt. Näidati, et vihmast mõjutatud andmete eemaldamine leebema filtreerimise teel annab tuule kiiruseks mõnevõrra suuremaid väärtusi, aga samal ajal suurendab märgatavalt ka andmete hulka, lubades niimoodi vaadelda eraldi lahe põhja- ja lõunaosa. SeaWinds mõõtis tuule kiirust ja suunda võrgusammuga 12.5 km ning ruumilise lahutusega 25 km ja neid tulemusi võrreldi mõõtmistega Kihnu ja Ruhnu saartel. Tuule kiirus maapealsetes meteoroloogiajaamades oli väiksem kui see, mida hinnati satelliidilt isegi siis, kui vihmast mõjutatud andmed eemaldati rangema filtreerimise teel. Kuigi leiti mõningaid erinevusi tuulteroosides, korreleerusid maapealsetes jaamades mõõdetud tuule suunad hästi satelliidilt mõõdetutega, näidates korrelatsioonikordajat üle 0.9. Korrelatsioon tuule suundade vahel oli mõnevõrra nõrgem – korrelatsioonikordajaga ligikaudu 0.6.

MetOp (Meteorological Operational) satelliidil paiknev ASCAT (Advanced Scatterometer) töötab alates aastast 2006. ASCATi andmeid (võrgusamm 12.5 km ning ruumiline lahutus 25 km) võrreldi Läänemere regioonis HIRLAMi prognoosidega 2009. aasta tormisel aastaajal. Kasutati kaht erineva lahutusega HIRLAMi varianti. Hinnati mõõtmiste ja prognooside kokkulangevust, mis osutus küllalt heaks ja tõstab nii satelliidiandmestiku kui ka HIRLAMi usaldusväarsust Läänemere tuulte hindamisel ja prognoosimisel. Ühel tsüklonaalse aktiivsuse juhtumil Läänemere regioonis leiti ka faasinihke viga HIRLAMi prognoosis.

HIRLAMi prognoosi parendamiseks katsetati ASCATi tuuleandmete (võrgusammuga 25 km ning ruumiline lahutus 50-km) assimileerimist mudelisse. Hinnati ASCATi andmete assimileerimise mõju HIRLAMi analüüsi kvaliteedile 2013. aasta kiiresti arenevate tormide ajal. Seda tehti kahe vaatlussüsteemi eksperimendi kaudu: ühel juhul toimus ASCATi andmete assimileerimine ja teisel

mitte. Mudeli väljundi kvaliteedi hindamiseks kasutati 10 meetri kõrgusel mere kohal registreeritud tuule ja keskmise õhurõhu andmeid. Tulemused näitavad, et olenevalt uuritava ala kaetusest ASCATi andmetega ja assimilatsioonihetkel saadaval olevast andmehulgast, võib tulemus olla enam või vähem täpne. Leiti ka, et mõnede kitsamate alade puhul Läänemeres (Botnia laht ja Soome laht) ASCATi andmete assimileerimine ei mõjuta oluliselt tulemusi. Tuuleprodukti spetsifikatsiooni käigus märgitakse ASCATi mõõtmised rannikualade lähedal tavaliselt maismaaga saastunuteks. Nendel aladel ASCATi tuuli ei analüüsita pärast HIRLAMi kvaliteedikontrolli ja põhjuseks on tõenäoliselt ranniku lähedus. Tulevikus võiks neil aladel ASCATi avameretuule produkti täiendada rannikutuule produktiga. Lisaks avastati mõned ASCATi andmeassimilatsiooni nõrgad kohad, mis tõstatab küsimuse ASCATi andmete optimaalsest kasutamisest. Leitakse, et tulemuste edasiseks parendamiseks on vaja proovida ASCATi mõõtmisi hõrendada enne assimileerimist või vähendada ajalist vahemikku HIRLAMi analüüsides.

REFERENCES

- Atlas, R., Hoffman, R.N., Leidner, S.M., Sienkiewicz, J., Yu, T.-W., Bloom, S.C., Brin, E., Ardizzone, J., Terry, J., Bungato, D., Jusem, J.C. 2001. The effects of marine winds from scatterometer data on weather analysis and forecasting, *Bull. Am. Meteorol. Soc.*, 82, 1965–1990.
- Bartalis, Z., Naeimi, V., Hasenauer, S., Wagner, W. 2008. ASCAT Soil Moisture Product Handbook. ASCAT Soil Moisture Report Series, No. 15, Institute of Photogrammetry and Remote Sensing, Vienna University of Technology, Austria.
- Bentamy, A., Croize-Fillon, D., Perigaud, C. 2008. Characterization of ASCAT measurements based on buoy and QuikSCAT wind vector observations. *Ocean Sci.*, 4 (4), 265–274.
- Bi, L., Jung, J., Morgan, M., Le Marshall, J., Baker, N., Santek, D. 2010. Impact of METOP ASCAT Ocean Surface Winds on Global Weather Forecasts. In: 10th International Winds Workshop, Tokyo, Japan, 22–26 February 2010. https://www.researchgate.net/publication/267700761_Impact_of_METOP_ASCAT_Ocean_Surface_Winds_on_Global_Weather_Forecasts, 11.04.2016.
- Cotton, J. 2013. The impact of ASCAT winds from Metop-B and a new scatterometer thinning scheme. Forecasting Research Technical Report No. 580, Met Office. <http://www.metoffice.gov.uk/media/pdf/3/1/FRTR580.pdf>, 20.10.2015.
- De Chiara, G., Janssen, P., English, S., Bidlot, J.-R. and Laloyaux, P. 2014. Scatterometer impact studies at ECMWF. In: Proceedings of the EUMETSAT Meteorological Satellite Conference, Geneva, Switzerland, 22–26 September 2014. <http://www.eumetsat.int/>, 20.10.2015.
- De Haan, S., Marseille, G.J., De Valk, P. and De Vries, J. 2013. Impact of ASCAT Scatterometer Wind Observations on the High-Resolution Limited-Area Model (HIRLAM) within an Operational Context. *Weather and Forecasting*, 28, 489–503.
- De Valk, P. 2013. ASCAT assimilation in the HIRLAM report. De Bilt, international report, IR-2013-02. <http://www.knmi.nl/bibliotheek/knmi/pubIR/IR2013-02.pdf>, 20.10.2015.
- Deutschländer, T., Friedrich, K., Haeseler, S. and Lefebvre, C. 2013. Severe storm XAVER across northern Europe from 5 to 7 December 2013. DWD. https://www.dwd.de/EN/ourservices/specialevents/storms/20131230_XAVER_europe_en.pdf?__blob=publicationFile&v=4, 11.04.2016.
- Figa-Saldaña, J., Wilson, J.W., Attema, E., Gelsthorpe, R., Drinkwater, M.R. and Stoffelen, A. 2002. The advanced scatterometer (ASCAT) on the

meteorological operational (MetOp) platform: A follow on for the European wind scatterometers. *Can. Jour. Remote Sensing*, 28(3), 404–412.

Gelsthorpe, R.V., Schied, E., Wilson, J.J.W. 2000. ASCAT-MetOp's advanced scatterometer. *ESA Bulletin* 102. <http://www.esa.int/esapub/bulletin/bullet102/Gelsthorpe102.pdf>, 19.05.2015.

Haeseler, S. and Lefebvre, C. 2013. Heavy storm CHRISTIAN on 28 October 2013. *DWD*. http://www.dwd.de/DE/presse/hintergrundberichte/2013/Orkantief_Christian_PDF.pdf?__blob=publicationFile&v=3, 18.10.2015.

Hersbach, H. and Janssen, P. 2007. Operational assimilation of surface wind data from the MetOp ASCAT scatterometer at ECMWF. *ECMWF Newsletter*, 113, 6–8.

Hersbach, H. and Janssen P. 2010. The Usage of Scatterometer Data at ECMWF. In: *International Ocean Vector Winds Meeting*, Barcelona, Spain, 18–20 May 2010. https://mdc.coaps.fsu.edu/scatterometry/meeting/docs/2010_may/gridded/hersbach.pdf, 28.03.2015

Hoffman, R.N. and Leidner, S.M. 2005. An Introduction to the Near-Real-Time QuikSCAT data. *Journal of weather and forecasting*, 20, 476–493.

Hsu, S.A., Meindl, E.A. and Gilhousen, D.B. 1994. Determining the Power-Law Wind-Profile Exponent under Near-Neutral Stability Conditions at Sea. *Applied Meteorology*, 33(6), June 1994.

Huang, X-Y., Morgensen, K.S. and Yang, X. 2002. First-guess at the appropriate time: the HIRLAM implementation and experiments. In: *Proceedings for HIRLAM workshop on variational data assimilation and remote sensing*, Helsinki, Finland, 22–23 January 2002, 28–43.

Huddleston, J.N. and Stiles, B.W. 2000. A Multidimensional Histogram Rain-Flagging Technique For SeaWinds on QuikSCAT. In: *Geoscience and Remote Sensing Symposium (IGARSS)*, Honolulu, USA, 24–28 July 2000, 1232–1234. ftp://podaac-ftp.jpl.nasa.gov/OceanWinds/quikscat/L2B12/docs/MUDH_Description_V3.pdf, 13.03.2012.

Ingleby, B. 2009. Factors affecting ship and buoy data quality. *Technical Report nr. 529*, Met Office, Meteorology Research and Development. http://research.metoffice.gov.uk/research/nwp/publications/papers/technical_reports/reports/529.pdf, 25.05.2015.

Keevallik, S., Männik, A. and Hinnov, J. 2009. Comparison of HIRLAM wind data with measurements at Estonian coastal meteorological stations. *Estonian Journal of Earth Sciences*, 59(1), 90–99.

Kleiss, J., Kelly, K., Thompson, L., Dickinson S. 2010. A comparison of QuikSCAT winds to in situ observations in the Western Boundary Current

regions. In: 2010 International Ocean Vector Winds Meeting, Barcelona, Spain, 18–20 May 2010. http://coaps.fsu.edu/scatterometry/meeting/docs/2010_may/calval/kleiss.pdf, 25.05.2015.

Lungu, T. and Callahan, S. 2006. QuikSCAT Science Data Product User's Manual. ftp://podaac-ftp.jpl.nasa.gov/OceanWinds/quikscat/L2B12/docs/QSUG_v3.pdf, 25.05.2015.

Mears, C., Wentz, F. and Smith, D. 2000. SeaWinds on QuikScat normalized objective function rain flag. Remote Sensing Systems, Santa Rosa, Calif, 1–13. ftp://podaac-ftp.jpl.nasa.gov/OceanWinds/quikscat/L2B12/docs/NOF_Description_V1.2.pdf, 15.03.2012.

National Research Council. 2007. Options to Ensure the Climate Record from the NPOESS and GOES-R Spacecraft: A Workshop Report. ISBN: 0-309-11277-X, 84 pages, 8 ½ x 11.

Nghiem, S.V., Leshkevich, G.A. and Stiles, B.W. 2004. Wind Fields over the Great Lakes Measured by the SeaWinds Scatterometer on the QuikSCAT Satellite. *Journal of Great Lakes Research*. 30(1), 148–165.

Ollinaho, P. 2010. Feasibility of assimilating ASCAT surface winds into a limited area model. M.S. thesis, Dept. of Physics, University of Helsinki, 81 pp. <https://helda.helsinki.fi/handle/10138/20968>, 27.03.2016

OSI-SAF Project Team. 2013. ASCAT Wind Product User Manual version 1.13, Technical Report Reference: 2013, SAF/OSI/CDOP/KNMI/TEC/MA/126.

Payan, C. 2010. Improvements in the use of scatterometer winds in the operational NWP system at Meteo-France. In: 10th International Winds Workshop, Tokyo, Japan, 22–26 February 2010. http://www.eumetsat.int/website/home/News/ConferencesandEvents/DAT_2042632.html, 11.04.2016.

Pickett, M.H, Tang, W., Rosenfeld, L.K. and Wash, C.H. 2003. QuikSCAT satellite comparisons with nearshore buoy wind data off US West Coast. *Journal of Atmospheric and Oceanic Technology*, 20, 1869–1879.

Portabella, M. 2002. Wind field retrieval from satellite radar systems. Thesis: University of Barcelona, Barcelona, Spain, 207 p. http://www.knmi.nl/publications/fulltexts/phd_thesis.pdf, 19.05. 2015.

Portabella, M. and Stoffelen, A. 2002. A comparison of KNMI Quality Control and JPL Rain Flag for SeaWinds. *Canadian Journal of Remote Sensing*, 28(3), 424–430.

Portabella, M. and Stoffelen, A. 2004. A probabilistic approach for SeaWinds data assimilation. *Quart. J. R. Met. Soc.*, 130(596), 127–152.

Portabella, M., Stoffelen, A., Verhoef, A., and Verspeek, J. 2012. A new method for improving ASCAT wind quality control. *IEEE Geoscience and Remote Sensing Letters*, 9(4), 579–583.

Sharma, N. and D'Sa, E. 2008. Assessment and analysis of QuikSCAT vector wind products for the Gulf of Mexico: a long-term and hurricane analysis. *Sensors (Basel)*, 8, 1927–1949.

Služenikina, J. and Männik, A. 2011. A comparison of ASCAT wind measurements and the HIRLAM model over the Baltic Sea. *Oceanologia*, 53(1-TI), 229–244.

Smith, D.K., Wentz, F.J. and Mears, C.A. 2002. Analysis of QuikSCAT rain-flagged winds within the tropical cyclone environment. In: 25th Conference on Hurricanes and Tropical Meteorology, San Diego, CA, 28 April – 03 May 2002, AMS, 507–508.

Spencer, M.W., Wu, C. and Long, D.G. 2000. Improved Resolution Backscatter Measurements with the SeaWinds Pencil-beam Scatterometer. *IEEE Transactions on Geoscience and Remote Sensing*, 38(1), 89–104.

Stiles, B.W. 1999. Special Wind Vector Data Product: Direction Interval Retrieval with Thresholded Nudging (DIRTH) Product Description. <ftp://podaac-ftp.jpl.nasa.gov/OceanWinds/quikscat/L2B12/docs/Dirth-Product-Description.pdf>, 15.03.2012.

Stiles, B.W., Veleva, S. and Dunbar, R.S. 2006. IMUDH Rain Impact Flagging Algorithm. In: 2006 International Ocean Vector Winds Meeting, Salt Lake City, USA, 5–7 July 2006. <http://coaps.fsu.edu/scatterometry/meeting/docs/2006/stiles.pdf>, 15.03.2012.

Stoffelen, A. 1998. Scatterometry. Thesis, Univ. Utrecht. <http://dspace.library.uu.nl/bitstream/handle/1874/636/full.pdf?sequence=1>, 19.05.2015.

Stoffelen, A., Vogelzang, J. and Verhoef A. 2010. Verification of Scatterometer Winds. In: 10th International Winds Workshop, Tokyo, Japan, 22–26 February 2010. <http://cimss.ssec.wisc.edu/iwwg/iww10/talks/stoffelen2.pdf>, 20.03.2012.

Stoffelen, A., Verhoef, A., Verspeek, J., Vogelzang, J., Driesenaar, T., Risheng, Y., Payan, C., De Chiara, G., Cotton, J., Bentamy, A., Portabella, M. and Marseille, G.J. 2013. Research and Development in Europe on Global Application of the OceanSat-2 Scatterometer Winds. Final Report of OceanSat-2 Cal/Val A0 project.

Storch, H., Feser, F., Haeseler, S., Iefebvre, C., Stendel, M. 2014. A violent midlatitude storm in northern Germany and Denmark, 28 October 2013. *BAMS*, 95(9), 76–78.

Suursaar, Ü., Kullas, T., Otsmann, M., Saaremäe, I., Kuik, J. and Merilain M. 2006. Cyclone Gudrun in January 2005 and modelling its hydrodynamic

consequences in the Estonian coastal waters. *Boreal Environment Research*, 11, 143–159.

Takahashi, M. 2010. Operational use of Scatterometer Winds at JMA. In: 10th International Winds Workshop, Tokyo, Japan, 22–26 February 2010.

Tang, W., Liu, W.T. and Stiles, B.W. 2004. Evaluation of High-Resolution Ocean Surface Vector Winds Measured by QuikSCAT Scatterometer in Coastal Regions. *IEEE Transactions on Geoscience and Remote Sensing*, 42(8), 1762–1769.

Tsai, W.-Y., Spencer, M., Wu, C., Kellogg, K. 2000. SeaWinds on QuikSCAT: Sensor Description and Mission Overview. In: *Geoscience and Remote Sensing Symposium 2000*, Honolulu, HI, 24–28 July 2000, 1021–1023.

Tveter, F. 2006. Assimilating ambiguous QuikScat scatterometer observations in HIRLAM 3-D-Var at the Norwegian Meteorological Institute. *Tellus*, 58A, 59–68.

Undén, P., Rontu, L., Järvinen, H., Lynch, P., Calvo, J., Cats, G., Cuxart, J., Eerola, K., Fortelius, C., Garcia-Moya, J.A., Jones, C., Lenderink, G., McDonald, A., McGrath, R., Navasques, B., Nielsen, N.W., Ødegaard, V., Rodrigues, E., Rummukainen, M., Rõõm, R., Sattler, K., Sass, B.H., Savijärvi, H., Schreur, B.W., Sigg, R., The, H., Tijn, A. 2002. HIRLAM-5 scientific documentation, <http://www.hirlam.org/>, 11.04.2015.

Valkonen, T. and Schyberg, H. 2015. The impact of ASCAT winds in storm cases using the HARMONIE model system. EUMETSAT Fellowship Programme: First year report. MET report 2/2015, ISSN 2387–4201, Norwegian Meteorological Institute, Norway. http://met.no/Forskning/Publikasjoner/MET_report/filestore/MetReport02-2015.pdf, 20.10.2015.

Verhoef, A., Portabella, M., Stoffelen, A. 2012. High-Resolution ASCAT scatterometer winds near the coast. *Geoscience and Remote Sensing*, 50(7), 2481–2487.

Verhoef, A. and Stoffelen, A. 2009. Validation of ASCAT 12.5-km winds, version 1.2. SAF/OSI/CDOP/KNMI/TEC/REP/147, EUMETSAT Tech. Rep., http://projects.knmi.nl/publications/fulltexts/validation_of_ascat_12.5km_winds_1.2.pdf, 02.05.2016.

Verhoef, A. and Stoffelen, A. 2011. ASCAT coastal winds validation report, OSI SAF Report, SAF/OSI/CDOP/KNMI/TEC/RP/176.

Verhoef, A. and Stoffelen, A. 2014. Algorithm Theoretical Basis Document for the OSI SAF wind products version 1.1, EUMETSAT.

Verhoef, A. and Stoffelen, A. 2015. RapidScat wind Product User Manual version 1.1. Technical Report Reference: 2015, SAF/OSI/CDOP2/KNMI/TEC/MA/227.

Verspeek, J., Stoffelen, A., Portabella, M., Verhoef, A., Vogelzang, J. 2007. ASCAT scatterometer cal/val and winds. In: EUMETSAT/AMS Satellite Meteorology and Oceanography conference, Amsterdam, The Netherlands, 24-28 September 2007.

Verspeek, J., Verhoef, A. and Stoffelen, A. 2013. ASCAT-B NWP Ocean Calibration and Validation. Technical Report SAF/OSI/CDOP2/KNMI/TEC/RP/199, EUMETSAT.

Yu, T.-W. and McPherson, R.D. 1984. Global Data Assimilation Experiments with Scatterometer Winds from SEASAT-A. Monthly Weather Review, 112, 368–376.

ELULOOKIRJELDUS

1. Isikuandmed

Ees- ja perekonnanimi Jekaterina Služenikina (Serebrijan)
Sünniaeg ja -koht 26.05.1983, Moldova
Kodakondsus Eesti
E-posti aadress lisjusha@gmail.com

2. Hariduskäik

Õppeasutus (nimetus lõpetamise ajal)	Lõpetamise aeg	Hariduskäik (eriala/kraad)
Tallinna Tehnikaülikool	2009	Maa-teadused/magistrikraad
Eesti Mereakadeemia	2006	Hüdrometeoroloogia ja loodushoid/rakenduskõrgharidus
Maardu Gümnaasium	2002	Keskharidus

3. Keelteoskus (alg-, kesk- või kõrgtase)

Keel	Tase
Vene keel	Emakeel
Eesti keel	Kõrgtase
Inglise keel	Keskstase

4. Täiendusõpe

Õppimise aeg	Täiendusõppe korraldaja nimetus
25.02.2014 – 21.01.2015	“Satellite Meteorology Training Course funded by EUMETSAT Training Placement Scheme” EUMETSAT/ESTEA
05.-09. detsember 2011	“Applications of Satellite Wind and Wave Products for Marine Forecasting” EUMETSAT/IODE
09.-13. juuni 2008	“International Training – Seminar on Satellite Meteorology” DWD

12.-14. mai 2008	“Using Satellite Data In Forecasting Severe Weather Events” EUMETSAT/EMHI
16.-27. oktoober 2006	“WMO/CGMS Virtual Laboratory High Profile Training Event” WMO

5. Teenistuskäik

Töötamise aeg	Tööandja nimetus	Ametikoht
2006-...	Keskonnaagentuur	Prognoosmudelite osakonna peaspetsialist

6. Teadustegevus, sh tunnustused ja juhendatud lõputööd

Služenikina, J., Männik, A. [ilmumas]. Impact of the ASCAT scatterometer winds on the HIRLAM analysis quality in case of severe storms. Proceedings of the Estonian Academy of Sciences, 2016, 65, 3, 177–194.

Služenikina, J., Keevallik, S. 2013. Winds in the Gulf of Riga from QuikSCAT and ground-based measurements. International Journal of Remote Sensing, 34 (16), 5731–5747.

Služenikina, J., Männik, A. 2011. A comparison of ASCAT wind measurements and the HIRLAM model over the Baltic Sea. Oceanologia, 53 (1, SI), 229–244.

7. Kaitstud lõputööd

Magistrikraad, 2009. Satelliidipõhine hetkennustussüsteem Eesti Meteoroloogia ja Hüdroloogia Instituudis, Tallinna Tehnikaülikool, TTÜ Meresüsteemide Instituut.

Diplomitöö, 2002. Eesti Meteoroloogia ja Hüdroloogia Instituudis töötava ilmaennustusmudeli HIRLAM sademete prognooside hindamine, Eesti Mereakadeemia.

CURRICULUM VITAE

1. Personal data

Name Jekaterina Služenikina (Serebrijan)
 Date and place of birth 26.05.1983, Moldova
 Citizenship Estonia
 E-mail address lisjusha@gmail.com

2. Education

Educational institution	Graduation year	Education (field of study/degree)
Tallinn University of Technology	2009	Earth Sciences/master's degree
Estonian Maritime Academy	2006	Hydrometeorology and Environmental Protection/higher professional education
Maardu Gymnasium	2002	Secondary education

3. Language competence/skills (fluent, average, basic skills)

Language	Level
Russian	Native language
Estonian	Fluent
English	Average

4. Special courses

Period	Educational or other organisation
25 February 2014 – 21 January 2015	“Satellite Meteorology Training Course funded by EUMETSAT Training Placement Scheme” EUMETSAT/ESTEA
05–09 December 2011	“Applications of Satellite Wind and Wave Products for Marine Forecasting” EUMETSAT/IODE
09–13 June 2008	“International Training – Seminar on Satellite Meteorology” DWD

12–14 May 2008	“Using Satellite Data In Forecasting Severe Weather Events” EUMETSAT/EMHI
16–27 October 2006	“WMO/CGMS Virtual Laboratory High Profile Training Event” WMO

5. Professional Employment

Period	Organisation	Position
2006-...	Estonian Environment Agency	Head specialist of numerical modelling department

6. Research activity, including honours and theses supervised

Služenikina, J., Männik, A. [accepted for publication]. Impact of the ASCAT scatterometer winds on the HIRLAM analysis quality in case of severe storms. Proceedings of the Estonian Academy of Sciences, 2016, 65, 3, 177–194.

Služenikina, J., Keevallik, S. 2013. Winds in the Gulf of Riga from QuikSCAT and ground-based measurements. International Journal of Remote Sensing, 34 (16), 5731–5747.

Služenikina, J., Männik, A. 2011. A comparison of ASCAT wind measurements and the HIRLAM model over the Baltic Sea. Oceanologia, 53 (1, SI), 229–244.

7. Defended theses

Master’s degree, 2009. Satellite-based nowcasting system in Estonian Meteorological and Hydrological Institute. Tallinn University of Technology, Marine Systems Institute.

Diploma work, 2002. Verification of HIRLAM precipitation forecasts. Estonian Maritime Academy.

APPENDIX A: PAPERS

Paper I

Služenikina, J., Keevallik, S. 2013. Winds in the Gulf of Riga from QuikSCAT and ground-based measurements. *International Journal of Remote Sensing*, 34 (16), 5731–5747.

Winds in the Gulf of Riga from QuikSCAT and ground-based measurements

Jekaterina Služenikina^{a*} and Sirje Keevallik^b

^aEstonian Meteorological and Hydrological Institute, Tallinn 10616, Estonia; ^bMarine Systems Institute, Tallinn University of Technology, Tallinn 12618, Estonia

(Received 30 March 2012; accepted 31 January 2013)

This article presents an overview of marine winds in the Gulf of Riga, measured by the SeaWinds instrument on the Quick Scatterometer (QuikSCAT) satellite during the whole lifetime period of the satellite, i.e. 1999–2009. The data were collected with a resolution of 12.5 km during the satellite overflights at 02–04 UTC and 16–18 UTC and referenced to the height of 10 m. The quality of the data was carefully checked, and necessary adjustment was applied to remove the contaminated recordings. Wind speed and direction were compared with those registered on the islands of Kihnu and Ruhnu. It has been shown that allowing lenient filtering of rain-contaminated data derives larger wind speed estimates but increases considerably the quantity of data, allowing separate analysis of the northern and southern parts of the gulf. Wind speed in the northern part is slightly higher, the wind roses for the early morning measurements are similar, but those for the evening measurements show that in spring and summer, the most frequent winds in the southern part are northwesterly and in the northern part are westerly. Wind speed measured on the islands is less than that estimated from the satellite even in the case when rain contamination is removed through application of strict criteria. Wind roses measured at Kihnu are practically similar to those estimated from satellites for the northern part of the gulf in the evening but show some differences during the early morning. In winter, ground-based measurements show maximal frequency of southerly winds, and satellite measurements show southwesterly winds. In spring, the secondary maximum in the wind rose shows northwesterly winds in ground-based records and easterly winds in satellite measurements. Ground-based wind directions are well correlated with those measured by the satellite showing correlation coefficients of over 0.9. For wind speed, this quantity is somewhat lower, i.e. around 0.6.

1. Introduction

It is widely known that satellite measurements offer the best spatial coverage to describe properties of the underlying surface and atmosphere. This is also valid for near-surface wind data, especially in marine areas where *in situ* wind measurements are quite sparse. Related to the events of dangerous combinations of high sea level and wave height (Suursaar et al. 2006), winds over the Gulf of Riga are of special interest.

The Gulf of Riga is a relatively closed, almost circular eastern sub-basin of the Baltic Sea. It has two openings – the Irbe Strait (with a sill depth of 25 m and a minimum cross-section area of 0.4 km²) in the west and the Virtsu Strait (with a sill depth of 5 m and a minimum cross-section area of 0.04 km²) in the north. The gulf has a surface area of

*Corresponding author. Email: jekaterina.sluzenikina@emhi.ee

14,000 km², a volume of 408 km³, a mean depth of 29 m, and a maximum depth of 55 m (Raudsepp, Beletsky, and Schwab 2003).

Marine winds measured by satellites give information about the wind speed and direction at 10 m height for the grid of defined resolution and coverage during the lifetime of the instrument. For the study of marine wind climatology in a relatively small area (Gulf of Riga), it was necessary to use high-resolution winds with the longest period of measurements. The highest resolution of 25 km with a grid spacing of 12.5 km was used for the ASCAT (Advanced Scatterometer) and SeaWinds instruments on board the MetOp (Meteorological Operational) and Quick Scatterometer (QuikSCAT) satellites. The ASCAT data usage in the Baltic Sea area has good potential for operational use (Služenikina and Männik 2011); however the wind data are available only from 2006. The longest data series for the current study has been from the QuikSCAT satellite launched on 19 June 1999, operated by the Jet Propulsion Laboratory (JPL) and managed by the National Aeronautic and Space Administration (NASA).

QuikSCAT is a polar-orbiting satellite with the SeaWinds scatterometer on board, whose primary objective is to measure ocean surface winds globally over ice-free areas in all weather conditions. QuikSCAT is in polar orbit approximately 800 km (500 miles) above the Earth's surface. The satellite completes its orbit in 101 min, and as this orbit migrates around the Earth, each ocean region is flown over once every 12 hours (Pickett et al. 2003). The SeaWinds scatterometer is an active microwave instrument that senses the roughness of the ocean surface by measuring the signal backscattered by the capillary waves generated by surface wind stress. By viewing the same ocean surface from several different azimuth angles, the ocean surface wind speed and direction can be obtained (Smith, Wentz, and Mears 2002). The SeaWinds instrument on the QuikSCAT satellite is a conical-scanning, pencil-beam scatterometer. It uses a rotating 1 m dish antenna with two spot beams, a horizontally polarized (H-pol) beam and a vertically polarized (V-pol) beam at incidence angles of 46° and 54°, respectively, that sweep in a circular pattern (see Figure 1). The antenna radiates microwave pulses at a frequency of 13.4 GHz (Ku-Band)

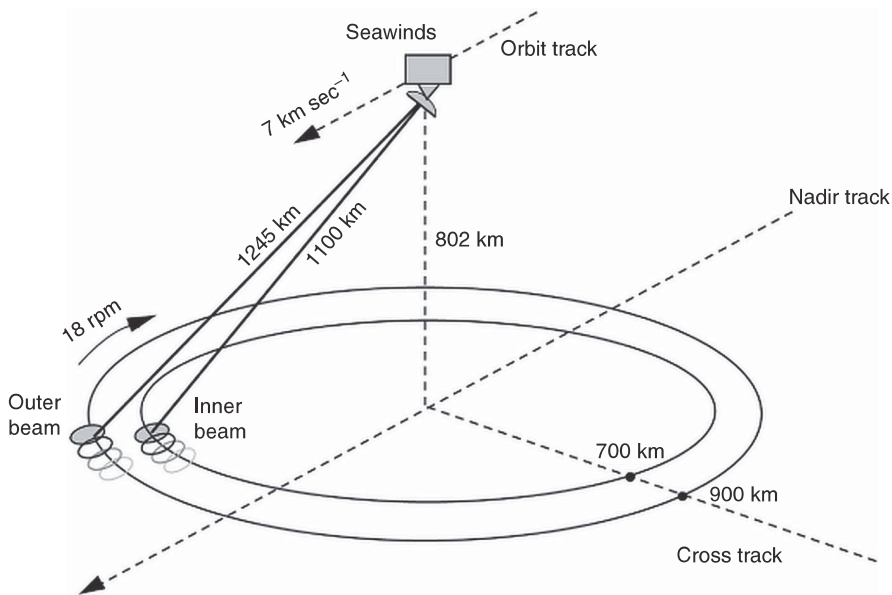


Figure 1. SeaWinds viewing geometry (Spencer, Wu, and Long 2000).

across a 1800 km wide swath centred on the spacecraft's nadir sub-track, making approximately 1.1 million 25 km ocean surface wind vector measurements and covering 90% of the Earth's surface every day (Portabella and Stoffelen 2002). However, because of the satellite's limited viewing area and the Earth's rotation, various sections of the coastal zone are only observed every few days (Pickett et al. 2003).

The SeaWinds backscatter (σ_0) measurements are collected over special equidistant wind vector cells (WVCs) with a grid resolution of $25 \times 25 \text{ km}^2$ and $12.5 \times 12.5 \text{ km}^2$. The QuikSCAT wind speed is referenced to the height of 10 m, and it is defined as neutral wind – the equivalent wind obtained with the stress and roughness length consistent with the atmospheric stratification when the stability adjustment is set to zero (Nghiem et al. 2004). The 12.5 km resolution level 2B winds are produced from 'slices' of the ellipsoidal instantaneous antenna footprint with a simplified backscatter averaging scheme and different land contamination criteria that are particularly useful to resolve the coastal winds (Tang, Liu, and Stiles 2004). In the standard QuikSCAT data product, slices from overlapping current and previous across-track sweeps of the radar beam are then combined and averaged to provide $25 \times 25 \text{ km}$ WVCs. Output is not used if any part of the field of view is contaminated by land, so QuikSCAT wind data are masked and, therefore, not available within 30 km of the coast (Pickett et al. 2003). Owing to conical scanning, a WVC is generally viewed when looking forward (fore) and a second time when looking aft. As such, up to four measurement classes emerge: H-pol fore, H-pol aft, V-pol fore, and V-pol aft, in each WVC (Portabella and Stoffelen 2002). The SeaWinds backscattered values registered at different azimuth and incidence angles are then converted to wind speed and wind direction. Wind stress over the ocean generates ripples and small waves, which roughen the sea surface. These waves modify the radar cross section (σ_0) of the ocean surface and hence the magnitude of backscattered power. To extract wind velocity from these measurements, one must know the relationship between σ_0 and near-surface winds – this relationship is known as the geophysical model function (Lungu and Callahan 2006).

The geophysical model function is used to transform backscattered signals from the sea surface into wind speed and wind direction at each WVC. Multiple measurements at different azimuth angles give a solution of wind vectors to remove ambiguities appearing at each WVC. The wind retrieval algorithm computes a set of wind vectors together with their relative likelihoods for each WVC. According to Bayes' theorem, the maximum likelihood estimation (MLE) value represents the probability of a trial wind vector (solution) being the 'true' wind. The SeaWinds optimization technique consists of looking for the minima, which represent the local solutions with maximum probability of being the true wind (Portabella and Stoffelen 2004). The solution closest to the true wind is called the 'closest' solution, and all the wind vector solutions found in each WVC are referred to as 'ambiguities'. The objective of the ambiguity removal algorithm is to choose the closest solution from the list of ambiguities (Lungu and Callahan 2006). MLE incorporates the numerical weather prediction (NWP), by the National Centers of Environmental Prediction (NCEP), output as the initial field, or 'first guess', to choose the best solution (nudging technique). The NWP wind field is spatially interpolated, and the 2.5° resolution 1000 mbar ($\approx 100 \text{ m}$) global data analysis model outputs closest in time to the QuikSCAT pass are chosen (Sharma and D'Sa 2008). It should be noted that the NWP winds used in the ambiguity removal algorithm are about 100 m above the sea level, while the QuikSCAT winds are 10 m neutral winds, and the difference in reference height may bring some uncertainty. In addition to the general ambiguity removal, some special techniques are applied for wind direction retrieval due to ambiguities appearing at different viewing angles during the scatterometer measurements.

Note that, unlike the fan-beam systems, the azimuth angle ‘mix’ of the σ_0 measurements going into the wind retrieval is not constant but varies from nadir out to the edge of the swath. Near nadir the forward and aft measurements are approximately 180° apart, while at the extreme edge of the swath, the azimuth angle between the measurements approaches 0° . Thus, the wind retrieval performance of SeaWinds is observed to vary as a function of the distance from the nadir track, which is generally optimum when the azimuth differences of the measurements are near 90° (Tsai et al. 2000). As a result, near nadir, due to non-optimal measurement geometry, there is a marked decrease in directional accuracy even when ambiguity removal works correctly. Two algorithms were developed, direction interval retrieval (DIR), to address the nadir performance issue, and threshold nudging (TN), to improve ambiguity removal at far swath (Stiles 1999). Both algorithms work independently and are used together to obtain the direction interval retrieval threshold nudging (DIRTH) solutions in the Level 2B product (Lungu and Callahan 2006). More information about the DIRTH algorithm can be found in Stiles (1999).

2. QuikSCAT data quality

The QuikSCAT wind data are in general of high quality; however, the accuracy of scatterometer winds can be affected by different factors, such as land, ice, and rain contamination, and very strong or very weak winds. The accuracy of the QuikSCAT 25 km product is required to have a root mean square error (RMSE) of less than 2 m s^{-1} in a wind speed interval of $3\text{--}30 \text{ m s}^{-1}$ or 10% in the interval of $20\text{--}30 \text{ m s}^{-1}$, and the wind direction RMSE is required to be less than 20° ($3\text{--}30 \text{ m s}^{-1}$) (Lungu and Callahan 2006). The buoy comparison with 25 km QuikSCAT winds by Stoffelen, Vogelzang, and Verhoef (2010) show similar results. The QuikSCAT winds weaker than 3 m s^{-1} or higher than 30 m s^{-1} are generally flagged as low or high wind speed. At light winds, for example, the uncertainties of wind retrievals are higher as the smoother sea surface appears more as a reflector than as a scatterer. Rain changes the roughness of the sea surface and attenuates measurements by acting as an opaque barrier for the radar signal and can artificially increase satellite wind speed data (Sharma and D’Sa 2008). In addition, direction errors decrease with increasing wind speed (Hoffman and Leidner 2005). Therefore, it is not recommended to analyse winds weaker than 1 m s^{-1} .

Rain is known to both attenuate and backscatter the microwave signal, affecting the quality of wind measurements. Rain drops are small compared to radar wavelengths and cause Rayleigh scattering (inversely proportional to the fourth power of the wavelength) (Portabella and Stoffelen 2002). In the presence of large rain drops, the impact is higher and the ‘splashing’ effect occurs. The roughness of the sea surface is increased because of splashing due to rain drops. This increases the radar backscatter (σ_0) measured, which in turn will affect the quality of wind speed (positive bias due to σ_0 increase) and direction (loss of anisotropy in the backscatter signal) retrievals (Portabella and Stoffelen 2002). In addition, as the rain rate increases, the space-borne instrument sees less and less of the radiation emitted by the surface and increasingly sees the radiation emitted by the rainy layer that becomes optically thick due to volumetric Rayleigh scattering (Portabella and Stoffelen 2002).

Several algorithms have been developed to detect rain-contaminated data for rain-flagging: normalized object function (NOF) rain flag (Mears et al. 2000) and multidimensional histogram (MUDH) rain flag (Huddleston and Stiles 2000a, 2000b). Both techniques are included for detecting rain contamination in the QuikSCAT Level 2B data; however, the impact-based MUDH (IMUDH) algorithm is used in the processing of Level 2B JPL

data; the NOF is incorporated as an additional parameter into the wind dataset (Lungu and Callahan 2006). The new IMUDH rain probability does not flag a specific rain rate, but a likelihood that the wind speed is perturbed by more than 2 m s^{-1} or the direction by more than 15° . The previous MUDH gave the probability of encountering a columnar rain rate that is greater than 2 km mm h^{-1} (Lungu and Callahan 2006). The new IMUDH algorithm is developed for 25 km Level 2B data, and in the case of the 12.5 km product, the IMUDH algorithm is applied to the corresponding cells only. The primary improvement of IMUDH over MUDH is in the reduction of the overflagging of high wind speeds and the removal of swath artefacts including overflagging in the outer swath (Lungu and Callahan 2006). Instead of flagging for rain, the IMUDH algorithm flag detects rain contamination of wind data and, as a result, flags fewer high winds and fewer overall (Stiles, Veleva, and Dunbar 2006). In addition, the NOF rain flag validation by Mears, Wentz and Smith (2000) showed that the NOF rain flag removes erroneous wind vectors almost as effectively as the Special Sensor Microwave Imager (SSM/I) collocated rain measurements, but does not require an SSM/I collocated measurement.

In general, rain contamination of QuikSCAT data causes two main effects, (1) higher derived wind speeds in low wind fields and (2) the presence of wind vectors, turned perpendicular to the satellite track in high wind and rain locations (referred to as cross-track winds) (Smith, Wentz, and Mears 2002). These two indicators of wrong wind speed and direction are used in operational forecasting when the rain-flagging technique is turned off to get more wind observations inside tropical or extra-tropical cyclones.

3. Data and methods

The QuikSCAT wind data used in this work were obtained from the Physical Oceanography Distributed Active Archive Centre (PO.DAAC) during the period of 6 October 2011 to 4 November 2011 from <http://podaac-ftp.jpl.nasa.gov/OceanWinds/quikscat/L2B12>; data are freely available worldwide and can be downloaded via file transfer protocol.

Level 2B QuikSCAT data at PO.DAAC present at 25 and 12.5 km grid resolution. For the Gulf of Riga, 12.5 km gridded ocean wind vectors were obtained from hierarchical data format and converted to ASCII by a FORTRAN program provided with the PO.DAAC data set. The wind direction conversion was also necessary due to the non-conventional wind direction detection of the QuikSCAT winds. For example, in the QuikSCAT data, the wind direction of 0° means the northward wind instead of the meteorological northerly direction.

The usage of a high-resolution data set is important for research of winds near the shoreline, which significantly increases the number of datapoints in a relatively small area of interest. Spatial resolution is particularly important to resolve the high variability of coastal winds under the influence of land. In standard QuikSCAT data processing, measurements with any part of its footprint touching land are excluded in the wind retrieval. This results in a data gap within 25 km from the shoreline (Tang, Liu, and Stiles 2004). That is why the high resolution 12.5 km winds were used.

At the first step of the wind data analysis, the wind vectors were selected geographically (57° N – 58.5° N , 22.5° E – 24.5° E). The period of acquired data is 1999–2009; however, the year 2003 was eliminated due to the large number of missing values. In addition, the year 1999 started on 1 August and the year 2009 lasted till the end of October. As previously noted, the measurements in the Gulf of Riga were from two time intervals: 02–04 UTC and 16–18 UTC. The satellite samples from the Gulf of Riga were at only two local times. The question arises how representative are these estimates for all winds. The daily cycle of the wind speed depends on the site and the season. Off-shore winds are characterized by a weak daily cycle. Therefore, an examination of the wind speed twice a day should

provide a sufficiently adequate picture. The amplitude of the wind speed (maximal minus minimal during a day) expressed as a fraction of the daily average value is negligible in winter at both measurement sites, up to 6% at Kihnu and up to 19% at Ruhnu in summer. These estimates are drawn from ground-based measurements during the period 1966–2005 (Žukova 2009).

The next step of data preparation is the usage of specially defined wind data with the chosen quality flags. For this reason, the data were filtered out by quality flags at each WVC. The data-flagging technique is described in the QuikSCAT science data product user's manual by Lungu and Callahan (2006). The winds used for this study possess good σ_0 values for wind retrieval (Lungu and Callahan 2006), without the presence of ice, but in some cases with land contamination. Although the coastal flag presence means that some portion of the WVC is over the land and it may indicate noisy wind measurements, elimination of these data significantly reduces the number of datapoints in the small area near the coastline. A difference when using high-resolution (12.5 km) data is that the slice data may not fall on land while another fraction or part of the cell data may fall on land. Thus, the high-resolution data have a lesser impact due to land effects and can be used to obtain winds closer to land (Nghiem et al. 2004).

Then the data with low wind speed flag (less than 3 m s^{-1}) and high wind speed flag (greater than 30 m s^{-1}) were eliminated due to some of the factors influencing the quality of data mentioned previously. According to rain contamination, two methods were used: (1) conservative elimination of all rain-contaminated data detected by the IMUDH algorithm and (2) more lenient filtering of rain-contaminated data.

In the case of conservative elimination (strict criteria), two data quality flags were chosen: Bit 12 – ‘Rain Flag Usable’ and Bit 13 – ‘Rain Flag’. The filtering of the wind data by strict criteria works when the IMUDH algorithm can provide a reasonably accurate estimate of the probability of the rain and the rain probability is detected. For more lenient rain filtering, we used special thresholds: MUDH less than 0.2 and NOF index of less than 50 as done by Kleiss et al. (2010).

Both methods of rain flagging were used in this study to compare the results. A more lenient method was used to increase the number of datapoints, especially for the northern part in the Gulf of Riga, where the number of observations were significantly decreased after first filtering, as shown in Figures 2(a) and (b). The major elimination of datapoints took place in the areas where the IMUDH algorithm was not usable because of land contamination or insufficient data provided for the quality estimate. The total number of datapoints in the Gulf of Riga with more lenient criteria is shown in Table 1.

In addition to satellite measurements, two wind observational stations have been used during the same period as the QuikSCAT measurements. Observational stations are located on the islands Kihnu ($58^\circ 06' \text{ N}$, $23^\circ 58' \text{ E}$) and Ruhnu ($57^\circ 47' \text{ N}$, $23^\circ 15' \text{ E}$), as shown in Figure 2. The winds are reported every 3 hours at 00, 03, 06, 09, 12, 15, 18, and 21 UTC. The wind speed is a 10 minute average value before the observation time and the wind direction is a two minute average accordingly.

4. Results

4.1. Analysis with strict criteria

The analysis of the wind field was focused on seasonal histograms of wind speed and direction for the two time intervals described previously (02–04 UTC and 16–18 UTC). While interpreting the data, one must keep in mind that wind speeds $<3 \text{ m s}^{-1}$ are not considered. The results show that the wind is the strongest in winter and autumn, when

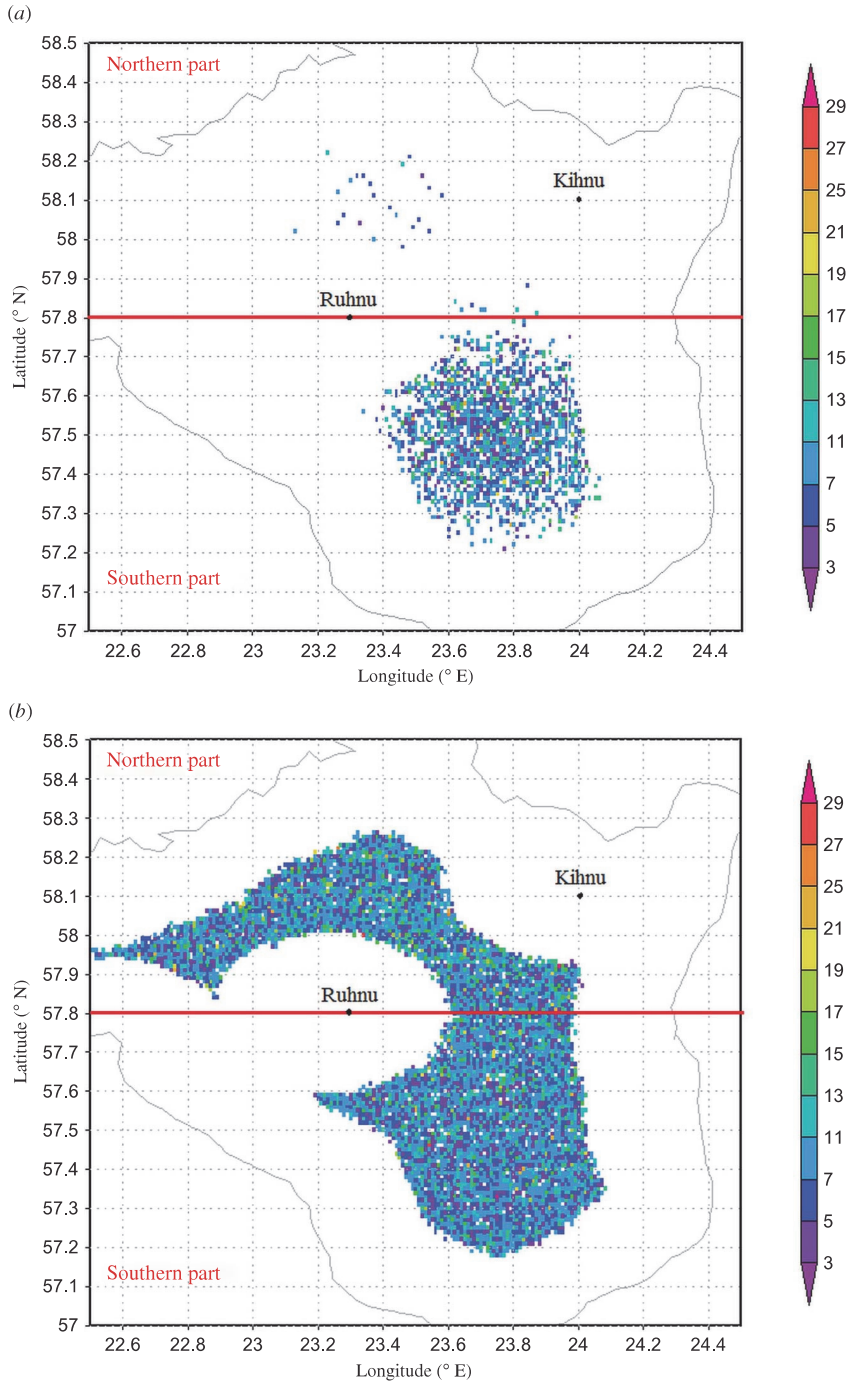


Figure 2. The coverage of QuikSCAT measurements for January 1999–2009 with strict criteria (a) and more lenient criteria (b).

Table 1. Number of datapoints by month and year with more lenient criteria.

	1999	2000	2001	2002	2003	2004	2005	2006	2007	2008	2009
Jan	0	2156	2183	2154	0	2167	2192	2085	2197	2165	2045
Feb	0	1941	1930	1828	0	1875	1933	602	1930	2006	1861
Mar	0	1854	1948	1833	0	1341	582	257	1697	2084	2051
Apr	0	1332	1488	1596	0	1622	1708	1243	1828	1394	1508
May	0	1809	1721	1574	0	1886	1579	1659	1526	1770	1810
June	0	1789	1663	1844	0	1584	1752	1734	1693	1777	1767
July	0	1723	1681	1711	0	1863	1762	1489	1876	1800	1765
Aug	1905	2054	1978	1617	0	1815	1971	1976	1656	1962	1626
Sep	1679	1795	1760	1861	0	1979	1933	1839	1832	1928	1778
Oct	2292	2198	2121	2171	0	2107	2002	2121	1849	2139	1520
Nov	2039	1937	1975	1938	0	2073	2168	1961	1848	1876	0
Dec	2287	2183	2052	2101	0	2122	2096	2192	2104	2108	0

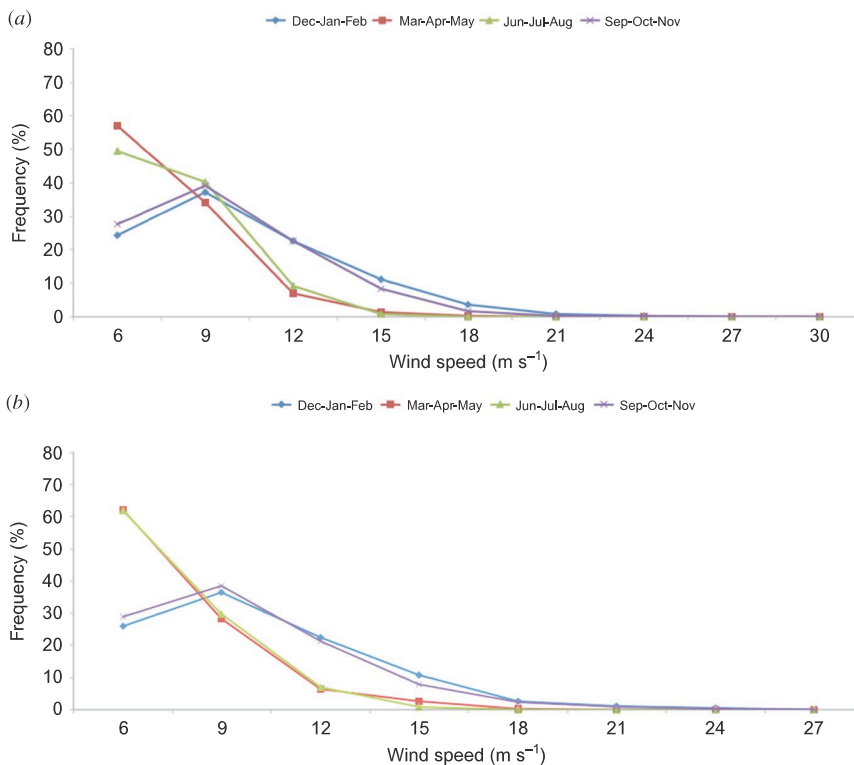


Figure 3. Wind speed seasonal histogram at 02–04 UTC (a) and 16–18 UTC (b).

prevailing wind speed V is $6 < V \leq 9 \text{ m s}^{-1}$ (see Figures 3(a) and (b)). In spring and summer, the most frequent wind speed is $3 \leq V \leq 6 \text{ m s}^{-1}$, in more than 50% of cases, while in the evening the frequency of those winds is somewhat higher.

The mean wind speed values (m s^{-1}) at different times of measurement are shown also in Table 2.

When the wind directions for different seasons at different measurements of time (see Figures 4(a) and (b)) were compared, some differences were observed. In winter and

Table 2. Average seasonal QuikSCAT wind speed (in this case, winds $<3 \text{ m s}^{-1}$ are not considered) with strict criteria (02–04 UTC and 16–18 UTC).

Time interval	Winter	Spring	Summer	Autumn
02–04 UTC	8.6	6.0	6.3	8.1
16–18 UTC	8.5	5.8	5.8	8.1

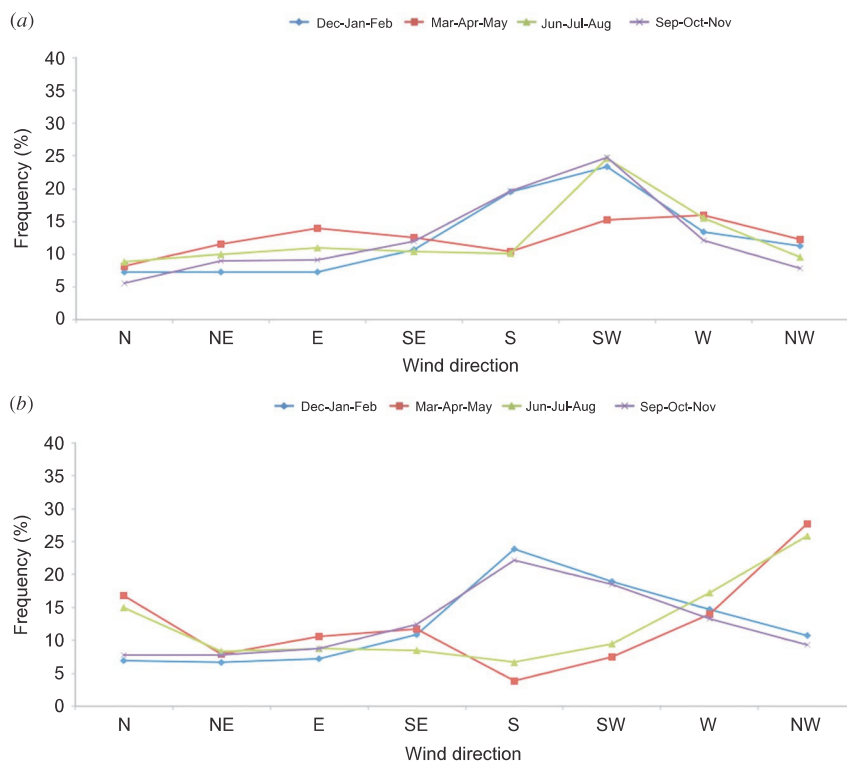


Figure 4. Wind direction seasonal histogram (wind rose) at 02–04 UTC (a) and 16–18 UTC (b).

autumn, the most frequent wind direction is southerly or southwesterly with minor differences between morning and evening recordings: At 02–04 UTC, southwesterly winds prevail and, at 16–18 UTC, southerly winds dominate. In spring, the prevalence of southwesterly and westerly winds is weakly expressed only in the morning wind rose, but the evening wind rose is highly anisotropic, showing 27% of northwesterly winds and 17% of northerly winds, while southerly winds are very seldom. The same feature can be noticed in summer with the exception that the morning wind rose shows a sharp maximum (25%) in the frequency of southwesterly winds.

4.2. Analysis with more lenient criteria

For a more detailed analysis of the wind speed distribution and the wind direction differences in the Gulf of Riga, the area of interest was divided into a northern part (57.8° N – 58.5° N) and a southern part (57° N – 57.8° N). When the wind speed distribution in these areas (not shown here) is compared with the wind speed chosen on the basis

Table 3. Average seasonal wind speed (in this case, winds $<3 \text{ m s}^{-1}$ are excluded) with more lenient criteria (02–04 UTC and 16–18 UTC).

Gulf of Riga	Time interval	Winter	Spring	Summer	Autumn
Northern part	02–04 UTC	9.1	6.7	6.6	8.4
	16–18 UTC	9.1	6.7	6.6	8.6
Southern part	02–04 UTC	8.7	6.3	6.6	8.3
	16–18 UTC	8.7	6.3	6.3	8.1

of strict criteria, no significant difference was found. The average wind for both areas is somewhat stronger than that without in the absence of rain (see Tables 2 and 3); however, the maximum difference between the values is not more than 0.9 m s^{-1} . This seems to be due to more lenient filtering of rain-contaminated data. The winds in the northern part are slightly stronger than those in the southern part.

The wind direction frequency distributions in the southern part of the gulf obtained by means of lenient criteria are similar to those for the whole gulf obtained by means of strict criteria (see Figure 4). This is understandable as the data for the analysis with strict criteria come mostly from the southern part (see Figure 2). The same can be said for the northern part during the early morning, but the evening frequency distributions are somewhat different: in winter and autumn, the differences are not noticeable, but in spring and summer the most frequent winds in the northern part are westerly and in the southern part are northwesterly (see Figures 5 and 4(b)).

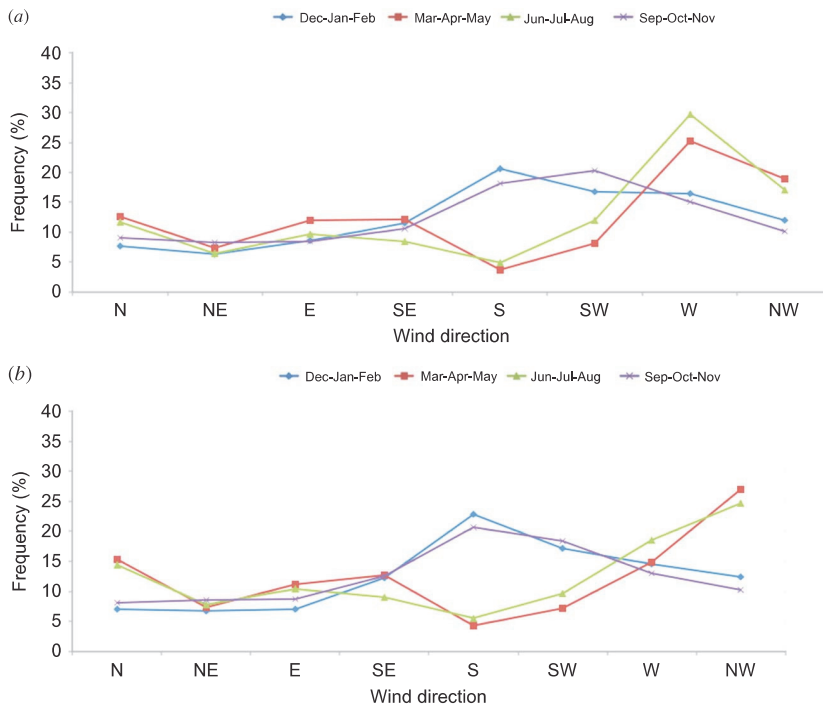


Figure 5. Wind direction seasonal histogram (wind rose) in the Gulf of Riga northern part (a) and southern part (b) at 16–18 UTC.

4.3. Wind measurements on the islands

For comparison of satellite measurements with Kihnu and Ruhnu data, the winds at 03 and 18 UTC are used. Table 4 shows that the winds on both islands are weaker. The elevation of the Kihnu station is 3 m above sea level and that of the Ruhnu station is 2 m. The major obstruction on the islands is the pine forest, which may cause a decrease of wind speed due to uniform friction on the land. Wind was measured at both sites at a height of 10 m.

As presented in the paper by Keevallik, Männik, and Hinnov (2009), Kihnu observational station is sheltered from the north and northeast directions and only partly open from the east, southeast, and northwest directions. On Ruhnu, the winds are totally sheltered from the north and northwest and partly from the northeast and west direction. As a result, the average wind speed is reduced. The higher difference between satellite winds and winds at the stations occurs in the period of the strongest winds, winter and autumn. Domination of weaker winds is more evident in the wind speed histograms in Figures 6(a) and (b) where, almost in all seasons, the prevailing winds are between 3 and 6 m s⁻¹. At the same time, the satellite measured 30–40% of all winds between 6.1 and 9 m s⁻¹ practically in all seasons with the maximum in winter and autumn. In addition, the wind speed STDEV shows that the higher wind speed variation appears in winter and autumn seasons both measured at ground-based stations and at the satellite. The wind speed variation is about 2–3 m s⁻¹.

Comparing the results with the wind direction on Kihnu and Ruhnu, it was noticed that in the evening Kihnu and Ruhnu wind directional histograms are very similar; only some slight quantitative differences can be seen in the northerly and northeasterly directions; therefore the histogram of Ruhnu is not shown here. In addition, Ruhnu observations at 03 UTC were not available. The Kihnu station is situated in the northern part of the Gulf, and therefore the comparison with the satellite is done with the same area.

The results show that in the morning measurements in winter at Kihnu more frequent winds are southerly, whereas the frequency of southwesterly and westerly winds is slightly less (see Figure 7(a)). The QuikSCAT measured more than 20% of southwesterly winds. In spring, the morning measurements at Kihnu show equal frequency of southwesterly, southerly, and westerly winds (about 15% of each); the satellite also measured southwesterly and westerly winds with the same value of frequency, but southerly winds were less frequent. Attention should be drawn to the secondary maximum in spring that is typical to

Table 4. Average seasonal wind speed (in this case, winds <3 m s⁻¹ are not considered) and the wind speed standard deviation (STDEV) estimated from the satellite data (with strict criteria) and measured at the meteorological stations.

Season		Kihnu 03 UTC	Satellite 02–04 UTC	Kihnu 18 UTC	Ruhnu 18 UTC	Satellite 16–18 UTC
Winter	Mean	7.6	8.6	7.6	7.0	8.5
	STDEV	3.1	3.4	3.2	2.9	3.5
Spring	Mean	5.5	6.0	5.4	5.0	5.8
	STDEV	2.2	2.2	2.4	1.9	2.3
Summer	Mean	6.0	6.3	5.8	5.3	5.8
	STDEV	2.4	2.1	2.5	2.0	2.1
Autumn	Mean	7.3	8.1	7.5	6.8	8.1
	STDEV	2.9	3.1	3.1	2.6	3.2

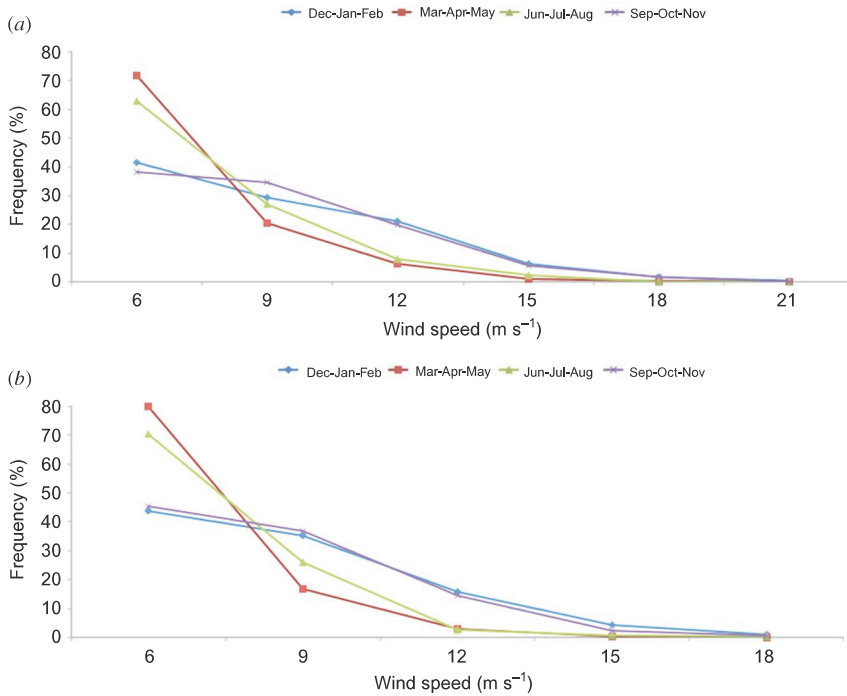


Figure 6. Wind speed seasonal histogram (wind rose) on Kihnu (a) and Ruhnu (b) at 18 UTC.

the wind roses of the Baltic Sea area. Ground measurements show this for northwesterly winds, and satellite measurements for easterly winds.

In the evening recordings at Kihnu in summer, the frequency of the westerly winds is more than 35%, whereas the satellite measures a frequency of less than 30%.

4.4. Correlation between ground-based and satellite measurements

To find out the correlation between ground-based and satellite measurements, the closest QuikSCAT recordings to Kihnu station were chosen. For the cases shown in Figures 8 and 9, the correlation coefficient for wind direction was 0.94 in summer and 0.95 in winter. During the calculation of the correlation coefficients, it was noted that the difference between the measurements did not exceed 180° : formal comparison of wind direction records may lead to the false result that the difference between 359° and 1° is not 2° but 358° . The correlation coefficient for wind speed was somewhat less – around 0.6.

Until 2003, the wind measurements were carried out by means of anemorhumbometer that recorded wind speed with an accuracy of 1 m s^{-1} and wind direction with 10° . In November 2003, manual measurements were replaced by the automatic weather station MILOS 520, which records data with a better resolution. This can be also seen in Figures 8 and 9, where ground-based measurements of the wind speed cluster at the values of 1, 2, and 3 m s^{-1} , etc., and the direction measurements cluster at the values of 10° , 20° , and 30° , etc.

Attention should be paid to the point in Figure 8(a) when the wind speed recorded at Kihnu was 25.2 m s^{-1} and that at the satellite was 24.4 m s^{-1} . This point describes the

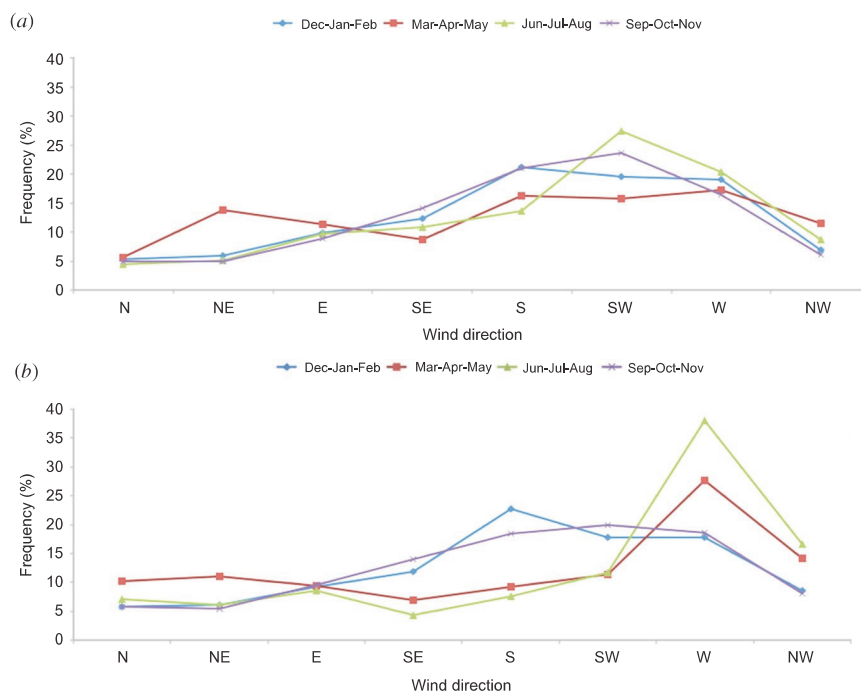


Figure 7. Wind direction seasonal histogram (wind rose) of Kihnu at 03 UTC (a) and 18 UTC (b).

situation on 9 January 2005 when the storm Gudrun devastated the coasts of the Gulf of Riga.

As can be seen in Table 5, the bias of the wind speed (average satellite record minus ground-based record) is positive, larger in winter, and smaller in summer. A positive bias in wind speed can be explained by the reported site obstructions that clearly affect the ground-based measurements but not the satellite measurements. The bias of the wind direction is negligible, but the RMSD estimates exceed the RMSE foreseen by the scatterometer design. It must be taken into account that the coordinates of the measurement sites are not exactly the same, and it cannot be expected that the measurements are carried out simultaneously.

5. Conclusions

As was described in Portabella and Stoffelen (2002), two quality control (QC) techniques were developed for the QuikSCAT data: the JPL and KNMI (Royal Netherlands Meteorological Institute) rain-flagging techniques. The results show that the KNMI QC is more efficient in rejecting low-quality data than the JPL rain flag, while the latter is more efficient in rejecting rain-contaminated data than the former. The JPL rain flag, however, rejects too many consistent wind data in dynamically active areas (Portabella and Stoffelen 2002). In the present study, we did not compare rain-flagged wind results from both JPL and KNMI data. However, a more lenient rain-flagging technique was applied to get many more observations in a relatively small area of the Baltic Sea. The results of the wind analysis show that the strict criteria for the wind speed gave practically the same results as the winds measured at the meteorological stations on the islands, whereas the analysis with

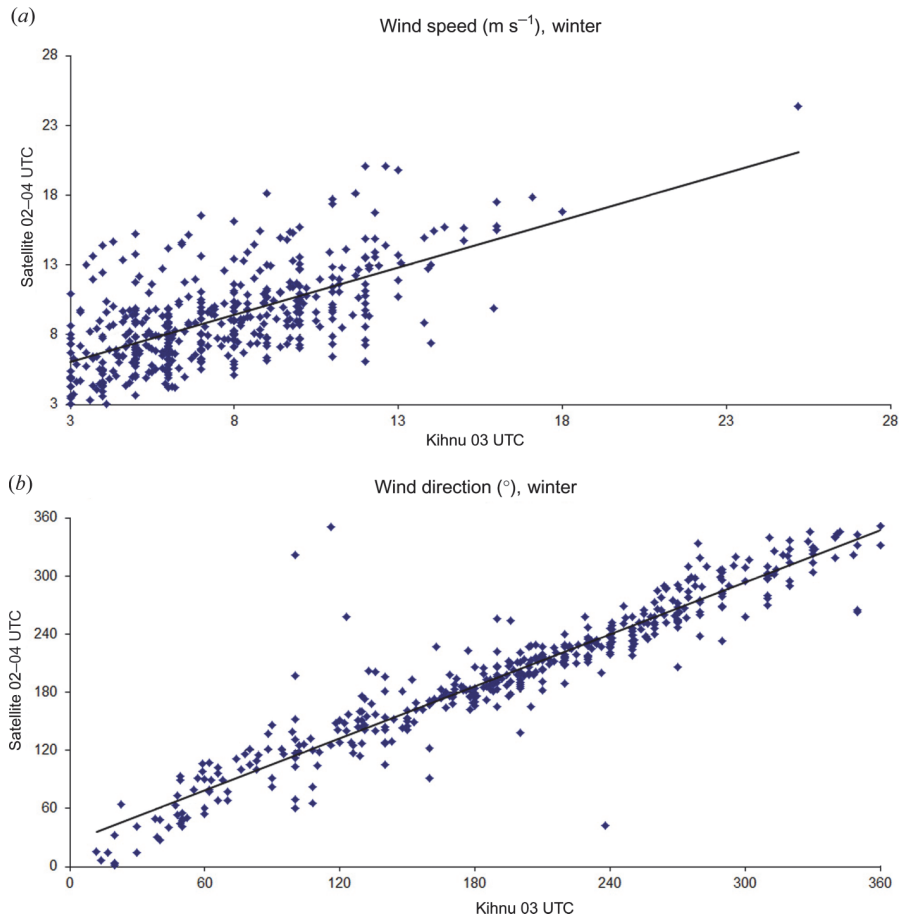


Figure 8. QuikSCAT and Kihnu wind speed (a) and direction (b) scatterplots in winter night.

more lenient criteria showed larger values – up to 0.9 m s^{-1} for the seasonal average. On the other hand, more lenient criteria enlarged essentially the number of datapoints in the area of interest and were a valuable source to describe differences in the wind roses for different parts of the gulf.

The article shows that

- Wind speed in the northern part of the gulf is slightly larger than that in the southern part.
- Wind speed measured at meteorological stations on the islands is less than that estimated from a satellite even in the case when rain contamination is removed through the application of strict criteria.
- Wind roses estimated from satellites for the northern and southern parts of the gulf are similar for the morning (02–04 UTC) data (not shown), but somewhat different in spring and summer for the evening (16–18 UTC) data: the most frequent winds in the southern part are northwesterly and in the northern part are westerly. Wind roses measured at Kihnu are practically similar to those estimated from

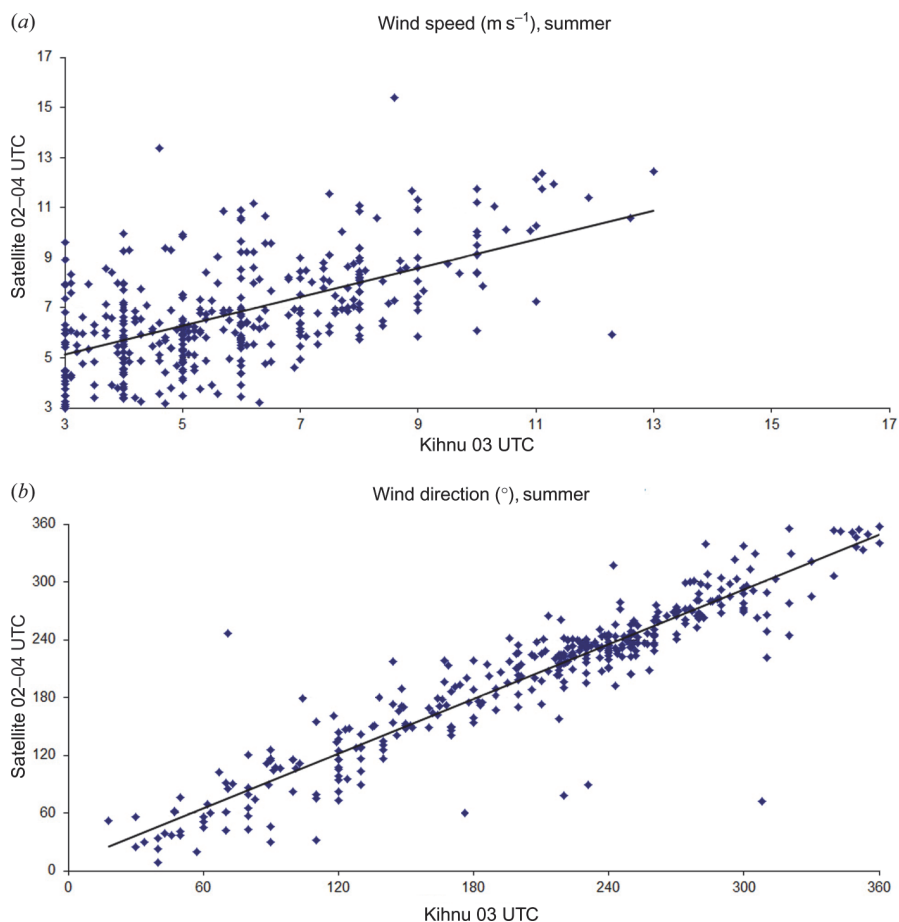


Figure 9. QuikSCAT and Kihnu wind speed (a) and direction (b) scatterplots in summer night.

Table 5. The bias and the root mean square deviation between the satellite and ground-based measurements.

Season		Satellite 02–04 UTC, Kihnu 03 UTC		Satellite 16–18 UTC, Kihnu 18 UTC	
		Speed (m s^{-1})	DIR ($^{\circ}$)	Speed (m s^{-1})	DIR ($^{\circ}$)
Winter	Bias	1.6	3.5	1.6	2.9
	RMSD	3.2	25.0	3.1	25.9
Summer	Bias	0.9	-2.3	0.4	8.5
	RMSD	2.1	29.2	2.6	36.7

satellites for the northern part of the gulf in the evening (16–18 UTC). Early morning (02–04 UTC) wind roses show differences in winter and spring. In winter the wind rose from ground-based measurements shows a maximal frequency of southerly winds, from satellite measurements – southwesterly winds. In spring, a similar difference is detected in the secondary maximum: northeasterly from ground-based measurements to easterly from satellite measurements.

- Correlation between satellite and island measurements is strong for wind direction (over 0.9) and somewhat weaker for wind speed (around 0.6). The weaker correlation for wind speed can be explained by sheltering of the ground-based measurement site or collocation errors.

Acknowledgements

The research is supported by the targeted financing by the Estonian Ministry of Education and Science (grant SF0140017s08) and the GORWIND (The Gulf of Riga as a Resource for Wind Energy) Project financed by the European Regional Development Fund and Estonian Environmental Investment Centre. Ground-based wind data are drawn from the archives of the Estonian Meteorological and Hydrological Institute. The first author is grateful to David Moroni (JPL PO.DAAC Ocean Wind and Scatterometry Data Engineer) for valuable consultations.

References

- Hoffman, R. N., and S. M. Leidner. 2005. "An Introduction to the Near-Real-Time QuikSCAT Data." *Journal of Weather and Forecasting* 20: 476–493.
- Huddleston, J. N., and B. W. Stiles. 2000a. "A Multidimensional Histogram Rain-Flagging Technique for SeaWinds on QuikSCAT." In *Geoscience and Remote Sensing Symposium (IGARSS)*, Honolulu, HI, July 24–28, 1232–1234.
- Huddleston, J. N., and B. W. Stiles. 2000b. *Multidimensional Histogram (MUDH) Rain Flag*. Accessed March 13, 2012. ftp://podaac-ftp.jpl.nasa.gov/OceanWinds/quikscat/L2B12/docs/MUDH_Description_V3.pdf
- Keevallik, S., A. Männik, and J. Hinnov. 2009. "Comparison of HIRLAM Wind Data with Measurements at Estonian Coastal Meteorological Stations." *Journal of Earth Sciences* 59: 90–99.
- Kleiss, J., K. Kelly, L. Thompson, and S. Dickinson. 2010. "A Comparison of QuickSCAT Winds to In Situ Observations in the Western Boundary Current Regions." In *2010 International Ocean Vector Winds Meeting*, Barcelona, May 18–20. Accessed March 13, 2012. http://coaps.fsu.edu/scatterometry/meeting/docs/2010_may/calval/kleiss.pdf
- Lungu, T., and S. Callahan. 2006. *QuikSCAT Science Data Product User's Manual*. Accessed March 13, 2012. ftp://podaac-ftp.jpl.nasa.gov/OceanWinds/quikscat/L2B12/docs/QSUG_v3.pdf
- Mears, C., F. Wentz, and D. Smith. 2000. *Special Product: SeaWinds on QuikScat Normalized Objective Function Rain Flag*, 1–13. Santa Rosa, CA: Remote Sensing Systems. Accessed March 15, 2012. ftp://podaac-ftp.jpl.nasa.gov/OceanWinds/quikscat/L2B12/docs/NOF_Description_V1.2.pdf
- Nghiem, S. V., G. A. Leshkevich, and B. W. Stiles. 2004. "Wind Fields over the Great Lakes Measured by the SeaWinds Scatterometer on the QuikSCAT Satellite." *Journal of Great Lakes Research* 30: 148–165.
- Pickett, M. H., W. Tang, L. K. Rosenfeld, and C. H. Wash. 2003. "QuikSCAT Satellite Comparisons with Near Shore Buoy Wind Data off US West Coast." *Journal of Atmospheric and Oceanic Technology* 20: 1869–1879.
- Portabella, M., and A. Stoffelen. 2002. "A Comparison of KNMI Quality Control and JPL Rain Flag for SeaWinds." *Canadian Journal of Remote Sensing (special issue on Remote Sensing of Marine Winds)* 28: 424–430.
- Portabella, M., and A. Stoffelen. 2004. "A Probabilistic Approach for SeaWinds Data Assimilation." *Quarterly Journal of the Royal Meteorological Society* 130 (596): 127–152.
- Raudsepp, U., D. Beletsky, and D. J. Schwab. 2003. "Basin-Scale Topographic Waves in the Gulf of Riga." *Journal of Physical Oceanography* 33: 1129–1140.
- Sharma, N., and E. D'sa. 2008. "Assessment and Analysis of QuikSCAT Vector Wind Products for the Gulf of Mexico: A Long-term and Hurricane Analysis." *Sensors* 2008 8: 1927–1949.
- Služenikina, J., and A. Männik. 2011. "A Comparison of ASCAT Wind Measurements and the HIRLAM Model over the Baltic Sea." *Oceanologia* 53 (1-TI): 229–244.

- Smith, D. K., F. J. Wentz, and C. A. Mears. 2002. "Analysis of QuikSCAT Rain-flagged Winds within the Tropical Cyclone Environment." In *25th Conference on Hurricanes and Tropical Meteorology*, April 28–May 3, 507–508. San Diego, CA: AMS.
- Spencer, M. W., C. Wu, and D. G. Long. 2000. "Improved Resolution Backscatter Measurements with the SeaWinds Pencil-beam Scatterometer." *IEEE Transactions on Geoscience and Remote Sensing* 38: 89–104.
- Stiles, B. W. 1999. *Special Wind Vector Data Product: Direction Interval Retrieval with Thresholded Nudging (DIRTH) Product Description*. Accessed March 15, 2012. <ftp://podaac-ftp.jpl.nasa.gov/OceanWinds/quikscat/L2B12/docs/Dirth-Product-Description.pdf>
- Stiles, B. W., S. Veleva, and R. S. Dunbar. 2006. "IMUDH Rain Impact Flagging Algorithm." In *2006 International Ocean Vector Winds Meeting*, Salt Lake City, UT, July 5–7. Accessed March 15, 2012. <http://coaps.fsu.edu/scatterometry/meeting/docs/2006/stiles.pdf>
- Stoffelen, A., J. Vogelzang, and A. Verhoef. 2010. "Verification of Scatterometer Winds." In *10th International Winds Workshop*, Tokyo, February 22–26. Accessed March 20, 2012. <http://cimss.ssec.wisc.edu/iwwg/iww10/talks/stoffelen2.pdf>
- Suursaar, Ü., T. Kullas, M. Otsmann, I. Saaremäe, J. Kuik, and M. Merilain. 2006. "Cyclone Gudrun in Consequences in the Estonian Coastal Waters." *Boreal Environment Research* 11: 143–159.
- Tang, W., W. T. Liu, and B. W. Stiles. 2004. "Evaluation of High-Resolution Ocean Surface Vector Winds Measured by QuikSCAT Scatterometer in Coastal Regions." *IEEE Transactions on Geoscience and Remote Sensing* 42: 1762–1769.
- Tsai W.-Y., M. Spencer, C. Wu, C. Winn, and K. Kellogg. 2000. "SeaWinds on QuikSCAT: Sensor Description and Mission Overview." In *Geoscience and Remote Sensing Symposium 2000*, Honolulu, HI, July 24–28, 1021–1023.
- Žukova, V. 2009. "Possibilities of Estimation of Marine Winds from Estonian Coastal Stations." Master's thesis, Tallinn University of Technology, Estonia (in Estonian).

APPENDIX A: PAPERS

Paper II

Služenikina, J., Männik, A. 2011. A comparison of ASCAT wind measurements and the HIRLAM model over the Baltic Sea. *Oceanologia*, 53 (1, SI), 229–244.

A comparison of ASCAT wind measurements and the HIRLAM model over the Baltic Sea*

OCEANOLOGIA, 53 (TI), 2011.
pp. 229–244.

© 2011, by Institute of
Oceanology PAS.

KEYWORDS

ASCAT
Scatterometer winds
HIRLAM model
Baltic Sea
Numerical weather prediction

JEKATERINA SLUŽENIKINA^{1,2,*}
AARNE MÄNNIK^{2,3}

¹ Tallinn University of Technology,
Ehitajate tee 5, Tallinn 19086, Estonia

² Estonian Meteorological and Hydrological Institute,
Toompuiestee 24, Tallinn 10149, Estonia;
jekaterina.sluzenikina@emhi.ee

*corresponding author

³ University of Tartu,
Ülikooli 18, Tartu 50090, Estonia

Received 6 October 2010, revised 14 February 2011, accepted 15 February 2011.

Abstract

This paper presents a comparison of the wind data measured by the ASCAT polar-orbiting satellite scatterometer and winds forecast by the numerical weather prediction model HIRLAM in the Baltic Sea region during the stormy season in 2009. Two different resolution models were used in the comparison. Mutual quality and uncertainty characteristics of the measurements and predictions are determined. The results of the study show that the ASCAT wind data are well

* This research is supported by European Social Fund's Doctoral Studies and Internationalization Programme DoRa and the Estonian Ministry of Education and Science research targeted financing theme SF0180038s08. The EARS ASCAT data used in this research was provided by the EUMETCast service of EUMETSAT OSI SAF project, and the software used in this work was developed at KNMI.

The complete text of the paper is available at <http://www.iopan.gda.pl/oceanologia/>

correlated with the HIRLAM predicted winds, which raises the credibility of both data sources in operational and hindcasting applications over the Baltic Sea. A case of phase error in a HIRLAM forecast of cyclonic activity over the Baltic Sea is discussed.

1. Introduction

The Advanced Scatterometer (ASCAT) on the Meteorological Operational (MetOp) satellite of the European Organization for the Exploitation of Meteorological Satellites (EUMETSAT) is a C band radar, whose primary objective is to determine the wind field at the ocean surface (Figa-Saldaña et al. 2002). Wind scatterometers are instruments that are used to infer data on wind speed and direction from radar measurements of the sea surface. They rely for their operation on the fact that winds blowing over the sea influence the radar backscattering properties of the surface in a manner that is related to wind speed and wind direction (Stoffelen 1998, Gelsthorpe et al. 2000, Portabella 2002, Chelton & Freilich 2005). The EUMETSAT ASCAT wind products provide the wind speed and direction measurements at 10 m above the sea surface. Data is provided either with a grid spacing of 12.5 km and a spatial resolution of 25 km or with a grid spacing of 25 km at a 50 km resolution across and along two 550-km wide swaths on either sides of the nadir track. The radar measurements are provided in three azimuth directions – fore, mid and aft – respectively pointing 45°, 90° and 135° away from the satellite propagation vector, to resolve the wind direction and speed (Figure 1).

The ASCAT data are processed and distributed jointly by the EUMETSAT Ocean and Sea Ice (OSI) Satellite Application Facility (SAF) and Advanced Retransmission Service (EARS) ground system, both implemented at the Koninklijk Nederlands Meteorologisch Instituut (KNMI). The ASCAT wind products are freely available worldwide (see www.knmi.nl/scatterometer/), either through EUMETCAST, FTP or GTS. The ASCAT 12.5 km wind data visualization in the Baltic Sea region has been operational at the Estonian Meteorological and Hydrological Institute (EMHI) since the spring of 2010.

The ASCAT mission has been primarily designed to provide global ocean wind vectors operationally. The main applications are in the use of the high-resolution ASCAT winds in operational nowcasting (Von Ahn et al. 2006) and assimilation of those winds into numerical weather prediction (NWP) models (Figa-Saldaña et al. 2002). The use of scatterometer observations in data assimilation systems can extend their usefulness substantially and lead to improved sea level pressure analyses, improved upper air analyses of both

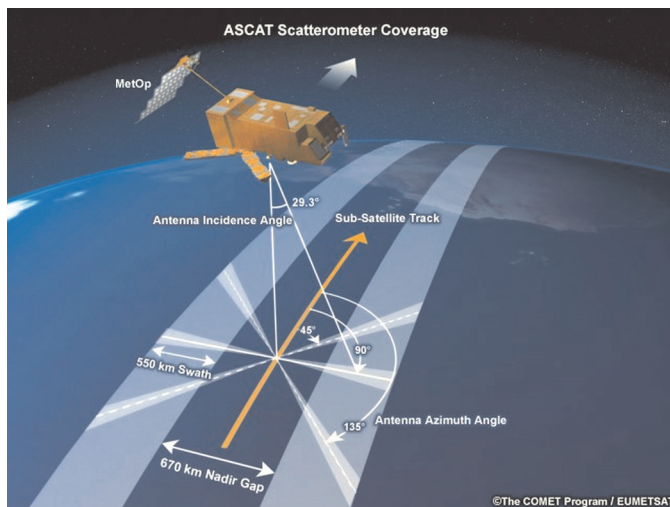


Figure 1. The ASCAT Scatterometer Coverage. (Source: COMET® <http://www.moisturemap.monash.edu.au/aacs/aacs-1/ascat.php> accessed on 28th Apr. 2010)

wind and geopotential, and improved short and extended-range numerical weather forecasts (Atlas et al. 2001).

In many applications, such as storm surge and wave prediction, marine warnings and ocean forcing, NWP analysis winds are used as input, but lacking in mesoscale detail. For both operational real-time marine applications and oceanographic research it is important to characterize the differences between the scatterometer and NWP products (Stoffelen et al. 2006). Global NWP models do not generally describe the small scales observed by scatterometers (Stoffelen et al. 2010), and it is of interest to investigate the assimilation of small scales by a high-resolution NWP model.

HIRLAM (Undén et al. 2002) is a High Resolution Limited Area Model, which serves as the main NWP platform for short-range, up to three days', operational weather forecasting and NWP applications in its member countries. HIRLAM gained operational status at EMHI in 2007. Besides its usual application as the weather prediction model, HIRLAM acts as the driving model for the local HIROMB marine modelling system (Funkquist et al. 2000), which is currently used for storm surge warnings.

Because of the scarcity of marine wind observations in the Baltic Sea region, EMHI is interested in the quality of satellite-based ASCAT winds

as a complementary data source of weather over the sea. The main interest of EMHI in the ASCAT winds as a possible solution for the operational monitoring of marine winds lies in the verification of storm warnings, as the network of coastal weather stations is insufficient for assessing weather conditions over the sea. The potential of ASCAT wind measurements as a means of improving the data assimilation process in HIRLAM is an area of interest as well. The current study compares ASCAT 10-m wind measurements with the respective numerical predictions of the operational HIRLAM models. The quality of the ASCAT winds has been assessed before, mostly over the large areas of oceans using comparisons with buoy measurements (Verhoef & Stoffelen 2009). The present study attempts to assess whether the same quality and uncertainty characteristics apply to the narrow, almost enclosed Baltic Sea basin as well. The comparison further aims to assess the quality and uncertainty range of HIRLAM NWP model predictions, as its output is often used for driving marine models in operational forecasting and hindcasting regimes. Two different resolutions of the NWP model are compared to see whether the resolution increase can play a significant role in forecasting over the enclosed Baltic Sea.

2. Material and methods

In the present study the EARS ASCAT 12.5-km gridded wind speed and wind direction were studied during the two-month period from 01.10 to 03.12.2009. The period was chosen to represent the stormy season over the Baltic Sea. HIRLAM forecasts from the archive of operational runs at the EMHI for the same period were used for comparison. Unfortunately, buoy measurements from the Baltic Sea were not available for inclusion in the study.

The NWP environment at EMHI is based on HIRLAM version 7.1.2 and consists of two modelling areas, ETA_II and ETB_II, with different grids. _II refers to EMHI's in-house second generation of modelling areas and will be omitted further on in the current manuscript for ease of reading.

Figure 2 illustrates the HIRLAM modelling areas and their geographical location. The ETA modelling domain has a horizontal grid distance of 11.1 km and the smaller ETB model domain has a 3.3 km grid. It should be noted that the HIRLAM has a rotated-pole latitude-longitude grid (here, the south pole is located at 30°S and 0°E). The boundary fields for the HIRLAM ETA model are provided by the European Centre for Medium-Range Weather Forecasting (ECMWF) model, and the boundary fields for the ETB model are provided by the ETA forecasts. The 54-hour forecasts of the ETA model are calculated four times a day with forecast starting-points at 00, 06, 12 and 18 UTC. For the ETB domain the 36-hour forecasts are

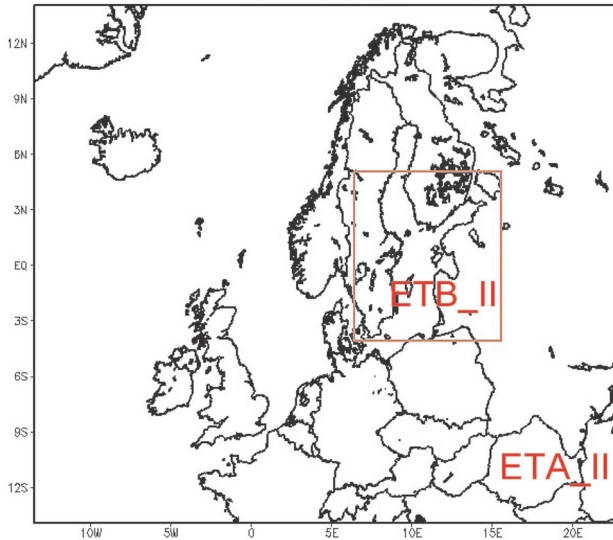


Figure 2. HIRLAM ETA and ETB modelling areas. The geographical coordinates are the latitudes and longitudes in the Earth's system with rotated poles as defined in HIRLAM

calculated twice a day with starting-points at 00 and 12 UTC. To maintain the analysis cycle, 6-hour forecasts at 06 and 18 UTC are calculated for ETB as well. Forecast fields are available with a 3-hour time resolution. Further properties of models and the parameterization schemes applied in the NWP environment at EMHI can be found in the paper by Keevallik et al. (2010).

The physical definition of the ASCAT winds is that of equivalent neutral winds. In the most common definition, equivalent neutral wind speed is the mean wind speed that would be observed if there was neutral atmospheric stratification (Geernaert & Katsaros 1986). The only difference between neutral and real ASCAT winds is a bias of $+0.2 \text{ m s}^{-1}$ for the neutral winds as compared to the real winds (Verhoef & Stoffelen 2009). Of course, the differences between the HIRLAM real and 10-m neutral winds will be variable, but with an expected statistical mean of 0.2 m s^{-1} (Hersbach 2010). In the assessment of ASCAT winds, the HIRLAM model forecast wind components at 10-metre height were used. The stability conditions in the forecasts were not checked, however.

The area of interest in the Baltic region was 55° – 62.3° N and 14.5° – 27.8° E. As ASCAT is an instrument on a polar orbiting satellite, the measurements in this area are made from one to three times per day and in the time interval around 17–20 UTC. For comparison of the ASCAT and HIRLAM winds, the time of the ASCAT data measurements had to be coordinated with the time of the HIRLAM wind forecasts. During this study 06-hour, 18-hour and 30-hour forecasts of both the ETA and the ETB model were used. While the ASCAT measurements were made about at 18 UTC, the HIRLAM 06-hour and 30-hour forecasts were chosen at the 12 UTC starting-point and the 18-hour forecast at the 00 UTC starting-point. If the ASCAT measurements were made more than once per day, the ASCAT data were chosen with a minimal time difference between the NWP model and ASCAT winds (less than one hour). The 10-m wind from the HIRLAM analyses were not used in the comparison as they are reported to be of lower quality than the short-range predictions by Keevallik et al. (2010).

The HIRLAM wind components at 10-m height were interpolated into the ASCAT points of measurements using the bilinear interpolation method. The bias, root mean square (RMS) error and correlation coefficient were calculated between the ASCAT and HIRLAM models for two wind speed intervals – 0 – 22 m s^{-1} and 4 – 22 m s^{-1} . The upper level of the wind speed was the maximum wind speed during the observed period. Comparison of wind data was performed through the wind speed and direction, and the wind velocity components, where u is the zonal and v is the meridional wind component. All statistical characteristics were computed on a homogenized dataset, which means that if one of the model forecasts was missing, the datum for comparison with the ASCAT winds was eliminated from the analysis. The quality characteristics used here are associated with sampling length distributions.

3. Results

3.1. Statistical comparison of HIRLAM and ASCAT

Over the evaluation period the observed winds in general showed remarkably good coincidence with those predicted by the model. As an example of good coincidence, Figure 3 presents the observed and predicted winds over the Baltic Sea on 03.11.2009. Unfortunately, the area of interest is not shown in full here (54.6° N– 60.3° N, 16° E– 24.5° E), owing to the high density of the wind barbs.

In wind verification, a speed of over 4 m s^{-1} is often used (Gelsthorpe et al. 2000, Verspeek et al. 2008, Verhoef & Stoffelen 2009) to estimate quality characteristics; this approach is followed here. In particular, this is

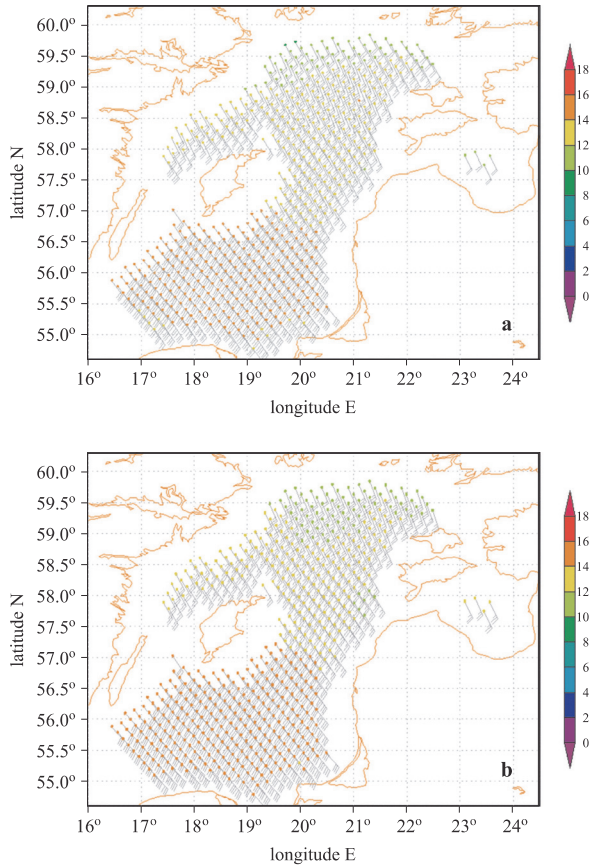


Figure 3. The winds of the ASCAT (top) 03.11.2009 at 18:09 UTC and the HIRLAM ETA model 03.11.2009 at 12 UTC 06-hour forecast (bottom)

done when computing wind direction statistics, which would otherwise be determined to a large extent by low winds (Stoffelen 1998).

The ETA 06-hour forecast and ASCAT measurement scatterplots of wind speed and direction are shown in Figure 4 ($0\text{--}22\text{ m s}^{-1}$) and Figure 5 ($4\text{--}22\text{ m s}^{-1}$). As seen in Figure 4, the coincidence of the ETA 06-hour forecast and ASCAT wind speed is reasonably good. The wind direction scatterplots also show good correlation, whereas the scattering is much smaller when low speed winds are filtered out (see Figure 5).

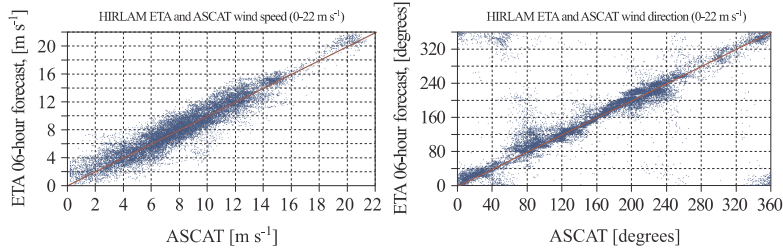


Figure 4. HIRLAM ETA 06-hour forecast and ASCAT wind direction and speed scatterplots (0–22 m s⁻¹)

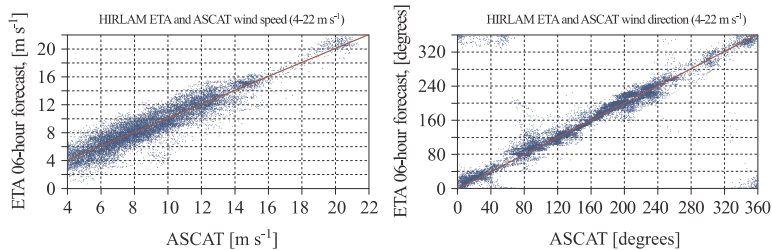


Figure 5. HIRLAM ETA 06-hour forecast and ASCAT wind direction and speed scatterplots (4–22 m s⁻¹)

Analysis of similar scatterplots of the HIRLAM ETB model and both models with forecast lengths of 18 and 30 hours shows that the characteristics of distribution do not change qualitatively in time. Thus, for the sake of brevity, the scatterplots are not shown here. The scatterplots of the wind components of the ASCAT and HIRLAM winds were also compared (see Figure 6). The scatterplots of the wind components show good coincidence between the observed and predicted wind components. However, scattering increases on both the type and model scatterplots with growing forecast length, which is a natural and expected effect. Some quality characteristics are computed for all forecast periods for both the ETA and the ETB models and are summarized in Tables 1 and 2. In computations of wind direction statistics the errors due to 360-degree aliasing were eliminated by manual inspection.

The quality characteristics are worse when all wind speeds are taken into account (compared only to the 4–22 m s⁻¹ range), which can be explained by the fact that, according to Stoffelen (1998), in the presence of weak winds, wind speed error distributions are skewed at low winds with slightly

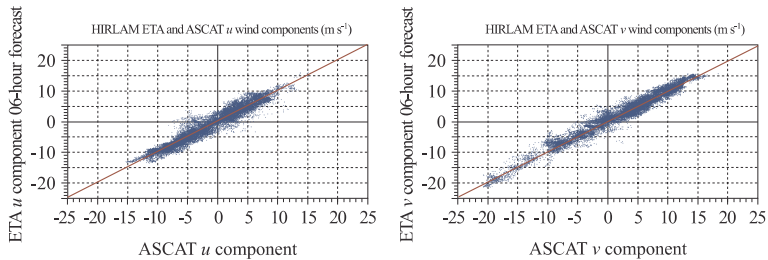


Figure 6. HIRLAM ETA 06-hour forecast and ASCAT u and v wind component scatterplots ($4\text{--}22\text{ m s}^{-1}$)

increased variance differences. The wind speed correlations decrease in the case of the $4\text{--}22\text{ m s}^{-1}$ range, since the correlation depends on the ratio of domain over scatter; hence, reducing the wind speed domain decreases the correlation. The differences are related mostly to effects of atmospheric wind variability and differences in spatial representation, which are well expressed as constant errors in the wind components. As far as the wind speed is concerned, the bias of both the ETA and ETB models in the $4\text{--}22\text{ m s}^{-1}$ range is almost non-existent, whereas a weak, negative bias growth may be noted with increasing forecast length. In the case of wind direction the bias is appreciable, and a weak anticlockwise turning with growing forecast length may be observed. The RMS error of the wind speed was mostly less than 2 m s^{-1} in all forecasts and wind speed intervals. The results in Table 2 show that the bias of the wind component is quite small and in some cases even decreases to 0 m s^{-1} . However, the RMS value gradually increases with the forecast length.

Comparison of the results in Tables 1 and 2 shows a higher correlation between the ASCAT and HIRLAM winds present in the wind components (> 0.90 for all the forecasts), whereas the correlation coefficients in Table 1 are much lower, especially in the wind direction. According to Stoffelen (1998), the wind component errors are better described than wind speed or wind direction. The wind component errors have a symmetrical distribution for the scatterometer and model forecast, and as mentioned before, the random errors of wind direction clearly depend on wind speed.

ETA seems to perform slightly better than the high resolution ETB model, whereas the expectation was that the high-resolution model would perform better. An explanation for this could be that when more small scales are represented in ETB than in ETA, these scales do not appear to tally with the scatterometer winds. The reason for this might be that the

Table 1. ASCAT and HIRLAM models: statistical characteristics (bias, RMS error, correlation) of wind speed and direction

		06-hour forecast			18-hour forecast			30-hour forecast		
		bias	RMS	corr.	bias	RMS	corr.	bias	RMS	corr.
HIRLAM ETA										
0–22 m s ⁻¹	wind speed	0.12	1.30	0.94	0.14	1.46	0.92	-0.10	2.05	0.85
	wind direction	5.34	24.89	0.75	4.53	27.13	0.76	2.14	33.23	0.72
4–22 m s ⁻¹	wind speed	0.03	1.28	0.93	0.01	1.39	0.91	-0.31	1.97	0.84
	wind direction	3.46	16.19	0.82	2.45	18.60	0.82	1.40	27.52	0.75
HIRLAM ETB										
		bias	RMS	corr.	bias	RMS	corr.	bias	RMS	corr.
0–22 m s ⁻¹	wind speed	0.12	1.38	0.94	0.12	1.51	0.92	-0.07	2.08	0.85
	wind direction	5.13	25.36	0.73	4.90	28.43	0.72	2.80	32.76	0.71
4–22 m s ⁻¹	wind speed	0.03	1.35	0.93	-0.01	1.46	0.91	-0.28	2.03	0.83
	wind direction	3.26	16.31	0.80	3.10	19.72	0.78	1.79	26.68	0.75

Table 2. ASCAT and HIRLAM models: statistical characteristics (bias, RMS error, correlation) of wind components

	06-hour forecast			18-hour forecast			30-hour forecast			
	bias	RMS	corr.	bias	RMS	corr.	bias	RMS	corr.	
HIRLAM ETA										
0-22 m s ⁻¹	<i>u</i> comp.	0.16	1.61	0.96	0.04	1.80	0.94	-0.01	2.22	0.92
	<i>v</i> comp.	0.34	1.58	0.98	0.15	1.77	0.97	-0.09	2.72	0.92
4-22 m s ⁻¹	<i>u</i> comp.	0.17	1.59	0.96	0.00	1.77	0.95	0.01	2.16	0.93
	<i>v</i> comp.	0.29	1.52	0.98	0.13	1.72	0.97	-0.15	2.78	0.93
HIRLAM ETB										
		bias	RMS	corr.	bias	RMS	corr.	bias	RMS	corr.
0-22 m s ⁻¹	<i>u</i> comp.	0.20	1.69	0.95	0.03	1.89	0.94	-0.01	2.24	0.92
	<i>v</i> comp.	0.28	1.66	0.97	0.15	1.84	0.96	-0.08	2.77	0.92
4-22 m s ⁻¹	<i>u</i> comp.	0.20	1.68	0.96	0.00	1.90	0.94	-0.01	2.20	0.93
	<i>v</i> comp.	0.23	1.61	0.98	0.12	1.82	0.97	-0.12	2.84	0.93

forcing of these scales in the HIRLAM model is weak and the phases of these small-scales are not well determined. In such a case, the added small-scale variance will not reduce the variance of the differences, but will tend to cause the difference variances to increase. This is usually referred to as the ‘double penalty’ in verification. To determine small scales, they need to be either observed or generated by downscale cascading and parameterizations. Other possible explanations may be that the HIRLAM parameterization schemes are fine-tuned to 15 km resolution and therefore do not work so well at high resolution, or that the proximity of the boundary conditions introduces distortions in small domains.

3.2. A case with phase error in cyclonic activity

ASCAT winds may be useful when NWP model phase shift errors need to be corrected over the open sea, as for example on 02.12.2009. Figures 7a and 7b illustrate the difference between the ASCAT and HIRLAM ETA 06-hour wind forecasts. In this figure the difference between the ASCAT and HIRLAM forecasts is not so significant. There are a few differences in

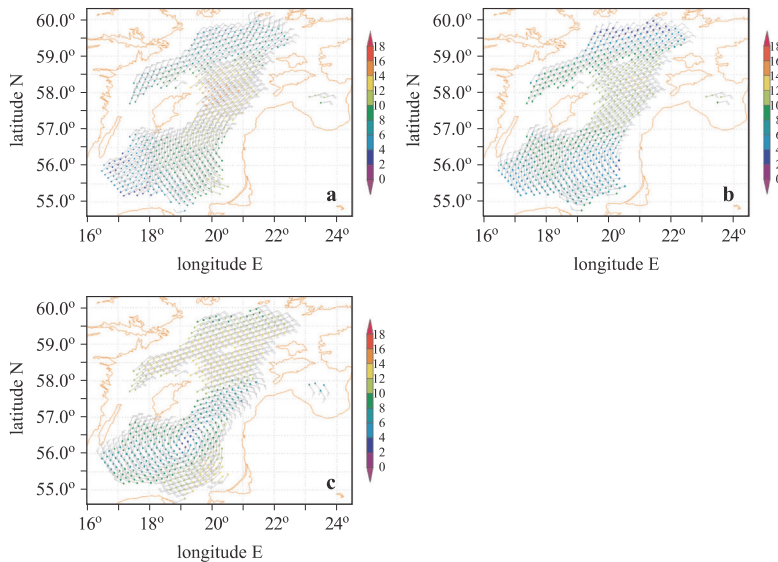


Figure 7. The winds of the ASCAT – 02.12.2009 at 18:09 UTC (a), HIRLAM ETA model – 02.12.2009 at 12 UTC 06-hour forecast (b), HIRLAM ETA model – 01.12.2009 at 12 UTC 30-hour forecast (c)

the wind direction between the ASCAT winds and the HIRLAM forecast for 02.12.2009 in the southern Baltic Sea at 18°E.

Comparison of the HIRLAM ETA 30-hour forecast with the ASCAT winds shows that there is a significant difference between wind directions in Figures 7a and 7c. On the southern part of the image the HIRLAM ETA model generates cyclonic winds, which do not fit the ASCAT winds. The results of the same forecasts from ETB model data show practically the same difference with the ASCAT winds. This is a clear signal that HIRLAM predicted a cyclonic development with a phase shift in the forecast with start time 12 UTC 01.01.2009 and corrected it later. The situation can be used to study the reasons for such phase shifts over the open sea and to correct them.

4. Discussion

HIRLAM ETA and HIRLAM ETB 10 m wind predictions show good correspondence with the measurements. The speed predictions practically lack a systematic error, although a very weak negative bias in wind speed may be observed with growing forecast length. This shows that the friction parameterization over the sea is roughly correct in HIRLAM. However, a small wind direction bias does exist.

The results of the higher resolution ETB model tend to be slightly worse than those of the operational suite; we may speculate that they are the result of the poor determination of 50-km scales over the Baltic, due to the relatively weak forcing and the lack of observations, or perhaps they are due to the proximity of the boundary zone, which introduces dynamic distortions in too small a domain, or they may be the effect of physical parameterizations not being tuned to such a high resolution.

The uncertainty ranges fit well with the expected quality characteristics reported in the literature. According to Gelsthorpe et al. (2000), determination of speeds in the range 4–24 m s⁻¹ with an accuracy of 2 m s⁻¹ (or 10%) and directions with an accuracy of ±20 deg is required. These criteria are met in both comparisons up to the 18-hour forecast lengths. In the case of the 30-hour forecasts these criteria are exceeded only slightly for the wind speed, but not for the wind direction. According to Figa-Saldaña et al. (2002), the accuracy target for ASCAT winds generated by the OSI SAF is 2 m s⁻¹ root mean square wind component error and 0.5 m s⁻¹ bias for all speeds below 25 m s⁻¹. The wind components of the HIRLAM and ASCAT presented in Table 2 show that the wind component statistics fit the required accuracy thresholds well. The RMS of wind components higher than 2 m s⁻¹ is present only in the 30-hour forecasts. The bias of the components is lower than that required in all HIRLAM forecasts.

In a comparison of the ASCAT and ECMWF analysis in northern oceanic areas (30°N–60°N), Bentamy et al. (2008) determined standard deviations of 1.77 m s⁻¹ for wind speed and 20 degrees for wind direction. According to Verhoef & Stoffelen (2010), the global ASCAT-ECMWF standard deviation of difference for wind speed is 1.26 m s⁻¹ and for wind direction is 15 degrees for the 25-km gridded product. The u wind component standard deviation of the ASCAT-ECMWF winds is 1.45 m s⁻¹; the corresponding v component is 1.63 m s⁻¹. More recently and in line with these results, Hersbach & Janssen reported at the 2010 International Ocean Vector Winds Meeting (18–20 May 2010) a vector RMS difference of ~ 2.2 m s⁻¹ in the Baltic (http://coaps.fsu.edu/scatterometry/meeting/docs/2010_may/gridded/hersbach.pdf). HIRLAM wind speeds and directions show similar or slightly worse results over these ranges. Again, the HIRLAM model may contain smaller scales than ECMWF that are not well resolved by the physical parameterizations and the observing systems. Generally, 100-km scales evolve fast and need to be sampled densely in both time and space. To reduce the uncertainty in HIRLAM wind predictions, more observations over the Baltic may be necessary. The fact that the comparison of ASCAT and HIRLAM winds is generally in line with results from other similar studies confirms that the ASCAT 10-m winds are a reliable data source over the Baltic Sea, which is of great importance for marine and NWP communities operating in the region. Unfortunately, sea buoy or ship measurements in the Baltic Sea region were not available for the study, but it would be really advantageous to extend the study in this respect.

A case of phase error in the HIRLAM predictions of cyclonic development over Baltic Sea was spotted on 2.12.2009. This situation needs further analysis to identify the causes of the phase error. Nonetheless, it illustrates the potential of ASCAT measurements for identifying such a phase shift error over open sea areas and may help in the development of better deterministic models in the future.

References

- Atlas R., Hoffman R.N., Leidner S.M., Sienkiewicz J., Yu T.-W., Bloom S.C., Brin E., Ardizzone J., Terry J., Bungato D., Jusem J.C., 2001, *The effects of marine winds from scatterometer data on weather analysis and forecasting*, Bull. Am. Meteorol. Soc., 82, 1965–1990.
- Bentamy A., Croize-Fillon D., Perigaud C., 2008, *Characterization of ASCAT measurements based on buoy and QuikSCAT wind vector observations*, Ocean Sci., 4 (4), 265–274.

- Chelton D.B., Freilich M.H., 2005, *Scatterometer-Based Assessment of 10-m Wind Analyses from the Operational ECMWF and NCEP Numerical Weather Prediction Models*, Mon. Weather Rev., 133 (2), 409–429.
- Figa-Saldaña J., Wilson J.W., Attema E., Gelsthorpe R., Drinkwater M.R., Stoffelen A., 2002, *The advanced scatterometer (ASCAT) on the meteorological operational (MetOp) platform: A follow on for the European wind scatterometers*, Can. J. Remote Sens., 28 (3), 404–412.
- Funkquist L., Kleine E., 2000, *An introduction to HIROMB, an operational baroclinic model for the Baltic Sea*, Tech. Rep. SMHL, Norrköping.
- Geernaert G.L., Katsaros K.B., 1986, *Incorporation of stratification effects on the oceanic roughness length in the derivation of the neutral drag coefficient*, J. Phys. Oceanogr., 16 (9), 1580–1584.
- Gelsthorpe R.V., Schied E., Wilson J.J.W., 2000, *ASCAT-MetOp's advanced scatterometer*, ESA Bull. 102, [<http://esapub.esrin.esa.it/bulletin/bullet102..htm>].
- Hersbach H., 2010, *Assimilation of scatterometer data as equivalent-neutral wind*, Tech. Memo., ECMWF, [http://www.ecmwf.int/publications/library/ecpublications/_pdf/tm/601-700/tm629.pdf].
- Keevalik S., Männik A., Hinnov J., 2010, *Comparison of HIRLAM wind data with measurements at Estonian coastal meteorological station*, Est. J. Earth Sci., 59 (1), 90–99.
- Portabella M., 2002, *Wind field retrieval from satellite radar systems*, Thesis, Univ. Barcelona, 207 pp., [http://www.knmi.nl/publications/fulltexts/phd_thesis.pdf].
- Stoffelen A., 1998, *Scatterometry*, Thesis, Univ. Utrecht., [<http://igitur-archive.library.uu.nl/dissertations/01840669/inhoud.htm>].
- Stoffelen A., Portabella M., Verhoef A., Verspeek J., Vogelzang J., *Mesoscale winds from the new ASCAT scatterometer*, KNMI Res. Biennial Rep. 2005–2006, [http://www.knmi.nl/research/biennial/05-06_ASCAT.pdf].
- Stoffelen A., Vogelzang J., Verhoef A., 2010, *Verification of scatterometer winds*, 10th Inter. Winds Workshop, [http://www.knmi.nl/publications/fulltexts/scat_iww10.pdf].
- Undén P., Rontu L., Järvinen H., Lynch P., Calvo J., Cats G., Cuxart J., Eerola K., Fortelius C., Garcia-Moya J.A., Jones C., Lenderink G., McDonald A., McGrath R., Navasques B., Nielsen N.W., Ødegaard V., Rodrigues E., Rummukainen M., Rööm R., Sattler K., Sass B.H., Savijärvi H., Schreur B.W., Sigg R., The H., Tijm A., 2002, *HIRLAM-5 scientific documentation*, [<http://www.hirlam.org/>].
- Verhoef A., Stoffelen A., 2009, *Validation of ASCAT 12.5-km winds, version 1.2*, SAF/OSI/CDOP/KNMI/TEC/RP/147, EUMETSAT Tech. Rep., [<http://www.knmi.nl/scatterometer/publications/>].
- Verhoef A., Stoffelen A., 2010, *ASCAT wind product user manual version 1.8*, SAF/OSI/CDOP/KNMI/TEC/MA/126, EUMETSAT, [<http://www.knmi.nl/scatterometer/publications/>].

- Verspeek J., Portabella M., Stoffelen A., Verhoef A., 2008, *Calibration and validation of ASCAT winds, version 4.0*, Doc. Extern. Proj., SAF/OSI/KNMI/TEC/TN/163, EUMETSAT.
- Von Ahn J., Sienkiewicz J.M., Chang P., 2006, *Operational impact of QuikSCAT winds at the NOAA Ocean Prediction Center*, *Weather Forecast.*, 21 (4), 523–539.

APPENDIX A: PAPERS

Paper III

Služenikina, J., Männik, A. [accepted for publication]. Impact of the ASCAT scatterometer winds on the HIRLAM analysis quality in case of severe storms. Proceedings of the Estonian Academy of Sciences, 2016, 65, 3, 177–194.



Impact of the ASCAT scatterometer winds on the quality of HIRLAM analysis in case of severe storms

Jekaterina Služenikina* and Aarne Männik

Estonian Environment Agency, Mustamäe tee 33, 10616 Tallinn, Estonia

Received 27 March 2015, revised 28 October 2015, accepted 1 February 2016, available online 2 May 2016

© 2016 Authors. This is an Open Access article distributed under the terms and conditions of the Creative Commons Attribution-NonCommercial 4.0 International License (<http://creativecommons.org/licenses/by-nc/4.0/>).

Abstract. The impact of the Advanced Scatterometer (ASCAT) data assimilation on the quality of HIRLAM analysis is assessed in cases of rapidly developing severe storms of 2013. The HIRLAM quality is analysed for two observing system experiments: with and without the ASCAT data assimilation. Mainly impact on the model analysis output is evaluated. Marine observations of 10-m wind speed and mean sea level pressure are used as measures of quality. The results show that depending on ASCAT data coverage in the HIRLAM domain and temporal availability of the data at the assimilation time moment, the impact may be either more or less accurate. It is also detected that some narrow places of the Baltic Sea (Bothnian Bay, Gulf of Finland) are not affected by the ASCAT data assimilation. According to the ASCAT Wind Product specification, ASCAT measurements near the shoreline are usually flagged as land contaminated. The ASCAT winds in these areas are not admitted to the analysis after the procedure of the HIRLAM quality control, most likely due to the proximity to the land. The use of the ASCAT Coastal Wind Product in the future may enlarge the ASCAT data coverage in these areas. In addition, some weaknesses of the ASCAT data assimilation were detected in the study raising the question of the optimal ASCAT data usage. Further attempts to improve the quality of the HIRLAM analyses are expected in the ASCAT data thinning before assimilation or by reducing time differences between the HIRLAM analyses.

Key words: ASCAT, marine winds, storm, HIRLAM, data assimilation, experiments.

List of acronyms and abbreviations

3DVAR – Three-Dimensional Variational data assimilation	MET Norway – Norwegian Meteorological Institute
AIREP – AIRcraft REPorts	Met Office – UK’s national weather service
AMO – Assimilated Marine Observations	MetOp – Meteorological Operational satellite
ASCAT – Advanced Scatterometer	MSLP – Mean Sea Level Pressure
ASCEXP – Experiments with ASCAT data assimilation	NWP – Numerical Weather Prediction
BSH – Federal Maritime and Hydrographic Agency of Germany	O–A – Surface-based Observation minus HIRLAM Analysis
C-band – 4.0–8.0 GHz electromagnetic spectrum frequency range	O–B – ASCAT Observation minus HIRLAM Background
DRIBU – DRifting BUoys	OSCAT – Oceansat-2 scatterometer
EARS – EUMETSAT Advanced Retransmission Service	OSE – Observing System Experiments
ECMWF – European Centre for Medium-Range Weather Forecasts	OSI SAF – Ocean and Sea Ice Satellite Application Facility
EUMETSAT – European Organization for the Exploitation of Meteorological Satellites	PILOT – Pilot-balloon stations
FGAT – First Guess at Appropriate Time	QuikSCAT – Quick Scatterometer
HARMONIE – Hirlam Aladin Regional/Mesoscale Operational NWP in Europe	REFEXP – Experiments without ASCAT data assimilation
HIRLAM – High Resolution Limited Area Model	RMSE – Root Mean Square Error
IMO – Independent Marine Observation	SHIP – Synoptic observations from ships
KNMI – Royal Netherlands Meteorological Institute	SD – Standard Deviation
MARNET – MARine Environmental Monitoring NETWORK in the North Sea and the Baltic Sea	SYNOP – Surface synoptic stations
	TEMP – Upper air soundings
	UTC – Coordinated Universal Time
	WVC – Wind Vector Cell

* Corresponding author, jekaterina.sluzenikina@envir.ee

1. INTRODUCTION

The Advanced Scatterometer (ASCAT) on the Meteorological Operational satellite (MetOp) of the European Organization for the Exploitation of Meteorological Satellites (EUMETSAT) is a C-band (5.255 GHz) radar, whose primary objective is to determine the wind field at the ocean surface (Figa-Saldaña et al., 2002). Scatterometers uniquely define the mesoscale wind vector field at the sea surface by measuring the radar backscatter signal (σ^0) from wind-generated cm-sized, so-called gravity-capillary sea waves (Stoffelen et al., 2006). It was found experimentally that the sensitivity to wind speed and direction describes well the changes in backscatter over the ocean at moderate incidence angles due to changes in surface roughness (OSI-SAF Project Team, 2013).

The ASCAT mission has been primarily designed to provide global ocean wind vectors operationally. The main applications are in the use of the high-resolution ASCAT winds in operational nowcasting and assimilation of marine winds into Numerical Weather Prediction (NWP) models (Figa-Saldaña et al., 2002; Stoffelen et al., 2013).

Most general weather centres such as ECMWF (European Centre for Medium-Range Weather Forecasts), Met Office (UK's national weather service), Japan Meteorological Agency, and Environment Canada already use the ASCAT data in the data assimilation process. The ECMWF was the first centre that assimilated the ASCAT winds into the global NWP model in 2007 and showed a positive effect on forecast skills, especially over the southern hemisphere where the number of marine observations is limited. In addition, for ocean waves a significant positive impact was observed in the tropics (Hersbach and Janssen, 2007).

The impact of the ASCAT data assimilation into numerical models is mainly analysed for global models and in general, the impact is neutral to positive (Hersbach and Janssen, 2007; Bi et al., 2010; Payan, 2010; Takahashi, 2010). More recent studies of the ASCAT-A and ASCAT-B (ASCAT measurements from MetOp-A and MetOp-B) data assimilation into the ECMWF by De Chiara et al. (2014) also show a positive effect when either or both the ASCAT data sets are assimilated together with Indian Oceansat-2 scatterometer (OSCAT) data. The impact of scatterometer observation results for severe storms such as tropical cyclones was also evaluated by De Chiara et al. (2014) showing generally the benefit into the model analyses and forecasts. Cotton (2013) evaluated the impact of the ASCAT-A and ASCAT-B scatterometer data assimilation into the global model of Met Office. To better exploit data from parallel ASCAT-A and ASCAT-B operations a new thinning scheme is proposed.

For limited area models the Master's Thesis by Ollinaho (2010) indicated a positive to neutral impact on the forecasts of the High Resolution Limited Area Model (HIRLAM) (Undén et al., 2002), which serves as the main NWP platform for short-term (up to three days) operational weather forecasting and NWP applications in many European countries. However, the impact of ASCAT assimilation was assessed only by means of station data over land. De Valk (2013) in his paper compared HIRLAM experiments with assimilated ASCAT winds and without ASCAT assimilation with data from moored buoys, ships, and coastal stations. The results showed that over land there is no significant difference between analyses minus first guess for both experiments, the same as for wind forecasts differences (3-hour forecast, 6-hour forecast); over sea the patterns remain only partly visible. Both De Valk (2013) and De Haan et al. (2013) analysed the impact of the ASCAT data assimilation into the HIRLAM (during a period of 10 weeks and shorter) and reported positive results. Valkonen and Schyberg (2015) assessed the impact of the ASCAT assimilation into the Hirlam Aladin Regional/Mesoscale Operational NWP in Europe (HARMONIE) model in case of severe storms and showed a slightly positive impact on forecasts in comparison with observations over land.

The general aim of our work was to assess the impact of the ASCAT data assimilation into the HIRLAM analysis in case of extreme events such as severe storms. The study is concentrated on the Observing System Experiments (OSEs) to inspect the analysis output quality and differences in the analysis output with ASCAT data assimilation and without it. The wind speed at 10-m height and the Mean Sea Level Pressure (MSLP) are compared with observations over marine areas. It is slightly different from the study by Valkonen and Schyberg (2015) where the impact of ASCAT data assimilation on the forecasts over land was assessed. In addition, the differences between the ASCAT observations and model background (O–B) and also between the model analysis after ASCAT assimilation (O–A) are inspected to assess how well the system is set for ASCAT winds.

The synoptic situations of severe storms can develop dramatically and accurate calculations of model analysis may improve the quality of forecasts of severe weather. As HIRLAM is the operational weather prediction model used in the Estonian Weather Service it is relevant to check if any significant differences arise from the assimilation of ASCAT winds and which approach could be more accurate.

The structure of this paper is as follows. Section 2 presents the data and methods of the current study and consists of four subsections. First, an overview of severe storm cases is given, then observational data (ASCAT ocean surface wind product and marine surface-based

measurements) are described. Next, an overview of the HIRLAM model and the data assimilation system applied in the Estonian Weather Service is presented. Section 3 shows the results: analyses of the model experiments are compared with surface-based measurements in three different case studies and then the differences ASCAT O–B and O–A are analysed. Finally, Section 4 summarizes the results of the study and draws conclusions.

2. DATA AND METHODS

2.1. Severe storm cases

In the current study three different cases of severe storms in 2013 were selected to investigate the impact of satellite-based measurements on the HIRLAM analysis output with the emphasis of the ASCAT data impact on the storm initialization accuracy. The storm cases were chosen to contain the highest possible density of the ASCAT stormy wind measurements (over 15 m s^{-1}) in the marine areas of the HIRLAM modelling domain (Fig. 1), where the impact of the ASCAT data is expected to be visible.

The first study case is the strong storm on 28 October 2013, named in Germany Christian, in Denmark Allan, and in the UK St Jude. The storm moved across northern Europe and caused massive damages and disruptions. The impact of the storm was considerable. At least 15 people perished, a large number of trees were blown down, power supply broke down, train connections were interrupted, streets were impassable, and the Øresund Bridge between Denmark and Sweden had to be closed (Storch et al., 2014). In Germany, peak wind speeds ranking 11 ($28.5\text{--}32.6 \text{ m s}^{-1}$) and 12 ($\geq 32.7 \text{ m s}^{-1}$) on the Beaufort scale were observed at many stations along the coasts of the North and Baltic seas as well as further inland, with a maximum of 47.7 m s^{-1} at St Peter Ording, a location facing the North Sea (Storch et al., 2014).

The second stormy wind case of 1 December 2013 observed in the current study was not so dramatic as the event in October. However, as the storm took place in the Baltic Sea region it was possible to analyse the impact of the ASCAT winds for the closed marine area near the Baltic countries.

The third interesting case is the severe storm Xaver (05.12.2013), where the ASCAT measured widely winds over 20 m s^{-1} , indicating the high power of the storm. The storm moved across northern Europe and caused severe winds with gusts of hurricane force across northern Germany and at higher sites. Shipping and rail traffic were shut down in several places and flights were cancelled. In addition, dangerous street conditions and road accidents affected by the storm Xaver were reported in other European countries. More than 10 people died Europe-wide due to the storm (Deutschländer et al., 2013).

2.2. The ASCAT ocean surface winds

The ASCAT ocean surface winds provided by the EUMETSAT as the ASCAT Wind Product give information about the equivalent-neutral wind speed and direction at 10 m above the sea surface. Scatterometer data are organized into the so-called Wind Vector Cells (WVCs), the averaged wind solution in the centre of a defined grid box. Two types of the ASCAT wind products are generally processed: with a grid spacing of 12.5 km at a spatial resolution of 25 km or with a grid spacing of 25 km at a 50 km resolution across and along two 550-km wide swaths on both sides of the nadir track. The radar backscatter measurements (σ^0) are provided in three azimuth directions: fore, mid, and aft pointing respectively 45° , 90° , and 135° away from the satellite propagation vector, to resolve the wind direction and speed (OSI-SAF Project Team, 2013). The translation of the radar backscatter measurements from the sea surface into the wind speed and direction is performed by a geophysical model function (Stoffelen, 1998). In addition, this model links the dependences of the backscatter signal from the frequency, polarization, and incidence angle of the emitted and returned microwave, as well as from the local wind direction, relative to the satellite azimuth look direction (Hersbach et al., 2007).

For each backscatter measurement the wind speed solution as a function of all possible wind directions is shown. Given the basic harmonic wind direction dependence of the backscatter signal, four solutions exist in this general case (Stoffelen, 1998). Each wind ambiguity is characterized by a solution probability that is determined based on the distance-to-cone residual in the wind inversion. The wind ambiguities, solution probabilities, and prior information from the ECMWF model (10-m background winds) are used in a two-dimensional variational ambiguity removal (2DVAR) procedure (Vogelzang et al., 2009) to produce the surface wind field. Most of the quality control and ambiguity removal procedure of the ASCAT data are carried out during the retrieval process.

The ASCAT Level 2 winds obtained for the current study were processed in near real-time by the Koninklijk Nederlands Meteorologisch Instituut (KNMI) (see <http://www.knmi.nl/scatterometer>) and afterwards disseminated to the users by EUMETSAT. Processing and further dissemination of operational ASCAT are performed in both global and regional frame. The regional product known as the EARS (EUMETSAT Advanced Retransmission Service) ASCAT Wind Product is acquired locally by the network of Advanced High Resolution Picture Transmission receiving stations, which helps to provide European countries with the ASCAT winds within 25 min after data acquisition. The ASCAT Level 2 Wind Product includes information on the backscatter measurements, selected wind solution from

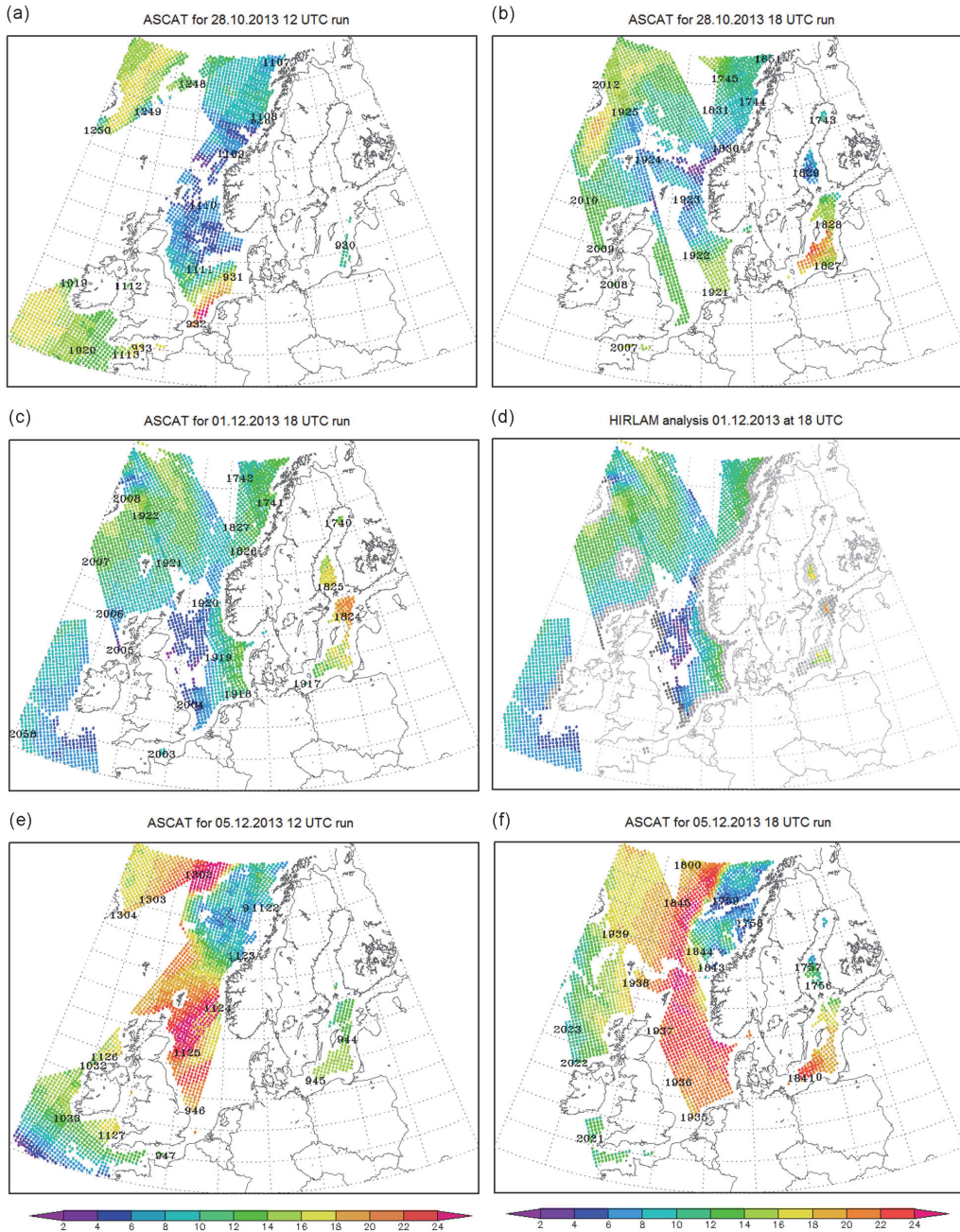


Fig. 1. Coverage of the EARS ASCAT overpasses in HIRLAM assimilation windows at 12 UTC and 18 UTC on 28.10.2013 (a, b), 01.12.2013 (c, d), and 05.12.2013 (e, f). HIRLAM analysis winds after ASCAT data assimilation at 18 UTC on 01.12.2013 (d): grey dots represent the ASCAT measurements rejected after quality control, probably due to proximity to the land. Three and/or four digit numbers in the figures show the ASCAT overpass time in UTC.

calculated ambiguous (up to four) wind solutions, scanning geometry, and the WVC quality flag in case of poor data quality (too large inversion residual, or too high noise value in the input product such as sea-ice or land contamination) among others. The procedure and improvements of the quality control performed at the KNMI are described in more detail by Portabella et al. (2012).

The coverage of the EARS ASCAT Level 2 data used in the HIRLAM assimilation window is not uniform during the day. The overpasses are quite sparse for HIRLAM 00 UTC and 06 UTC analyses while for HIRLAM analyses at 12 UTC and 18 UTC the HIRLAM domain is more densely filled with the ASCAT data (Fig. 1).

The accuracy of the ASCAT winds is validated against in situ wind measurements from buoys, platforms, or ships and against NWP data. Even better, the errors of all NWP model winds, in situ data, and scatterometer winds are computed in a triple collocation exercise. The performance is rather constant over the globe and depends mainly on the sub-footprint wind variability. The performance of the products issued by the Ocean and Sea Ice Satellite Application Facilities (OSI SAF) and EARS is characterized by a wind component RMS error smaller than 2 m s^{-1} and a bias of less than 0.5 m s^{-1} in wind speed (OSI-SAF Project Team, 2013).

In April 2013 the EUMETSAT began to disseminate operationally the ASCAT measurements from MetOp-B, which enlarged the coverage of the ASCAT measurements. As reported in the ASCAT Wind Product User Manual (OSI-SAF Project Team, 2013), both MetOp-A and MetOp-B ASCAT winds have the expected accuracy (compared with buoy data), the wind speed bias of -0.02 m s^{-1} for MetOp-A and 0.05 m s^{-1} for MetOp-B, the standard deviation is 1.78 m s^{-1} for MetOp-A and 1.80 m s^{-1} for MetOp-B. Buoy collocations and a triple collocation study made by Verspeek et al. (2013a) show also that there are no significant differences in wind quality between the ASCAT-A and ASCAT-B wind products; therefore ASCAT data from both satellites can be successfully used in operational work or in the data assimilation procedure. Verspeek et al. (2013b) used the so-called NWP Ocean Calibration (NOC) method to assess the errors of the ASCAT-A and ASCAT-B winds; data from the global oceans between latitudes 55°N and 65°S (sea ice-free areas) are used for this purpose. The error variances of the buoy data, ASCAT-A and ASCAT-B 25-km wind product, and ECMWF background winds showed standard deviations in line with the expected accuracy defined by OSI-SAF Project Team (2013). In our study both the ASCAT-A and ASCAT-B data are used for assimilation into HIRLAM.

2.3. Surface-based measurements

As the most significant impact of scatterometer observations on NWP forecasts is expected over sea and near-coastal regions, close to where the observations are made (De Valk, 2013), it is important to find out observations in marine areas on the HIRLAM domain. Two different types of observations are used for this purpose.

In our study we used two types of surface-based measurements: Independent Marine Observation (denoted here as IMO), which is not used in the HIRLAM data assimilation cycle, and Assimilated Marine Observations (denoted here as AMO), which belong to conventional data assimilated operationally into the HIRLAM. The IMO data are collected from moored buoys, lighthouses, lightships, oil platforms, and marine stations while the AMO data are collected mainly from islands or stations near the shoreline. The historical IMO data from UK Met Office buoys, lightships, and private industry oil platforms were obtained manually from the webpage <http://www.wunderground.com/MAR/ukm.html>. The measurements from Vädöarna buoy were provided by the Swedish Meteorological and Hydrological Institute; wind data from Vaindloo Island came from the Estonian Weather Service; marine data from some German buoys, lighthouses, and lightships were obtained via the Marine Environmental Monitoring Network in the North Sea and the Baltic Sea (MARNET) (http://www.bsh.de/en/Marine_data/Observations/MARNET_monitoring_network/index.jsp) and received from the Bundesamt für Seeschifffahrt und Hydrographie – Federal Maritime and Hydrographic Agency of Germany (BSH). In addition, it was a good opportunity to use the free access climate database <http://eklima.met.no/> for marine data from the Norwegian Meteorological Institute (MET Norway). All surface-based measurements used in the analysis were carried out mainly at 12:00 UTC and 18:00 UTC, except measurements on the Kiel lighthouse with 09-min delay (at 12:09 UTC, 18:09 UTC).

An overview of IMO data is presented in Table 1. To adjust the wind speed to 10 m from buoys, lighthouses, and lightships, the method described by Hsu et al. (1994) was used:

$$u_2 = u_1 (z_2/z_1)^P, \quad (1)$$

where u_2 is the wind speed at the desired reference height z_2 , u_1 is the wind speed measured at height z_1 , P is an empirically derived coefficient that varies dependent upon the stability of the atmosphere. For neutral stability conditions P is equal to 0.11, which is more appropriate for open water surfaces (Hsu et al., 1994). As reported by Ingleby (2009), all selected here private industry oil platforms report the wind

Table 1. Overview of independent marine observational (IMO) data points. WMO is World Meteorological Organization, HEIGHT means the actual height of the anemometer or the level to which the wind measurements are adjusted, MSLP shows the availability of data for MSLP data verification

WMO ID	Name	Lat, deg	Lon, deg	Type	HEIGHT, m	Owned and maintained by	MSLP
	Vaindloo	59.8	26.4	Station	10	Estonian Weather Service	No
	Vädöarna	58.5	10.9	Buoy	3	SMHI Sweden	Yes
62105	K4	55.0	-13.2	Buoy	3	Met Office UK	Yes
62029	K1	48.7	-12.4	Buoy	3	Met Office UK	Yes
62103	Channel	49.9	-2.9	Lightship	14	Met Office UK	Yes
62107	Seven Stones	50.1	-6.1	Lightship	14	Met Office UK	Yes
62304	Sandettie	51.2	1.8	Lightship	14	Met Office UK	Yes
62142	North Sea	53.0	2.1	Oil platform	10	Private industry	Yes
62145	North Sea	53.1	2.8	Oil platform	10	Private industry	Yes
62144	North Sea	53.4	1.7	Oil platform	10	Private industry	Yes
62301	Aberporth	52.4	-4.7	Buoy	3	Met Office UK	Yes
62081	K2	51.0	-13.4	Buoy	3	Met Office UK	Yes
62120	E Scotland	56.4	2.1	Oil platform	10		Yes
62164	North Sea	57.2	0.8	Oil platform	10	Private industry	Yes
64046	K7	60.5	-4.2	Buoy	3	Met Office UK	Yes
63117	North Sea	61.3	1.1	Oil platform	10	Private industry	Yes
63110	North Sea	59.5	1.5	Oil platform	10	Private industry	Yes
63113	North Sea	61.0	1.7	Oil platform	10	Private industry	Yes
62095	M6	53.0	-15.9	Buoy	4.5	Met Office UK & Met Eireann	Yes
62303	Pembroke	51.6	-5.1	Buoy	3	Met Office UK	Yes
64045	K5	59.1	-11.7	Buoy	3	Met Office UK	Yes
1300	Gullfaks C	61.2	2.3	Oil platform	10	MET Norway	No
1402	Sleipner A	58.4	1.9	Oil platform	10	MET Norway	No
1309	Troll A	60.6	3.7	Oil platform	10	MET Norway	No
1404	Heimdal	59.6	2.2	Oil platform	10	MET Norway	No
1202	Draugen	64.4	7.8	Oil platform	10	MET Norway	No
1201	Heidrun	65.3	7.3	Oil platform	10	MET Norway	No
1200	Norne	66.0	8.1	Oil platform	10	MET Norway	No
66021	Arkona Becken	54.9	13.9	Buoy	10	BSH Germany	Yes
66022	Oder Bank	54.1	14.2	Buoy	9	BSH Germany	Yes
66024	Darsser Schwelle	54.7	12.7	Buoy	9	BSH Germany	Yes
	Kiel	54.5	10.3	Lighthouse	34	BSH Germany	Yes

measurements adjusted to 10-m height. In addition, marine winds measured in the Norwegian Sea are also adjusted to 10 m. Figure 2 shows the geographical location of IMO and AMO observations. The AMO measurements are carried out mainly on islands and chosen manually depending on the location from the shoreline or in case it has been established that the measurements can represent marine winds. However, the effects of slowing down the wind speed and wind turning caused by land friction have to be taken into account.

In addition to statistical calculations, a visual comparison of the wind speed and the MSLP analysis was made for both OSEs. The number values in figures represent the difference between observational data and analysis (O–A). Some data points with close locations were eliminated from figures for clarity's sake.

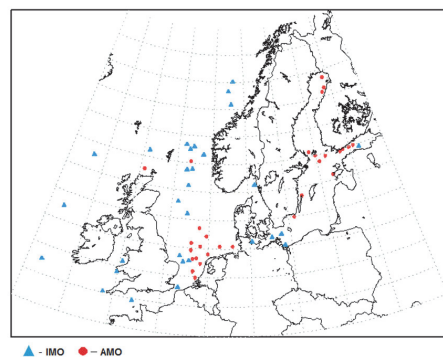


Fig. 2. Geographical location of the marine wind observations. The IMO datapoints are marked by blue colour, AMO datapoints are red.

2.4. HIRLAM and data assimilation

The HIRLAM is a hydrostatic grid-point model whose dynamics is based on a semi-implicit semi-Lagrangian discretization using hybrid vertical coordinates. The model equations and their numerical aspects are described in more detail by Undén et al. (2002). At present, the Estonian Weather Service uses the HIRLAM 7.4 version. The HIRLAM ETA domain, which covers with a horizontal resolution of 11.1 km the northern area of European countries, is used for OSEs. A more detailed overview of the HIRLAM environment in Estonia is presented by Männik et al. (2014).

The boundary fields for the HIRLAM operational model are provided by the ECMWF model. The 54-h forecasts of the HIRLAM are calculated four times a day with forecast starting-points at 00, 06, 12, and 18 UTC. Besides its usual application as the weather prediction model, the HIRLAM acts as the driving model for the local High Resolution Operational Model for the Baltic marine modelling system, which is currently used for storm surge warnings (Služenikina and Männik, 2011). In case of a positive impact of the ASCAT data assimilation on the HIRLAM, it may improve the quality of marine forecasts.

The current data assimilation system in the HIRLAM is Three-Dimensional Variational (3DVAR), the assimilation window is 06 h, -03 h from the analysis time, and +03 h ahead. Some conventional observations are generally assimilated into the local HIRLAM. The surface observations include the observations from synoptic stations (SYNOP), ships (SHIP), and from drifting buoys (DRIBU). The upper air observations include the measurements from radiosoundings (TEMP), aircraft reports (AIREP), and from pilot-balloon stations (PILOT). An overview of meteorological parameters assimilated into the HIRLAM is given in Table 2.

The First Guess at Appropriate Time (FGAT) is applied for both the conventional and ASCAT data assimilation in the operational HIRLAM. Traditionally,

3DVAR uses only a short-range forecast valid at the analysis time to compute the innovations (observations minus background); however, in the FGAT option all short-range forecasts are taken into account in the assimilation time window, and for each observation the closest forecast is selected (Huang et al., 2002). This option helps to approximate the model analysis time with observational data sampled at asynoptic time and to improve the accuracy of the model analysis output. However, in the HIRLAM 3DVAR this scheme is not used for in situ observations such as SYNOP, TEMP, and PILOT to avoid data redundancy associated with the assumption about a static observation increment (HIRLAM System Documentation, www.hirlam.org).

The algorithm of the ASCAT data assimilation in the HIRLAM 7.4 is written by De Valk (2013) with John De Vries and is optional for calculations. The principle of SeaWinds Quick Scatterometer (QuikSCAT) satellite data assimilation is applied for the ASCAT. As the ASCAT and SeaWinds have different data structures, the reading routines had to be adapted. Once the wind vector cell information is ingested, the consecutive steps for the ASCAT and SeaWinds data assimilation are similar (De Valk, 2013). A more detailed description of the SeaWinds 3DVAR assimilation algorithm is given by Tveter (2006).

The spatial and temporal screening procedure of the ASCAT observations is performed before the admission of the ASCAT data into the HIRLAM analysis: location of each WVC is compared with the HIRLAM domain and the ASCAT observational time should fit into the time window of a given assimilation cycle. Then, the WVC quality flag from the ASCAT wind product is used to ensure the high quality of the backscatter measurements and successful inversion. The ASCAT data that are land or sea-ice contaminated as well as the data with the wind speeds exceeding 30 m s⁻¹ are rejected during the quality control. In addition, the HIRLAM checks the number of ambiguities calculated for each WVC and takes the wind solutions only from the WVCs where up to two ambiguities exist. As the ASCAT wind information consists of wind ambiguities, no first-guess check is carried out and in the analysis variational quality control is not active for ASCAT (De Valk, 2013). The wind vector ambiguous solutions at each WVC are compared with the HIRLAM background winds, and the closest solution is finally selected, other wind solutions are rejected in the HIRLAM analysis.

It is well known that global models lack variance on scales below 200 km. As a consequence, the representativeness error of closely spaced observations (separated by less than 200 km) is correlated. However, nowadays assimilation systems assume uncorrelated observations. To account for this inconsistency, NWP centres apply data thinning and/or inflate the observation

Table 2. Conventional observations assimilated into the HIRLAM 3DVAR system, where z is geopotential height, u is zonal wind component, v is meridional wind component, T is temperature, and q is specific humidity

	Observation type	Parameters assimilated
Surface	SYNOP	z
	SHIP	z
	DRIBU	z
Upper air	TEMP	u, v, T, q
	AIREP	u, v, T
	PILOT	u, v

error variances to reduce the weight of the observations in the analysis (De Haan et al., 2013). In our study observational error for both wind components is 1.8 m s^{-1} , no data thinning or error inflation was applied for the ASCAT 25-km data assimilation as it is done by De Haan et al. (2013) and De Valk (2013); so more weight is given to the ASCAT observations.

In this paper two different OSEs are carried out: with ASCAT data (named 'ASCEXP') and without ASCAT data assimilation (named 'REFEXP'). As mentioned above, three different case studies are analysed:

- 28.10.2013 at 12 UTC and 18 UTC
- 01.12.2013 at 18 UTC
- 05.12.2013 at 12 UTC and 18 UTC.

The experiments are recalculated for the selected cases in the past using the backgrounds from the operational HIRLAM archive. For each case the calculations are started with the backgrounds one day before the cases at 06 UTC to avoid the 'cold start' of the model and the ASCEXP analyses are recalculated with the same method adding the ASCAT measurements in each analysis cycle. In the current study only results of OSEs analyses are compared with observations to investigate, first of all, the impact of the assimilation of the ASCAT winds into the model in case of a stormy wind situation. The bias, Root Mean Square Error (RMSE), and correlation coefficients calculated for both parameters are analysed. In addition, the differences between the ASCAT winds and model background winds (O–B) as well as model analysis after ASCAT assimilation (O–A) are calculated.

3. RESULTS

3.1. Storm Christian (St Jude, Allan) 28.10.2013

The case of the storm Christian is evaluated for two assimilation cycles at 12 and 18 UTC. The highest wind speeds measured by ASCAT for 12 UTC assimilation window were across the Belgian coast, the Netherlands, and Germany (max 25.8 m s^{-1}) and for 18 UTC assimilation window over the southern part of the Baltic Sea (max 23.9 m s^{-1}) (see Figs 1a and 1b).

The fields of the wind speed and the MSLP analysis at 12 UTC mainly differ in the centre of the storm Christian, as it is shown in Figs 3 and 4. The REFEXP calculated stormy winds in the larger marine area, while in the ASCEXP stormy winds are pressed together and shifted more to the east, and the area of weak winds has already developed in the tail of the rapidly moving storm. In addition, slightly stronger winds are calculated across the coastline of Belgium and the Netherlands in ASCEXP.

Verification with surface-based observations (O–A) detected wind speed underestimation in the tail of the storm, in some points even up to $7\text{--}8 \text{ m s}^{-1}$. The ASCAT measurements were significantly lower than the HIRLAM background winds before assimilation, but after data assimilation HIRLAM winds decreased (Fig. 3). What could be the reason that the ASCAT winds were lower than the actual winds? Haeseler and Lefebvre (2013) analysed the storm Christian in more detail and report that with the forward speed of 1200 km in 12 h , Christian was a rapidly moving low. On 28 October at 07 UTC

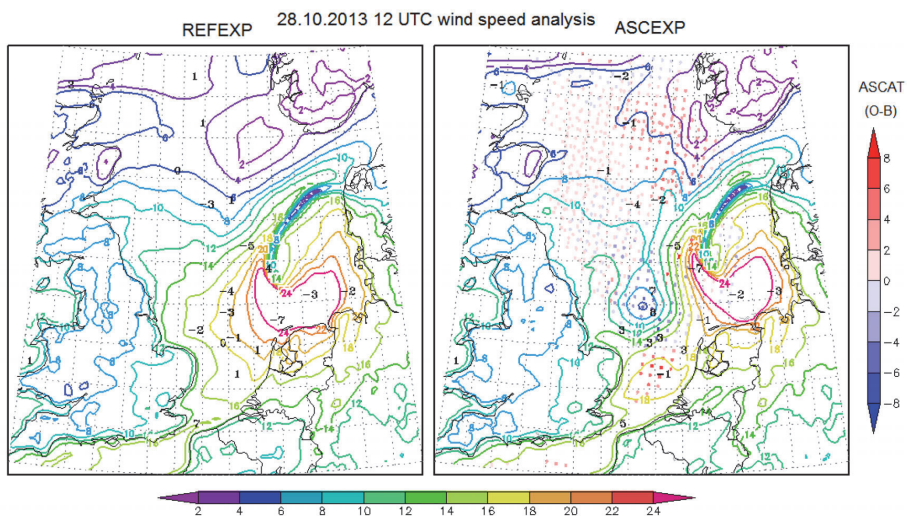


Fig. 3. The HIRLAM 10-m wind speed analyses 28.10.2013 at 12 UTC: REFEXP (left), ASCEXP (right). The number values: surface-based observation minus analysis (O–A); colour dots: ASCAT observation minus HIRLAM background (O–B) before assimilation.

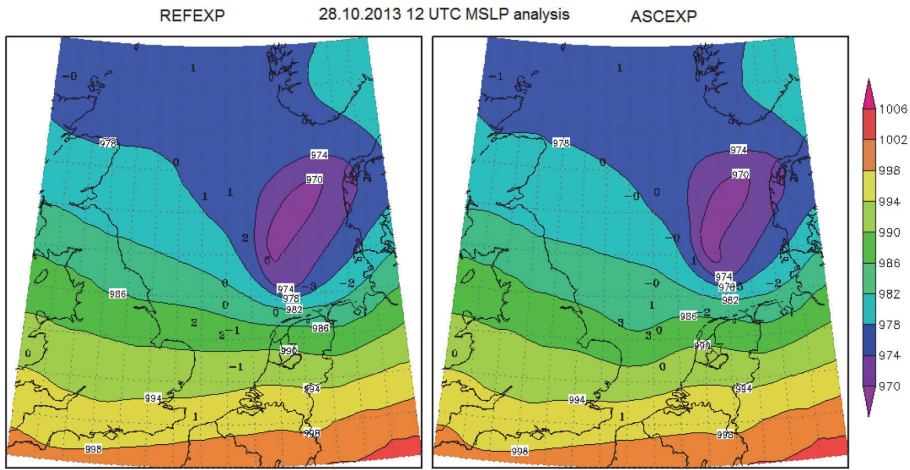


Fig. 4. The HIRLAM MSLP analyses 28.10.2013 at 12 UTC: REFEXP (left), ASCEXP (right). The number values: surface-based observation minus analysis (O–A).

the centre of the storm with a pressure of 977 hPa was located over the East Midlands, UK. Inspection of the ASCAT overpasses in the same area reveals that the ASCAT measurements were made at 09:31–09:32 UTC. This fact confirms that the centre of the low had moved slightly in two hours and that the ASCAT still gave accurate measurements. The problem lies in the fact that the ASCAT measured weaker winds in the tail of the moving storm in this time moment and the analysis at 12 UTC follows the ASCAT measurements made about two hours before the analysis time moment.

The statistics for wind speed and MSLP for 28.10.2013 at 12 UTC (Table 3) shows that the results

of OSEs are either more or less accurate depending on the area of inspection. The most notable in the MSLP analysis is that the isobars between the UK and the Netherlands (Fig. 4) shifted slightly to the south in the ASCEXP. Deepening of the low in this region probably is related with the strong winds registered there by the ASCAT. In spite of this fact, the field of the lowest pressure is more accurate in ASCEXP, which is moved more to the east unlike the REFEXP.

The visual comparison of OSEs analyses for 28.10.2013 at 18 UTC (Fig. 5) does not show significant differences. In the ASCEXP the area of stronger winds is extended more to the southern part of the Baltic Sea and

Table 3. The HIRLAM REFEXP and ASCEXP bias, RMSE, and correlation (CORR) with observed values of the 10-m wind speed and MSLP 28.10.2013 at 12 UTC (left) and 18 UTC (right)

10-m wind speed					10-m wind speed				
20131028 12 UTC		BIAS	RMSE	CORR	20131028 18 UTC		BIAS	RMSE	CORR
ASCEXP	IMO	0.00	2.17	0.95	ASCEXP	IMO	−0.63	2.11	0.91
REFEXP		0.45	2.25	0.94	REFEXP		−0.08	1.68	0.94
ASCEXP	AMO	0.56	3.24	0.81	ASCEXP	AMO	0.37	2.13	0.89
REFEXP		−0.36	3.11	0.87	REFEXP		0.53	2.12	0.89
ASCEXP	ALL	0.29	2.77	0.88	ASCEXP	ALL	−0.23	2.11	0.88
REFEXP		0.03	2.73	0.90	REFEXP		0.16	1.87	0.92
MSLP					MSLP				
ASCEXP	IMO	−0.08	2.07	0.98	ASCEXP	IMO	−0.20	0.98	1.00
REFEXP		−0.28	1.57	0.99	REFEXP		−0.15	0.98	1.00
ASCEXP	AMO	−0.50	1.26	0.98	ASCEXP	AMO	−0.71	0.77	1.00
REFEXP		−0.02	1.49	0.97	REFEXP		−0.78	0.83	1.00
ASCEXP	ALL	−0.31	1.67	0.98	ASCEXP	ALL	−0.41	0.90	1.00
REFEXP		−0.13	1.52	0.98	REFEXP		−0.41	0.92	1.00

the winds are stronger in the northern part of the Norwegian Sea. In this case we have two ASCAT overpasses across the Baltic Sea region starting at 17:43 UTC and 18:27 UTC, both showing strong winds in the Baltic Sea region. Unfortunately, the southern part of the Baltic Sea is not covered enough with observational data and we cannot check model accuracy sufficiently.

Statistical parameters for 28.10.2015 at 18 UTC are worse in the ASCEXP in the wind speed analysis compared with IMO data. The differences from IMO data points can be clearly observed near the coast of the Norwegian Sea, where the ASCEXP values follow the ASCAT wind speed values registered in this assimilation

window. Unfortunately, the comparison with IMO data points detects overestimation. This overestimation stems from the stronger ASCAT wind measurements in comparison with IMO (Fig. 1b and Fig. 5, right). The model assimilates ASCAT winds and becomes ‘incorrect’ in respect to IMO. It is difficult to assess to which observations should be given priority here.

The MSLP statistics is more accurate in AMO data points in ASCEXP analysis and takes into account all marine MSLP observations. The visual comparison of the MSLP 28.10.2013 at 18 UTC is represented only by REFEXP analysis and the difference between the OSEs analyses (Fig. 6), as the output in MSLP for both OSEs,

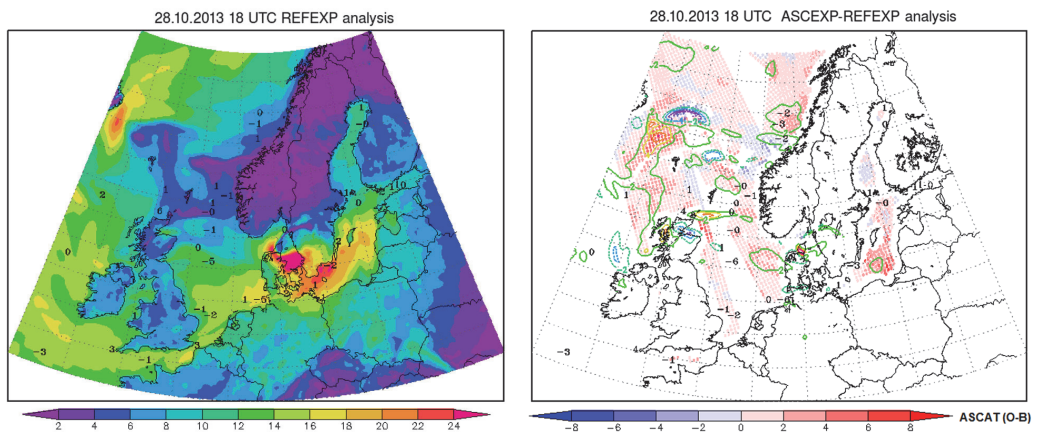


Fig. 5. HIRLAM 10-m wind speed analyses 28.10.2013 at 18 UTC: REFEXP (left), ASCEXP–REFEXP (right). The number values: surface-based observation minus analysis (O–A); colour dots: ASCAT observation minus HIRLAM background (O–B) before assimilation; colour contours (2 m s⁻¹ step) represent wind speed analyses difference (ASCEXP–REFEXP).

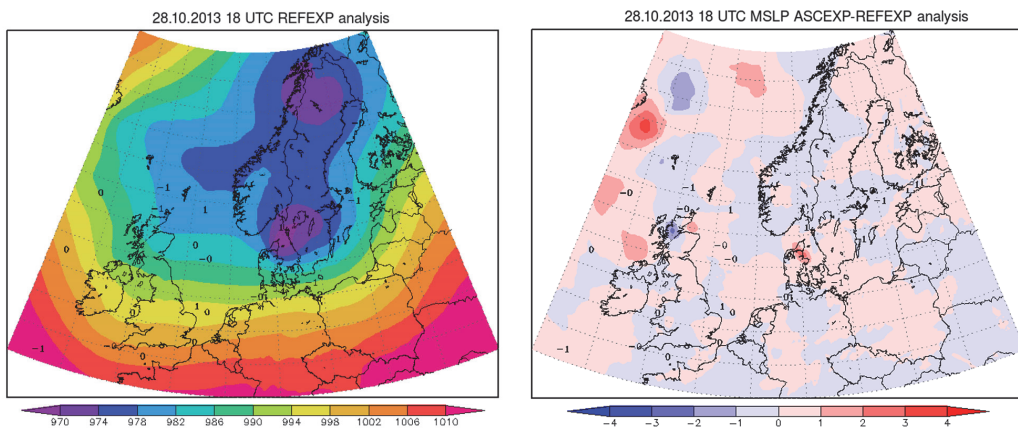


Fig. 6. The HIRLAM MSLP analyses 28.10.2013 at 18 UTC: REFEXP (left), ASCEXP–REFEXP MSLP analysis difference (right). The number values: surface-based observation minus analysis (O–A).

is very similar. Some differences were detected in the area where the accuracy cannot be checked by marine observations.

3.2. Stormy winds over the Baltic Sea 01.12.2013 at 18 UTC

In this case study we omit the OSE for 01.12.2013 at 12 UTC because of relatively sparse coverage of the ASCAT data in the HIRLAM domain, with missing measurements in the Baltic Sea. Fortunately, for 18 UTC run we have the ASCAT overpasses in the Baltic Sea region starting at 17:40 UTC and 18:24 UTC providing a good coverage of ASCAT measurements (Fig. 1c).

Two HIRLAM wind speed analyses of 01.12.2013 at 18 UTC are shown in Fig. 7. The main OSEs differences appear over the Baltic Sea, over the North Sea, and in the northwestern part of the HIRLAM domain. In all these areas the ASCEXP calculates stronger winds. Unfortu-

nately, the most distinctive difference features appear in places that are not verifiable with independent data.

In both OSEs strong underestimation of the wind speed is detected in the Gulf of Bothnia (7 m s^{-1}) and widely in the Gulf of Finland (4 m s^{-1}). It is well known that the ASCAT wind product with the grid spacing of 25 km measures the winds about 70 km away from the coastline, the WVCs closer than $\sim 70 \text{ km}$ from the coast are flagged because of land contamination (Verhoef et al., 2012). The ASCAT winds in these areas are not admitted, most likely due to their proximity to the land (Fig. 1d), although they were full of ASCAT measurements. Unfortunately, the ASCAT measurements could not improve the analysis of the storm over the Baltic Sea.

The results of statistical comparison with marine observations are presented in Table 4. The RMSEs in the ASCEXP are slightly lower in both the wind speed and the MSLP compared with IMO data; however, the RMSEs of AMO data in both parameters are higher than

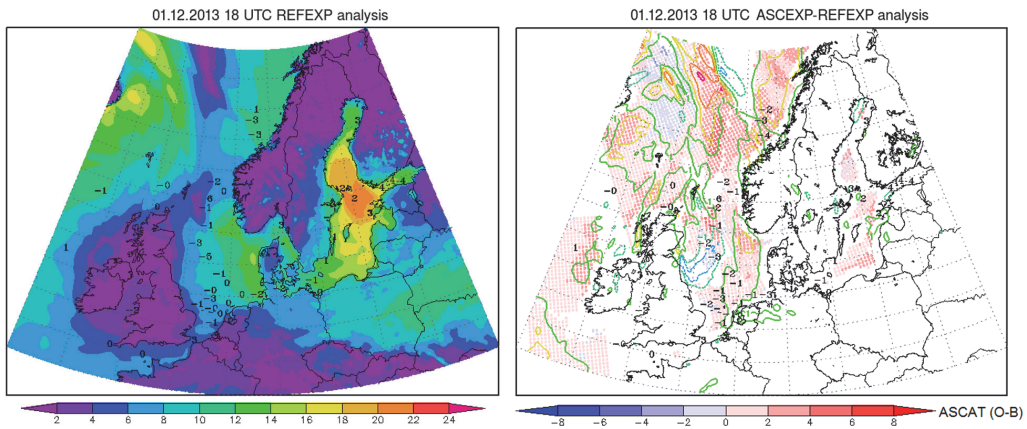


Fig. 7. HIRLAM 10-m wind speed analyses 01.12.2013 at 18 UTC: REFEXP (left), ASCEXP–REFEXP analyses difference (right). The number values: surface-based observation minus analysis (O–A); colour dots: ASCAT observation minus HIRLAM background (O–B) before assimilation; colour contours (1 m s^{-1} step) represent wind speed analyses difference (ASCEXP–REFEXP).

Table 4. The HIRLAM REFEXP and ASCEXP bias, RMSE, and correlation coefficients (CORR) of 10-m wind speed and MSLP on 01.12.2013 at 18 UTC

10-m wind speed					MSLP				
20131201 18 UTC		BIAS	RMSE	CORR	20131201 18 UTC		BIAS	RMSE	CORR
ASCEXP	IMO	-1.10	2.13	0.79	ASCEXP	IMO	-0.27	0.84	0.99
REFEXP		-0.96	2.18	0.75	REFEXP		-0.16	0.89	0.99
ASCEXP	AMO	0.48	2.82	0.86	ASCEXP	AMO	-0.65	0.85	1.00
REFEXP		0.87	2.72	0.88	REFEXP		-0.45	0.75	1.00
ASCEXP	ALL	-0.34	2.49	0.88	ASCEXP	ALL	-0.47	0.85	1.00
REFEXP		-0.08	2.46	0.88	REFEXP		-0.31	0.82	1.00

in REFEXP. An overestimation of the wind speed can be detected (Fig. 7, right) in the ASCEXP, which shows higher differences from AMO data points over the North Sea. The ASCAT overpasses after 19 UTC over the North Sea and in the northwestern part of the HIRLAM domain may cause wind speed overestimations in these regions. The cause of wind speed overestimations over the Norwegian Sea is not known, the ASCAT measurements are quite close to the assimilation moment.

The visual comparison of the MSLP shows similar results except the difference over the Norwegian Sea; here the isobars of the ASCEXP are more extended to the north and shifted slightly to the east (Fig. 8).

3.3. Storm Xaver 05.12.2013

The storm Xaver brought very high wind speeds over a large marine area of Europe; ASCAT registered the maximum for 12 UTC HIRLAM run with 28.6 m s^{-1} and for 18 UTC run 25.5 m s^{-1} . Here we evaluate two HIRLAM runs: at 12 UTC and 18 UTC. The results of the two experiments at 12 UTC (Fig. 9) differ considerably for the Norwegian Sea but show only small differences in other marine areas. The statistical output in this case (Table 5) shows more accurate wind speed analysis in REFEXP compared with IMO data. Here we observe a very strong wind speed overestimation over

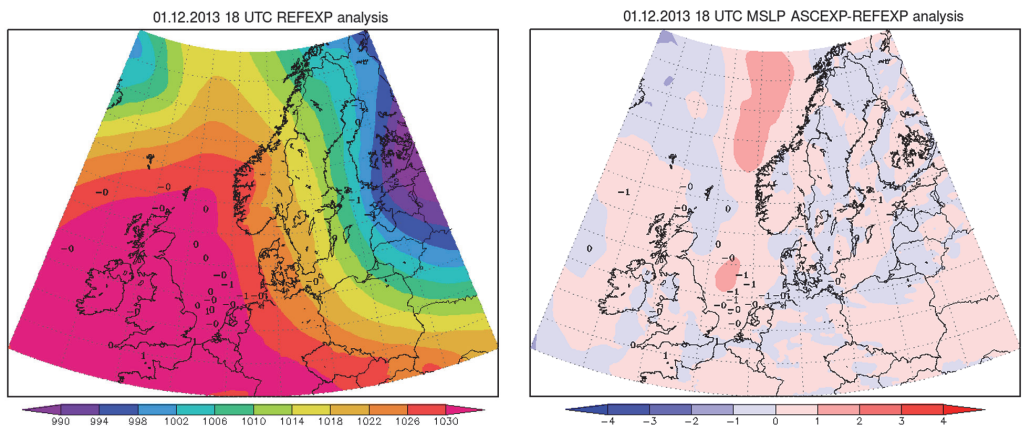


Fig. 8. The HIRLAM MSLP analyses 01.12.2013 at 18 UTC: REFEXP (left), ASCEXP–REFEXP MSLP analyses difference (right). The number values: surface-based observation minus analysis (O–A).

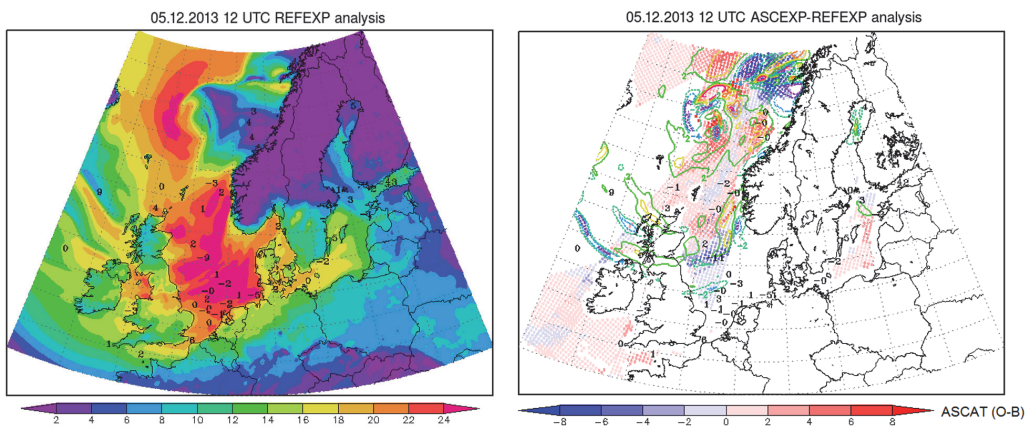


Fig. 9. HIRLAM 10-m wind speed analyses 05.12.2013 at 12 UTC: REFEXP (left), ASCEXP–REFEXP analyses difference (right). The number values: surface-based observation minus analysis (O–A); colour dots: ASCAT observation minus HIRLAM background (O–B) before assimilation; colour contours (2 m s^{-1} step) represent wind speed analyses difference (ASCEXP–REFEXP).

Table 5. The HIRLAM REFEXP and ASCEXP bias, RMSE, and correlation (CORR) with observed values of 10-m wind speed and MSLP on 05.12.2013 at 12 UTC (left) and 18 UTC (right)

10-m wind speed					10-m wind speed				
20131205 12 UTC		BIAS	RMSE	CORR	20131205 18 UTC		BIAS	RMSE	CORR
ASCEXP	IMO	0.20	3.35	0.82	ASCEXP	IMO	-1.77	4.12	0.81
REFEXP		0.90	3.27	0.86	REFEXP		-0.73	3.46	0.86
ASCEXP	AMO	-0.45	4.06	0.84	ASCEXP	AMO	0.42	3.41	0.80
REFEXP		-0.33	4.10	0.84	REFEXP		0.55	2.89	0.85
ASCEXP	ALL	-0.12	3.71	0.83	ASCEXP	ALL	-0.67	3.78	0.79
REFEXP		0.30	3.70	0.85	REFEXP		-0.09	3.19	0.85
MSLP					MSLP				
ASCEXP	IMO	-0.45	1.53	1.00	ASCEXP	IMO	-0.03	1.42	1.00
REFEXP		-0.45	1.54	1.00	REFEXP		0.10	1.35	1.00
ASCEXP	AMO	-0.91	1.16	1.00	ASCEXP	AMO	-0.61	0.86	1.00
REFEXP		-0.99	1.29	1.00	REFEXP		-0.72	0.99	1.00
ASCEXP	ALL	-0.69	1.35	1.00	ASCEXP	ALL	-0.34	1.16	1.00
REFEXP		-0.73	1.42	1.00	REFEXP		-0.34	1.17	1.00

the North Sea (-11 m s^{-1}). This overestimation is caused again by differences in the measurement time: the ASCAT measurements in this area were carried out at 09:45 UTC. However, over the Norwegian Sea the ASCEXP analysis is very accurate and fits with IMO data points because of the more appropriate time of measurement (11:23 UTC).

An important fact in this case is that about 2.0% of all ASCAT measurements used in the current assimilation window are winds over 25 m s^{-1} . Although the ASCAT Wind Product User Manual (OSI-SAF Project Team, 2013) gives the data range of the ASCAT winds $0-50 \text{ m s}^{-1}$, the wind speeds over 25 m s^{-1} are generally known to be less reliable. At strong winds wave breaking will further intensify, causing air bubbles, foam, and spray at the ocean surface, and a more and

more complicated ocean topography (Verhoef and Stoffelen, 2014). The buoy measurements in high wind/wave conditions may also show underestimated wind due to the flow disturbance extending beyond the anemometer height (Ingleby, 2009). It is also known that the model calculations may not be perfectly fitted for severe weather conditions. All these facts may lead to large variations between observed and analysed wind speed differences, especially in closely located observational data points.

In the case of 05.12.2013 at 12 UTC the ASCAT measurements over 25 m s^{-1} are used in the assimilation cycle, but in general the analysis winds are reduced to be closer to the background winds. However, at 09:42 UTC the analysis winds strengthened and were closer to the ASCAT measurements (Fig. 10). Unfortu-

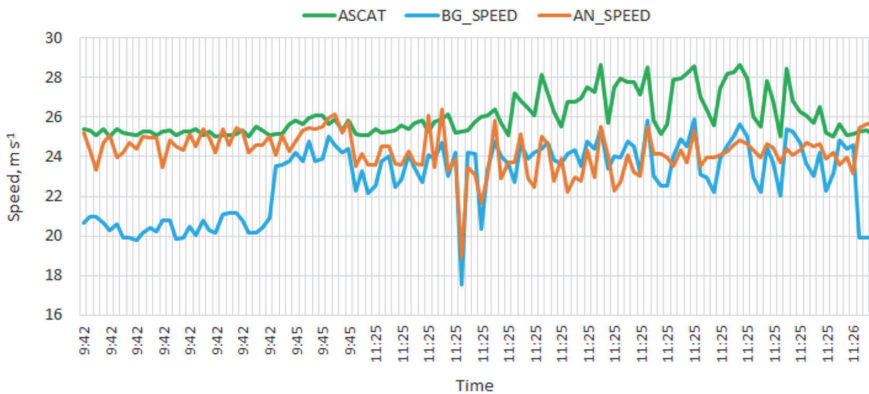


Fig. 10. The ASCAT winds over 25 m s^{-1} assimilated into the HIRLAM (ASCAT), analysis winds after assimilation (AN_SPEED), and the background winds (BG_SPEED) on 05.12.2013 at 12 UTC.

nately, as this area is located in the northern part of the Norwegian Sea, the accuracy of the analysis cannot be checked by surface-based marine observations.

The storm Xaver on 05.12.2013 at 18 UTC intensified and winds were very strong already in the southern part of the Baltic Sea (Fig. 11). The ASCEXP calculates stronger winds across the Norwegian coast and in the southern part of the Norwegian Sea, and the differences from marine observations may reach -12 m s^{-1} . Here again we observe a strong variation of the wind speed measurements in closely located data points inside the storm. At 18 UTC the wind speed statistics is more accurate in the REFEXP for all marine observations (Table 5), which is most likely caused by wind speed

overestimations in the ASCEXP analysis. The wind speed analyses in the Baltic Sea region are very similar in both OSEs.

Visual comparison of the MSLP in both analysis cycles shows significant differences over the Norwegian Sea (Fig. 12). Most likely, the strong ASCAT winds and their assimilation in this area (Fig. 1f) deepen the low-pressure system in comparison to the REFEXP. Unfortunately, the accuracy of OSEs output cannot be checked with observational data in these areas because of the missing MSLP measurements. Here we omit the ASCEXP analyses showing only REFEXP analyses and the ASCEXP–REFEXP differences.

The statistics of the MSLP 05.12.2013 at 12 UTC (Table 5) give smaller errors in the ASCEXP for all types of marine observations and, in general, show a better fit with observed MSLP than the statistics for 18 UTC. The MSLP statistics at 18 UTC are rather similar for both experiments.

3.4. ASCAT winds and HIRLAM

To study how the model backgrounds in severe storm cases fit with scatterometer observations, the ASCAT winds admitted into the HIRLAM analysis were compared with the model background (O–B) and with the analysis winds after assimilation (O–A). In all severe storm cases the mean O–B is more than 1 m s^{-1} (Fig. 13), which indicates that the ASCAT instrument measured stronger winds than the HIRLAM forecasts calculate. After the ASCAT data assimilation the mean O–A is less than 0.5 m s^{-1} and the mean standard deviation of the wind speed is less than 2 m s^{-1} , as it should be expected for the background winds. However, such general statistics hide the details of phase shifts by including effects that cancel each other.

It should be useful to analyse a longer period of ASCAT data for the evaluation of the O–B biases. In case the biases are systematic, the bias correction before the ASCAT assimilation should be undertaken. Presently no bias correction is applied in the HIRLAM.

The O–B scatterplot against time difference between the ASCAT observation time and analysis time (Fig. 14) detects that in case of the storm Xaver (05.12.2013) the wind speed deviations are the highest and occur even at the assimilation time moment. If we consider other cases, the ASCAT consistency with HIRLAM background winds is better when the ASCAT measurements are closer to the assimilation time moment. This means that in case of extremely strong storms such as the storm Xaver, higher discrepancy with the HIRLAM background winds may be expected. First, the ASCAT winds over 25 m s^{-1} are generally known to be less reliable, but they are taken into assimilation and then the limited area model calculations may not be perfectly fitted for extreme weather conditions.

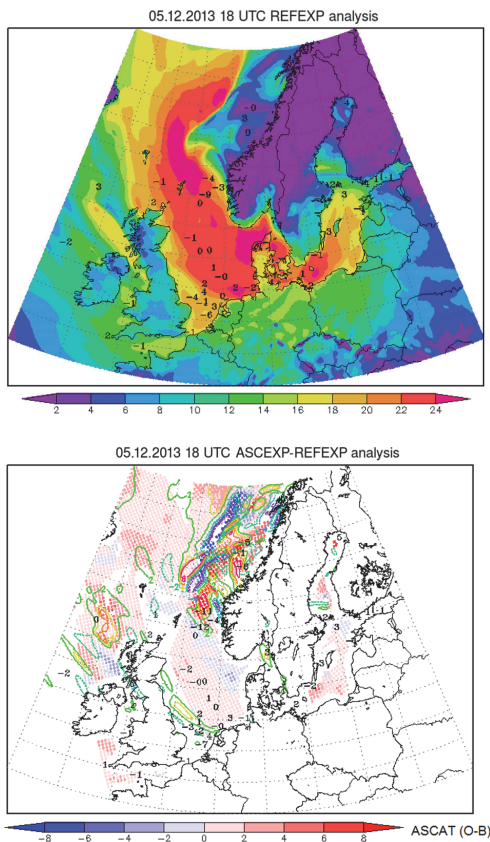


Fig. 11. HIRLAM 10-m wind speed analyses 05.12.2013 at 18 UTC: REFEXP (top), ASCEXP–REFEXP analyses difference (bottom). The number values: surface-based observation minus analysis (O–A); colour dots: ASCAT observation minus HIRLAM background (O–B) before assimilation; colour contours (2 m s^{-1} step) represent wind speed analyses difference (ASCEXP–REFEXP).

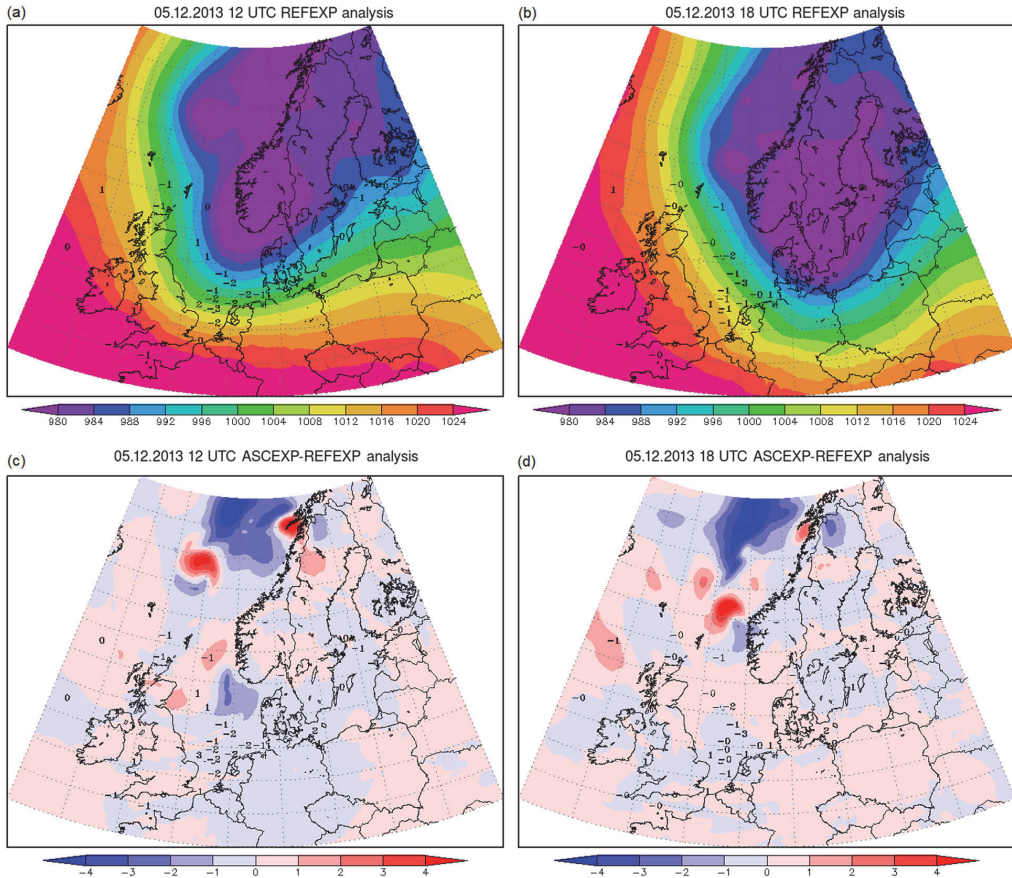


Fig. 12. HIRLAM MSLP analyses of the reference experiment REFEXP at 12 UTC (a) and 18 UTC (b), and ASCAT data containing analyses difference from the reference ASCEXP–REFEXP at 12 UTC (c) and 18 UTC (d) on 05.12.2013.

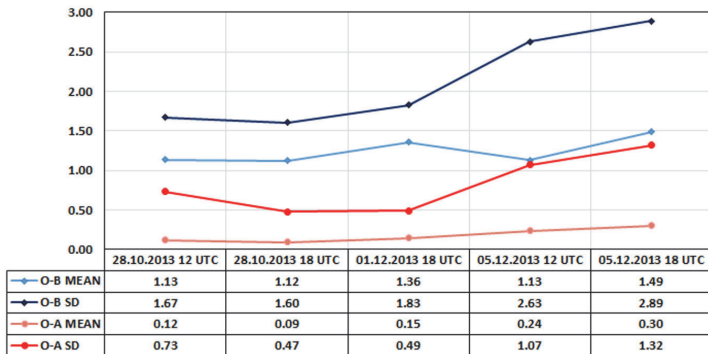


Fig. 13. The mean and standard deviation (SD) of ASCAT and HIRLAM wind speed differences (m s^{-1}) before assimilation (O–B) and after ASCAT assimilation (O–A), severe storm cases in 2013.

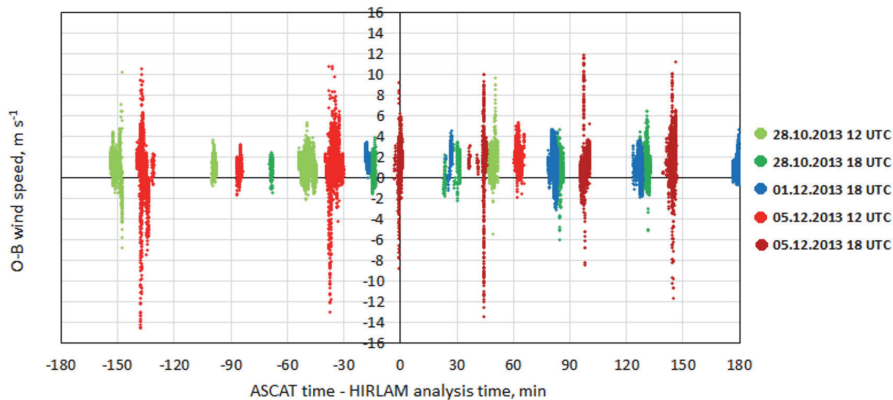


Fig. 14. Scatterplot of O–B wind speed difference versus ASCAT time minus HIRLAM analysis time for all severe storm cases.

4. CONCLUSIONS

In this paper the impact of the ASCAT measurements on the HIRLAM data assimilation quality is assessed in cases of severe storms caused by fast moving mid-latitude cyclones. The quality of the assimilation is examined in marine areas of the HIRLAM domain against in situ observations (10-m wind speed and MSLP) and the ASCAT measurements.

The results of verification show that sometimes the ASCAT data assimilation improves the analysis, but in some cases the REFEXP gives more accurate results. It is clear that case studies provide fewer statistics for the overall quality assessment of the ASCAT data assimilation in comparison with statistics collected over longer periods. On the other hand, the case studies may give more information about the model behaviour in specific synoptic situations. Valkonen and Schyberg (2015) also demonstrated strong day-to-day variations in the standard deviations of the ASCAT data compared to the model background (O–B) and the analysis (O–A). Such variations show how the model fits with instantaneous ASCAT measurements performed in the assimilation time window.

Verification of the OSEs in this study was performed separately for each case. The smallest RMSE of the wind speed appeared in the storm Christian (2.11 m s^{-1}) and the highest in the storm Xaver (3.78 m s^{-1}). De Valk (2013) analysed the impact of the ASCAT 25-km wind data assimilation on the HIRLAM during one-week experiments in wintertime and showed similar results: the mean standard deviation of the model initial state (00 length forecast) from marine observations was about 3.5 m s^{-1} . Statistical calculations of the MSLP showed also that the ASCAT data assimilation has an impact on the changes in the MSLP and in locations of the low-pressure systems.

Areas of no impact after the ASCAT data assimilation were detected as well. It was found that the HIRLAM rejected most of the ASCAT observations located close to the shoreline after the procedure of quality control. As a result, in the Baltic Sea storm of 01.12.2013 at 18 UTC (Fig. 7) the wind speeds were significantly underestimated in both OSEs, the same was detected in the storm Xaver 05.12.2013 at 12 UTC. It would be of interest to investigate possibilities of the application of the ASCAT Coastal Wind Product, which may increase the impact of the ASCAT data assimilation in these areas.

Assimilation of extremely strong ASCAT winds is also highlighted in this study. In the storm Xaver HIRLAM assimilated the ASCAT winds over 25 m s^{-1} . The analysis winds mainly followed HIRLAM background winds, which are weaker than the ASCAT measurements (Fig. 10). This result is contrary to the study by Valkonen and Schyberg (2015), which showed that in the case of the strong ASCAT winds (over 23 m s^{-1}) HARMONIE background winds were always higher than ASCAT. This may be attributed to the different tunings or systematic differences of HIRLAM and HARMONIE background forecast models. Some large differences in case of extremely strong ASCAT winds were detected between the ASCAT and HIRLAM background winds observed in our study as well. Unfortunately, the lack of independent marine observations in the area where large departures occurred does not allow comprehensive evaluation of the impact on the data assimilation quality.

Results from case studies of severe storms show that the impact of the ASCAT data assimilation into HIRLAM is considerable and well visible in both the wind and MSLP analyses. However, we demonstrate that strong winds measured by ASCAT may affect adversely the analysis quality and can create significant phase errors

in case of relatively fast moving severe storms. No adjustments in the system such as data thinning or observation error setting were made in the study, similar to the studies by De Valk (2013) and De Haan et al. (2013), which gave more weight to the ASCAT measurements. Some negative results detected in the study raise the question about the optimal use of the ASCAT data. Probably, the ASCAT observations should be thinned to get better results, especially in areas where measurements are performed simultaneously from both satellites. Such technique was applied by Valkonen and Schyberg (2015), De Chiara et al. (2014), and Ollinaho (2010) and shows positive to neutral results. Another approach that could improve the quality of the HIRLAM analyses is to shorten the time interval between the analyses. In our studies the FGAT is applied, but it still seems to be insufficient to avoid large differences in observations and background in the assimilation cycle. As improving the quality of severe storm forecasting is very important for society, further research is necessary to improve the data assimilation methods for ASCAT winds to avoid such negative impacts.

ACKNOWLEDGEMENTS

This work was supported by research grant No. 9140 of the Estonian Science Foundation and Institutional research funding IUT20-11 of the Estonian Ministry of Education and Research. The analysis was carried out with the ASCAT data distributed jointly by the EUMETSAT and OSI SAF project and through the participation in the HIRLAM project. The observational data used in the current study were provided by the Federal Maritime and Hydrographic Agency of Germany (BSH), Estonian Weather Service, and Swedish Meteorological Institute.

The authors are thankful for cooperation and consultations to Vello Loooris, who provided the environment to make the HIRLAM OSEs possible. We would like to thank Kalle Eerola, Pirkka Ollinaho, and Tuuli Perttula from the Finnish Meteorological Institute for their advice and consultations of the ASCAT assimilation into NWP models.

REFERENCES

- Bi, L., Jung, J., Morgan, M., Le Marshall, J., Baker, N., and Santek, D. 2010. Impact of METOP ASCAT Ocean Surface Winds on Global Weather Forecasts. In *10th International Winds Workshop, Tokyo, Japan, 22–26 February 2010*. https://www.researchgate.net/publication/267700761_Impact_of_METOP_ASCAT_Ocean_Surface_Winds_on_Global_Weather_Forecasts (accessed 2016-04-04).
- Cotton, J. 2013. The impact of ASCAT winds from Metop-B and a new scatterometer thinning scheme. Forecasting Research Technical Report No. 580, Met Office. <http://www.metoffice.gov.uk/media/pdf/3/1/FRTR580.pdf> (accessed 2015-10-20).
- De Chiara, G., Janssen, P., English, S., Bidlot, J.-R., and Laloyaux, P. 2014. Scatterometer impact studies at ECMWF. In *Proceedings of the EUMETSAT Meteorological Satellite Conference, Geneva, Switzerland, 22–26 September 2014*. <http://www.eumetsat.int/> (accessed 2015-10-20).
- De Haan, S., Marseille, G.-J., De Valk, P., and De Vries, J. 2013. Impact of ASCAT Scatterometer wind observations on the High-Resolution Limited-Area Model (HIRLAM) within an operational context. *Weather Forecast.*, **28**, 489–503.
- De Valk, P. 2013. ASCAT assimilation in the HIRLAM report. De Bilt, international report, IR-2013-02. <http://www.knmi.nl/bibliotheek/knmi/pubIR/IR2013-02.pdf> (accessed 2015-10-20).
- Deutschländer, T., Friedrich, K., Haeseler, S., and Lefebvre, C. 2013. Severe storm XAVER across northern Europe from 5 to 7 December 2013. Deutscher Wetterdienst. https://www.dwd.de/EN/ourservices/specialevents/storms/20131230_XAVER_europe_en.pdf?__blob=publicationFile&v=4 (accessed 2016-04-04).
- Figa-Saldaña, J., Wilson, J. W., Attema, E., Gelsthorpe, R., Drinkwater, M. R., and Stoffelen, A. 2002. The advanced scatterometer (ASCAT) on the meteorological operational (MetOp) platform: a follow on for the European wind scatterometers. *Can. J. Remote Sens.*, **28**(3), 404–412.
- Haeseler, S. and Lefebvre, C. 2013. Heavy storm CHRISTIAN on 28 October 2013. Deutscher Wetterdienst. http://www.dwd.de/DE/presse/hintergrundberichte/2013/Orkantief_Christian_PDF.pdf?__blob=publicationFile&v=3 (accessed 2015-10-18).
- Hersbach, H. and Janssen, P. 2007. Operational assimilation of surface wind data from the MetOp ASCAT scatterometer at ECMWF. *ECMWF Newsletter*, **113**, 6–8.
- Hersbach, H., Stoffelen, A., and de Haan, S. 2007. An improved C-band ocean geophysical model function: CMOD-5. *J. Geophys. Res.*, **112**, C03006.
- Hsu, S. A., Meindl, E. A., and Gilhouse, D. B. 1994. Determining the power-law wind-profile exponent under near-neutral stability conditions at sea. *Appl. Meteorol.*, **33**(6), 757–765.
- Huang, X.-Y., Morgensen, K. S., and Yang, X. 2002. First-guess at the appropriate time: the HIRLAM implementation and experiments. In *Proceedings for HIRLAM workshop on variational data assimilation and remote sensing, Helsinki, 22–23 January 2002*, pp. 28–43.
- Ingleby, B. 2009. Factors affecting ship and buoy data quality. Technical Report No. 529, Met Office, Meteorology Research and Development. http://research.metoffice.gov.uk/research/nwp/publications/papers/technical_reports/reports/529.pdf (accessed 2015-10-20).
- Männik, A., Luhamaa, A., Loooris, V., and Toll, V. 2014. Numerical weather prediction environment in Estonian Environmental Agency. In *Joint 24th ALADIN Workshop & HIRLAM All Staff Meeting 2014, 7–11 April 2014, Romania*. http://www.cnrm.meteo.fr/aladin/IMG/pdf/nationalposterkaur_asm2014.pdf (accessed 2015-10-16).

- Ollinaho, P. 2010. Feasibility of Assimilating ASCAT Surface Winds into a Limited Area Model. M.S. thesis, Department of Physics, University of Helsinki. <https://helda.helsinki.fi/bitstream/handle/10138/20968/feasibil.pdf> (accessed 2015-10-20).
- OSI-SAF Project Team. 2013. ASCAT Wind Product User Manual version 1.13 May. KNMI, De Bilt, The Netherlands. Technical Report Reference: SAF/OSI/CDOP/KNMI/TEC/MA/126. http://projects.knmi.nl/scatterometer/publications/pdf/ASCAT_Product_Manual.pdf (accessed 2015-10-20).
- Payan, C. 2010. Improvements in the use of scatterometer winds in the operational NWP system at Météo-France. 10th International Winds Workshop, Tokyo, Japan, 22–26 February 2010. www.eumetsat.int/.../ConferencesandEvents/DAT_2042632... (accessed 2016-04-04).
- Portabella, M., Stoffelen, A., Verhoef, A., and Verspeek, J. 2012. A new method for improving ASCAT wind quality control. *IEEE Geoscience and Remote Sensing Letters*, 9(4), 579–583.
- Služenikina, J. and Männik, A. 2011. A comparison of ASCAT wind measurements and the HIRLAM model over the Baltic Sea. *Oceanologia*, 53(1, SI), 229–244.
- Stoffelen, A. 1998. Scatterometry. Thesis, Universiteit Utrecht. <http://dspace.library.uu.nl/bitstream/handle/1874/636/full.pdf?sequence=1> (accessed 2015-10-20).
- Stoffelen, A., Portabella, M., Verhoef, A., Verspeek, J., and Vogelzang, J. 2006. Mesoscale winds from the new ASCAT scatterometer. *KNMI Res. Biennial Rep. 2005–2006*, 30–35.
- Stoffelen, A., Verhoef, A., Verspeek, J., Vogelzang, J., Driessenaar, T., Risheng, Y., et al. 2013. Research and Development in Europe on Global Application of the OceanSat-2 Scatterometer Winds. Final Report of OceanSat-2 Cal/Val A0 project.
- Storch, H., Feser, F., Haeseler, S., Lefebvre, C., and Stendel, M. 2014. A violent mid-latitude storm in northern Germany and Denmark, 28 October 2013. *BAMS*, 95(9). <http://www.hvnonstorch.de/klima/pdf/BAMS-Christian-Allan-2013.pdf> (accessed 2015-10-20).
- Takahashi, M. 2010. Operational use of Scatterometer Winds at JMA. In *Proceedings of 10th International Winds Workshop, Tokyo, Japan, 22–26 February 2010*.
- Tveter, F. 2006. Assimilating ambiguous QuikScat scatterometer observations in HIRLAM 3-D-Var at the Norwegian Meteorological Institute. *Tellus*, 58A, 59–68.
- Undén, P., Rontu, L., Järvinen, H., Lynch, P., Calvo, J., Cats, G., et al. 2002. HIRLAM-5 scientific documentation. http://www.hirlam.org/index.php/meeting-reports-and-presentations/cat_view/114-model-and-system-documentation/131-hirlam-documentation (accessed 2015-10-20).
- Valkonen, T. and Schyberg, H. 2015. The impact of ASCAT winds in storm cases using the HARMONIE model system. EUMETSAT Fellowship Programme: First year report. MET report 2/2015, ISSN 2387-4201, Norwegian Meteorological Institute, Norway. http://met.no/Forskning/Publikasjoner/MET_report/fil_estore/MetReport02-2015.pdf (accessed 2015-10-20).
- Verhoef, A. and Stoffelen, A. 2014. Algorithm Theoretical Basis Document for the OSI SAF wind products version 1.1. Document external project: SAF/OSI/CDOP2/KNMI/SCI/MA/197.
- Verhoef, A., Portabella, M., and Stoffelen, A. 2012. High-Resolution ASCAT scatterometer winds near the coast. *Geoscience and Remote Sensing*, 50(7), 2481–2487.
- Verspeek, J., Verhoef, A., and Stoffelen, A. 2013a. ASCAT-B NWP Ocean Calibration and Validation. Technical Report Reference: SAF/OSI/CDOP2/KNMI/TEC/RP/199.
- Verspeek, J., Stoffelen, A., Verhoef, A., Portabella, M., and Vogelzang, J. 2013b. ASCAT-B ocean calibration and wind product results. In *2013 EUMETSAT Meteorological Satellite Conference, Vienna, Austria, 16–20 September 2013*.
- Vogelzang, J., Stoffelen, A., Verhoef, A., De Vries, J., and Bonekamp, H. 2009. Validation of two-dimensional variational ambiguity removal on SeaWinds scatterometer data. *J. Atm. Oceanic Technol.*, 7(26), 1229–1245.

Skatteromeetri ASCAT tuuleandmete assimileerimise mõju HIRLAM-i analüüsi kvaliteedile tugevate tormide puhul

Jekaterina Služenikina ja Arne Männik

On hinnatud skatteromeetri ASCAT andmete assimileerimise mõju ilmaennustustarkvara HIRLAM väljundi kvaliteedile 2013. aasta kiiresti arenevate tormide ajal. Seda on tehtud kahe vaatlussüsteemi eksperimendi kaudu: ühel juhul toimub ASCAT-i andmete assimileerimine ja teisel mitte. Mudeli väljundi kvaliteedi hindamiseks on kasutatud kümme meetri kõrgusel mere kohal registreeritud tuule ja keskmise õhurõhu andmeid. Tulemused näitavad, et olenevalt uuritava ala kaetusest ASCAT-i andmetega ja assimilatsiooni hetkel saadaolevast andmehulgast võib tulemus olla enam või vähem täpne. On ka leitud, et mõnede kitsamate alade puhul Läänemeres (Botnia ja Soome laht) ei mõjuta ASCAT-i andmete assimileerimine oluliselt tulemusi. Tuuleprodukti spetsifikatsiooni käigus näitavad ASCAT-i mõõtmised rannikualade lähedal tavaliselt maismaaga saastumist. Nendel aladel ei analüüsita ASCAT-i tuuli pärast HIRLAM-i kvaliteedikontrolli, põhjuseks on tõenäoliselt ranniku lähedus. Tulevikus võiks neil aladel ASCAT-i avameretuule produkti täiendada rannikutuule produktiga. Lisaks avastati mõned ASCAT-i andmeassimilatsiooni nõrgad kohad, mis tõstatab küsimuse ASCAT-i andmete optimaalsest kasutamisest. On leitud, et tulemuste edasiseks parendamiseks on vaja proovida ASCAT-i mõõtmisi hõrendada enne assimileerimist või vähendada ajalist vahemikku HIRLAM-i analüüsides.

**DISSERTATIONS DEFENDED AT
TALLINN UNIVERSITY OF TECHNOLOGY ON
NATURAL AND EXACT SCIENCES**

1. **Olav Kongas**. Nonlinear Dynamics in Modeling Cardiac Arrhythmias. 1998.
2. **Kalju Vanatalu**. Optimization of Processes of Microbial Biosynthesis of Isotopically Labeled Biomolecules and Their Complexes. 1999.
3. **Ahto Buldas**. An Algebraic Approach to the Structure of Graphs. 1999.
4. **Monika Drews**. A Metabolic Study of Insect Cells in Batch and Continuous Culture: Application of Chemostat and Turbidostat to the Production of Recombinant Proteins. 1999.
5. **Eola Valdre**. Endothelial-Specific Regulation of Vessel Formation: Role of Receptor Tyrosine Kinases. 2000.
6. **Kalju Lott**. Doping and Defect Thermodynamic Equilibrium in ZnS. 2000.
7. **Reet Koljak**. Novel Fatty Acid Dioxygenases from the Corals *Plexaura homomalla* and *Gersemia fruticosa*. 2001.
8. **Anne Paju**. Asymmetric oxidation of Prochiral and Racemic Ketones by Using Sharpless Catalyst. 2001.
9. **Marko Vendelin**. Cardiac Mechanoenergetics *in silico*. 2001.
10. **Pearu Peterson**. Multi-Soliton Interactions and the Inverse Problem of Wave Crest. 2001.
11. **Anne Menert**. Microcalorimetry of Anaerobic Digestion. 2001.
12. **Toomas Tiivel**. The Role of the Mitochondrial Outer Membrane in *in vivo* Regulation of Respiration in Normal Heart and Skeletal Muscle Cell. 2002.
13. **Olle Hints**. Ordovician Scolecodonts of Estonia and Neighbouring Areas: Taxonomy, Distribution, Palaeoecology, and Application. 2002.
14. **Jaak Nõlvak**. Chitinozoan Biostratigraphy in the Ordovician of Baltoscandia. 2002.
15. **Liivi Kluge**. On Algebraic Structure of Pre-Operad. 2002.
16. **Jaanus Lass**. Biosignal Interpretation: Study of Cardiac Arrhythmias and Electromagnetic Field Effects on Human Nervous System. 2002.
17. **Janek Peterson**. Synthesis, Structural Characterization and Modification of PAMAM Dendrimers. 2002.
18. **Merike Vaher**. Room Temperature Ionic Liquids as Background Electrolyte Additives in Capillary Electrophoresis. 2002.
19. **Valdek Mikli**. Electron Microscopy and Image Analysis Study of Powdered Hardmetal Materials and Optoelectronic Thin Films. 2003.
20. **Mart Viljus**. The Microstructure and Properties of Fine-Grained Cermets. 2003.
21. **Signe Kask**. Identification and Characterization of Dairy-Related *Lactobacillus*. 2003.
22. **Tiiu-Mai Laht**. Influence of Microstructure of the Curd on Enzymatic and Microbiological Processes in Swiss-Type Cheese. 2003.
23. **Anne Kuusksalu**. 2–5A Synthetase in the Marine Sponge *Geodia cydonium*. 2003.
24. **Sergei Bereznev**. Solar Cells Based on Polycrystalline Copper-Indium Chalcogenides and Conductive Polymers. 2003.

25. **Kadri Kriis.** Asymmetric Synthesis of C₂-Symmetric Bimorpholines and Their Application as Chiral Ligands in the Transfer Hydrogenation of Aromatic Ketones. 2004.
26. **Jekaterina Reut.** Polypyrrole Coatings on Conducting and Insulating Substrates. 2004.
27. **Sven Nõmm.** Realization and Identification of Discrete-Time Nonlinear Systems. 2004.
28. **Olga Kijatkina.** Deposition of Copper Indium Disulphide Films by Chemical Spray Pyrolysis. 2004.
29. **Gert Tamberg.** On Sampling Operators Defined by Rogosinski, Hann and Blackman Windows. 2004.
30. **Monika Übner.** Interaction of Humic Substances with Metal Cations. 2004.
31. **Kaarel Adamberg.** Growth Characteristics of Non-Starter Lactic Acid Bacteria from Cheese. 2004.
32. **Imre Vallikivi.** Lipase-Catalysed Reactions of Prostaglandins. 2004.
33. **Merike Peld.** Substituted Apatites as Sorbents for Heavy Metals. 2005.
34. **Vitali Syritski.** Study of Synthesis and Redox Switching of Polypyrrole and Poly(3,4-ethylenedioxythiophene) by Using *in-situ* Techniques. 2004.
35. **Lee Põllumaa.** Evaluation of Ecotoxicological Effects Related to Oil Shale Industry. 2004.
36. **Riina Aav.** Synthesis of 9,11-Secosterols Intermediates. 2005.
37. **Andres Braunbrück.** Wave Interaction in Weakly Inhomogeneous Materials. 2005.
38. **Robert Kitt.** Generalised Scale-Invariance in Financial Time Series. 2005.
39. **Juss Pavelson.** Mesoscale Physical Processes and the Related Impact on the Summer Nutrient Fields and Phytoplankton Blooms in the Western Gulf of Finland. 2005.
40. **Olari Ilison.** Solitons and Solitary Waves in Media with Higher Order Dispersive and Nonlinear Effects. 2005.
41. **Maksim Säkki.** Intermittency and Long-Range Structurization of Heart Rate. 2005.
42. **Enli Kiipli.** Modelling Seawater Chemistry of the East Baltic Basin in the Late Ordovician–Early Silurian. 2005.
43. **Igor Golovtsov.** Modification of Conductive Properties and Processability of Polyparaphenylene, Polypyrrole and polyaniline. 2005.
44. **Katrin Laos.** Interaction Between Furcellaran and the Globular Proteins (Bovine Serum Albumin β -Lactoglobulin). 2005.
45. **Arvo Mere.** Structural and Electrical Properties of Spray Deposited Copper Indium Disulphide Films for Solar Cells. 2006.
46. **Sille Ehala.** Development and Application of Various On- and Off-Line Analytical Methods for the Analysis of Bioactive Compounds. 2006.
47. **Maria Kulp.** Capillary Electrophoretic Monitoring of Biochemical Reaction Kinetics. 2006.
48. **Anu Aaspõllu.** Proteinases from *Vipera lebetina* Snake Venom Affecting Hemostasis. 2006.

49. **Lyudmila Chekulayeva.** Photosensitized Inactivation of Tumor Cells by Porphyrins and Chlorins. 2006.
50. **Merle Uudsemaa.** Quantum-Chemical Modeling of Solvated First Row Transition Metal Ions. 2006.
51. **Tagli Pitsi.** Nutrition Situation of Pre-School Children in Estonia from 1995 to 2004. 2006.
52. **Angela Ivask.** Luminescent Recombinant Sensor Bacteria for the Analysis of Bioavailable Heavy Metals. 2006.
53. **Tiina Lõugas.** Study on Physico-Chemical Properties and Some Bioactive Compounds of Sea Buckthorn (*Hippophae rhamnoides* L.). 2006.
54. **Kaja Kasemets.** Effect of Changing Environmental Conditions on the Fermentative Growth of *Saccharomyces cerevisiae* S288C: Auxo-accelerostat Study. 2006.
55. **Ildar Nisamedtinov.** Application of ¹³C and Fluorescence Labeling in Metabolic Studies of *Saccharomyces* spp. 2006.
56. **Alar Leibak.** On Additive Generalisation of Voronoï's Theory of Perfect Forms over Algebraic Number Fields. 2006.
57. **Andri Jagomägi.** Photoluminescence of Chalcopyrite Tellurides. 2006.
58. **Tõnu Martma.** Application of Carbon Isotopes to the Study of the Ordovician and Silurian of the Baltic. 2006.
59. **Marit Kauk.** Chemical Composition of CuInSe₂ Monograin Powders for Solar Cell Application. 2006.
60. **Julia Kois.** Electrochemical Deposition of CuInSe₂ Thin Films for Photovoltaic Applications. 2006.
61. **Iiona Oja Açıık.** Sol-Gel Deposition of Titanium Dioxide Films. 2007.
62. **Tiia Anmann.** Integrated and Organized Cellular Bioenergetic Systems in Heart and Brain. 2007.
63. **Katrin Trummal.** Purification, Characterization and Specificity Studies of Metalloproteinases from *Vipera lebetina* Snake Venom. 2007.
64. **Gennadi Lessin.** Biochemical Definition of Coastal Zone Using Numerical Modeling and Measurement Data. 2007.
65. **Enno Pais.** Inverse problems to determine non-homogeneous degenerate memory kernels in heat flow. 2007.
66. **Maria Borissova.** Capillary Electrophoresis on Alkylimidazolium Salts. 2007.
67. **Karin Valmsen.** Prostaglandin Synthesis in the Coral *Plexaura homomalla*: Control of Prostaglandin Stereochemistry at Carbon 15 by Cyclooxygenases. 2007.
68. **Kristjan Piirimäe.** Long-Term Changes of Nutrient Fluxes in the Drainage Basin of the Gulf of Finland – Application of the PolFlow Model. 2007.
69. **Tatjana Dedova.** Chemical Spray Pyrolysis Deposition of Zinc Sulfide Thin Films and Zinc Oxide Nanostructured Layers. 2007.
70. **Katrin Tomson.** Production of Labelled Recombinant Proteins in Fed-Batch Systems in *Escherichia coli*. 2007.
71. **Cecilia Sarmiento.** Suppressors of RNA Silencing in Plants. 2008.
72. **Vilja Mardla.** Inhibition of Platelet Aggregation with Combination of Antiplatelet Agents. 2008.

73. **Maie Bachmann.** Effect of Modulated Microwave Radiation on Human Resting Electroencephalographic Signal. 2008.
74. **Dan Hivonen.** Terahertz Spectroscopy of Low-Dimensional Spin Systems. 2008.
75. **Ly Villo.** Stereoselective Chemoenzymatic Synthesis of Deoxy Sugar Esters Involving *Candida antarctica* Lipase B. 2008.
76. **Johan Anton.** Technology of Integrated Photoelasticity for Residual Stress Measurement in Glass Articles of Axisymmetric Shape. 2008.
77. **Olga Volobujeva.** SEM Study of Selenization of Different Thin Metallic Films. 2008.
78. **Artur Jogi.** Synthesis of 4'-Substituted 2,3'-dideoxynucleoside Analogues. 2008.
79. **Mario Kadastik.** Doubly Charged Higgs Boson Decays and Implications on Neutrino Physics. 2008.
80. **Fernando Perez-Caballero.** Carbon Aerogels from 5-Methylresorcinol-Formaldehyde Gels. 2008.
81. **Sirje Vaask.** The Comparability, Reproducibility and Validity of Estonian Food Consumption Surveys. 2008.
82. **Anna Menaker.** Electrosynthesized Conducting Polymers, Polypyrrole and Poly(3,4-ethylenedioxythiophene), for Molecular Imprinting. 2009.
83. **Lauri Ilison.** Solitons and Solitary Waves in Hierarchical Korteweg-de Vries Type Systems. 2009.
84. **Kaia Ernits.** Study of In₂S₃ and ZnS Thin Films Deposited by Ultrasonic Spray Pyrolysis and Chemical Deposition. 2009.
85. **Veljo Sinivee.** Portable Spectrometer for Ionizing Radiation "Gammamapper". 2009.
86. **Juri Virkepu.** On Lagrange Formalism for Lie Theory and Operadic Harmonic Oscillator in Low Dimensions. 2009.
87. **Marko Piirsoo.** Deciphering Molecular Basis of Schwann Cell Development. 2009.
88. **Kati Helmja.** Determination of Phenolic Compounds and Their Antioxidative Capability in Plant Extracts. 2010.
89. **Merike Sõmera.** Sobemoviruses: Genomic Organization, Potential for Recombination and Necessity of P1 in Systemic Infection. 2010.
90. **Kristjan Laes.** Preparation and Impedance Spectroscopy of Hybrid Structures Based on CuIn₃Se₅ Photoabsorber. 2010.
91. **Kristin Lippur.** Asymmetric Synthesis of 2,2'-Bimorpholine and its 5,5'-Substituted Derivatives. 2010.
92. **Merike Luman.** Dialysis Dose and Nutrition Assessment by an Optical Method. 2010.
93. **Mihhail Berezovski.** Numerical Simulation of Wave Propagation in Heterogeneous and Microstructured Materials. 2010.
94. **Tamara Aid-Pavlidis.** Structure and Regulation of BDNF Gene. 2010.
95. **Olga Bragina.** The Role of Sonic Hedgehog Pathway in Neuro- and Tumorigenesis. 2010.
96. **Merle Randrt.** Wave Propagation in Microstructured Solids: Solitary and Periodic Waves. 2010.

97. **Marju Laars.** Asymmetric Organocatalytic Michael and Aldol Reactions Mediated by Cyclic Amines. 2010.
98. **Maarja Grossberg.** Optical Properties of Multinary Semiconductor Compounds for Photovoltaic Applications. 2010.
99. **Alla Maloverjan.** Vertebrate Homologues of Drosophila Fused Kinase and Their Role in Sonic Hedgehog Signalling Pathway. 2010.
100. **Priit Pruunsild.** Neuronal Activity-Dependent Transcription Factors and Regulation of Human *BDNF* Gene. 2010.
101. **Tatjana Knjazeva.** New Approaches in Capillary Electrophoresis for Separation and Study of Proteins. 2011.
102. **Atanas Katerski.** Chemical Composition of Sprayed Copper Indium Disulfide Films for Nanostructured Solar Cells. 2011.
103. **Kristi Timmo.** Formation of Properties of CuInSe_2 and $\text{Cu}_2\text{ZnSn}(\text{S,Se})_4$ Monograin Powders Synthesized in Molten KI. 2011.
104. **Kert Tamm.** Wave Propagation and Interaction in Mindlin-Type Microstructured Solids: Numerical Simulation. 2011.
105. **Adrian Popp.** Ordovician Proetid Trilobites in Baltoscandia and Germany. 2011.
106. **Ove Pärn.** Sea Ice Deformation Events in the Gulf of Finland and This Impact on Shipping. 2011.
107. **Germo Väli.** Numerical Experiments on Matter Transport in the Baltic Sea. 2011.
108. **Andrus Seiman.** Point-of-Care Analyser Based on Capillary Electrophoresis. 2011.
109. **Olga Katargina.** Tick-Borne Pathogens Circulating in Estonia (Tick-Borne Encephalitis Virus, *Anaplasma phagocytophilum*, *Babesia* Species): Their Prevalence and Genetic Characterization. 2011.
110. **Ingrid Sumeri.** The Study of Probiotic Bacteria in Human Gastrointestinal Tract Simulator. 2011.
111. **Kairit Zovo.** Functional Characterization of Cellular Copper Proteome. 2011.
112. **Natalja Makarytsheva.** Analysis of Organic Species in Sediments and Soil by High Performance Separation Methods. 2011.
113. **Monika Mortimer.** Evaluation of the Biological Effects of Engineered Nanoparticles on Unicellular Pro- and Eukaryotic Organisms. 2011.
114. **Kersti Tepp.** Molecular System Bioenergetics of Cardiac Cells: Quantitative Analysis of Structure-Function Relationship. 2011.
115. **Anna-Liisa Peikolainen.** Organic Aerogels Based on 5-Methylresorcinol. 2011.
116. **Leeli Amon.** Palaeoecological Reconstruction of Late-Glacial Vegetation Dynamics in Eastern Baltic Area: A View Based on Plant Macrofossil Analysis. 2011.
117. **Tanel Peets.** Dispersion Analysis of Wave Motion in Microstructured Solids. 2011.
118. **Liina Kaupmees.** Selenization of Molybdenum as Contact Material in Solar Cells. 2011.
119. **Allan Olsper.** Properties of VPg and Coat Protein of Sobemoviruses. 2011.
120. **Kadri Koppel.** Food Category Appraisal Using Sensory Methods. 2011.

121. **Jelena Gorbatšova**. Development of Methods for CE Analysis of Plant Phenolics and Vitamins. 2011.
122. **Karin Viipsi**. Impact of EDTA and Humic Substances on the Removal of Cd and Zn from Aqueous Solutions by Apatite. 2012.
123. **David Schryer**. Metabolic Flux Analysis of Compartmentalized Systems Using Dynamic Isotopologue Modeling. 2012.
124. **Ardo Illaste**. Analysis of Molecular Movements in Cardiac Myocytes. 2012.
125. **Indrek Reile**. 3-Alkylcyclopentane-1,2-Diones in Asymmetric Oxidation and Alkylation Reactions. 2012.
126. **Tatjana Tamberg**. Some Classes of Finite 2-Groups and Their Endomorphism Semigroups. 2012.
127. **Taavi Liblik**. Variability of Thermohaline Structure in the Gulf of Finland in Summer. 2012.
128. **Priidik Lagemaa**. Operational Forecasting in Estonian Marine Waters. 2012.
129. **Andrei Errapart**. Photoelastic Tomography in Linear and Non-linear Approximation. 2012.
130. **Külliki Krabbi**. Biochemical Diagnosis of Classical Galactosemia and Mucopolysaccharidoses in Estonia. 2012.
131. **Kristel Kaseleht**. Identification of Aroma Compounds in Food using SPME-GC/MS and GC-Olfactometry. 2012.
132. **Kristel Kodar**. Immunoglobulin G Glycosylation Profiling in Patients with Gastric Cancer. 2012.
133. **Kai Rosin**. Solar Radiation and Wind as Agents of the Formation of the Radiation Regime in Water Bodies. 2012.
134. **Ann Tiiman**. Interactions of Alzheimer's Amyloid-Beta Peptides with Zn(II) and Cu(II) Ions. 2012.
135. **Olga Gavrilova**. Application and Elaboration of Accounting Approaches for Sustainable Development. 2012.
136. **Olesja Bondarenko**. Development of Bacterial Biosensors and Human Stem Cell-Based *In Vitro* Assays for the Toxicological Profiling of Synthetic Nanoparticles. 2012.
137. **Katri Muska**. Study of Composition and Thermal Treatments of Quaternary Compounds for Monograin Layer Solar Cells. 2012.
138. **Ranno Nahku**. Validation of Critical Factors for the Quantitative Characterization of Bacterial Physiology in Accelerostat Cultures. 2012.
139. **Petri-Jaan Lahtvee**. Quantitative Omics-level Analysis of Growth Rate Dependent Energy Metabolism in *Lactococcus lactis*. 2012.
140. **Kerti Orumets**. Molecular Mechanisms Controlling Intracellular Glutathione Levels in Baker's Yeast *Saccharomyces cerevisiae* and its Random Mutagenized Glutathione Over-Accumulating Isolate. 2012.
141. **Loreida Timberg**. Spice-Cured Sprats Ripening, Sensory Parameters Development, and Quality Indicators. 2012.
142. **Anna Mihhalevski**. Rye Sourdough Fermentation and Bread Stability. 2012.
143. **Liisa Arike**. Quantitative Proteomics of *Escherichia coli*: From Relative to Absolute Scale. 2012.
144. **Kairi Otto**. Deposition of In₂S₃ Thin Films by Chemical Spray Pyrolysis. 2012.

145. **Mari Sepp.** Functions of the Basic Helix-Loop-Helix Transcription Factor TCF4 in Health and Disease. 2012.
146. **Anna Suhhova.** Detection of the Effect of Weak Stressors on Human Resting Electroencephalographic Signal. 2012.
147. **Aram Kazarjan.** Development and Production of Extruded Food and Feed Products Containing Probiotic Microorganisms. 2012.
148. **Rivo Uiboupin.** Application of Remote Sensing Methods for the Investigation of Spatio-Temporal Variability of Sea Surface Temperature and Chlorophyll Fields in the Gulf of Finland. 2013.
149. **Tiina Kriščiunaite.** A Study of Milk Coagulability. 2013.
150. **Tuuli Levandi.** Comparative Study of Cereal Varieties by Analytical Separation Methods and Chemometrics. 2013.
151. **Natalja Kabanova.** Development of a Microcalorimetric Method for the Study of Fermentation Processes. 2013.
152. **Himani Khanduri.** Magnetic Properties of Functional Oxides. 2013.
153. **Julia Smirnova.** Investigation of Properties and Reaction Mechanisms of Redox-Active Proteins by ESI MS. 2013.
154. **Mervi Sepp.** Estimation of Diffusion Restrictions in Cardiomyocytes Using Kinetic Measurements. 2013.
155. **Kersti Jääger.** Differentiation and Heterogeneity of Mesenchymal Stem Cells. 2013.
156. **Victor Alari.** Multi-Scale Wind Wave Modeling in the Baltic Sea. 2013.
157. **Taavi Päll.** Studies of CD44 Hyaluronan Binding Domain as Novel Angiogenesis Inhibitor. 2013.
158. **Allan Niidu.** Synthesis of Cyclopentane and Tetrahydrofuran Derivatives. 2013.
159. **Julia Geller.** Detection and Genetic Characterization of *Borrelia* Species Circulating in Tick Population in Estonia. 2013.
160. **Irina Stulova.** The Effects of Milk Composition and Treatment on the Growth of Lactic Acid Bacteria. 2013.
161. **Jana Holmar.** Optical Method for Uric Acid Removal Assessment During Dialysis. 2013.
162. **Kerti Ausmees.** Synthesis of Heterobicyclo[3.2.0]heptane Derivatives *via* Multicomponent Cascade Reaction. 2013.
163. **Minna Varikmaa.** Structural and Functional Studies of Mitochondrial Respiration Regulation in Muscle Cells. 2013.
164. **Indrek Koppel.** Transcriptional Mechanisms of BDNF Gene Regulation. 2014.
165. **Kristjan Pilt.** Optical Pulse Wave Signal Analysis for Determination of Early Arterial Ageing in Diabetic Patients. 2014.
166. **Andres Anier.** Estimation of the Complexity of the Electroencephalogram for Brain Monitoring in Intensive Care. 2014.
167. **Toivo Kallaste.** Pyroclastic Sanidine in the Lower Palaeozoic Bentonites – A Tool for Regional Geological Correlations. 2014.
168. **Erki Kärber.** Properties of ZnO-nanorod/In₂S₃/CuInS₂ Solar Cell and the Constituent Layers Deposited by Chemical Spray Method. 2014.
169. **Julia Lehner.** Formation of Cu₂ZnSnS₄ and Cu₂ZnSnSe₄ by Chalcogenisation of Electrochemically Deposited Precursor Layers. 2014.

170. **Peep Pitk.** Protein- and Lipid-rich Solid Slaughterhouse Waste Anaerobic Co-digestion: Resource Analysis and Process Optimization. 2014.
171. **Kaspar Valgepea.** Absolute Quantitative Multi-omics Characterization of Specific Growth Rate-dependent Metabolism of *Escherichia coli*. 2014.
172. **Artur Noole.** Asymmetric Organocatalytic Synthesis of 3,3'-Disubstituted Oxindoles. 2014.
173. **Robert Tsanev.** Identification and Structure-Functional Characterisation of the Gene Transcriptional Repressor Domain of Human Gli Proteins. 2014.
174. **Dmitri Kartofelev.** Nonlinear Sound Generation Mechanisms in Musical Acoustic. 2014.
175. **Sigrid Hade.** GIS Applications in the Studies of the Palaeozoic Graptolite Argillite and Landscape Change. 2014.
176. **Agne Velthut-Meikas.** Ovarian Follicle as the Environment of Oocyte Maturation: The Role of Granulosa Cells and Follicular Fluid at Pre-Ovulatory Development. 2014.
177. **Kristel Hälvin.** Determination of B-group Vitamins in Food Using an LC-MS Stable Isotope Dilution Assay. 2014.
178. **Mailis Pääri.** Characterization of the Oligoadenylate Synthetase Subgroup from Phylum Porifera. 2014.
179. **Jekaterina Kazantseva.** Alternative Splicing of *TAF4*: A Dynamic Switch between Distinct Cell Functions. 2014.
180. **Jaanus Suurväli.** Regulator of G Protein Signalling 16 (RGS16): Functions in Immunity and Genomic Location in an Ancient MHC-Related Evolutionarily Conserved Synteny Group. 2014.
181. **Ene Viiard.** Diversity and Stability of Lactic Acid Bacteria During Rye Sourdough Propagation. 2014.
182. **Kristella Hansen.** Prostaglandin Synthesis in Marine Arthropods and Red Algae. 2014.
183. **Helike Lõhelaid.** Allene Oxide Synthase-lipoxygenase Pathway in Coral Stress Response. 2015.
184. **Normunds Stivrīnš.** Postglacial Environmental Conditions, Vegetation Succession and Human Impact in Latvia. 2015.
185. **Mary-Liis Kütt.** Identification and Characterization of Bioactive Peptides with Antimicrobial and Immunoregulating Properties Derived from Bovine Colostrum and Milk. 2015.
186. **Kazbulat Šogenov.** Petrophysical Models of the CO₂ Plume at Prospective Storage Sites in the Baltic Basin. 2015.
187. **Taavi Raadik.** Application of Modulation Spectroscopy Methods in Photovoltaic Materials Research. 2015.
188. **Reio Pöder.** Study of Oxygen Vacancy Dynamics in Sc-doped Ceria with NMR Techniques. 2015.
189. **Sven Siir.** Internal Geochemical Stratification of Bentonites (Altered Volcanic Ash Beds) and its Interpretation. 2015.
190. **Kaur Jaanson.** Novel Transgenic Models Based on Bacterial Artificial Chromosomes for Studying BDNF Gene Regulation. 2015.

191. **Niina Karro**. Analysis of ADP Compartmentation in Cardiomyocytes and Its Role in Protection Against Mitochondrial Permeability Transition Pore Opening. 2015.
192. **Piret Laht**. B-plexins Regulate the Maturation of Neurons Through Microtubule Dynamics. 2015.
193. **Sergei Žari**. Organocatalytic Asymmetric Addition to Unsaturated 1,4-Dicarbonyl Compounds. 2015.
194. **Natalja Buhhallo**. Processes Influencing the Spatio-temporal Dynamics of Nutrients and Phytoplankton in Summer in the Gulf of Finland, Baltic Sea. 2015.
195. **Natalia Maticiu**. Mechanism of Changes in the Properties of Chemically Deposited CdS Thin Films Induced by Thermal Annealing. 2015.
196. **Mario Öeren**. Computational Study of Cyclohexylhemicucurbiturils. 2015.
197. **Mari Kalda**. Mechanoenergetics of a Single Cardiomyocyte. 2015.
198. **Ieva Grudzinska**. Diatom Stratigraphy and Relative Sea Level Changes of the Eastern Baltic Sea over the Holocene. 2015.
199. **Anna Kazantseva**. Alternative Splicing in Health and Disease. 2015.
200. **Jana Kazarjan**. Investigation of Endogenous Antioxidants and Their Synthetic Analogues by Capillary Electrophoresis. 2016.
201. **Maria Safonova**. SnS Thin Films Deposition by Chemical Solution Method and Characterization. 2016.
202. **Jekaterina Mazina**. Detection of Psycho- and Bioactive Drugs in Different Sample Matrices by Fluorescence Spectroscopy and Capillary Electrophoresis. 2016.
203. **Karin Rosenstein**. Genes Regulated by Estrogen and Progesterone in Human Endometrium. 2016.
204. **Aleksei Tretjakov**. A Macromolecular Imprinting Approach to Design Synthetic Receptors for Label-Free Biosensing Applications. 2016.
205. **Mati Danilson**. Temperature Dependent Electrical Properties of Kesterite Monograin Layer Solar Cells. 2016.